Freie Universität Berlin

DRFZ BERLIN
Deutsches Rheuma-Forschungszentrum
Ein Institut der Leibniz-Gemeinschaft

Analysis of T Cell Receptor-Induced Signaling Modules by Mass Spectrometry: NFAT Interactions and the CBM-Complex.

Inaugural-Dissertation
to obtain the academic degree
Doctor rerum naturalium (Dr. rer. nat.)

submitted to the Department of Biology, Chemistry and Pharmacy
of Freie Universität Berlin

by

CHRISTIAN GABRIEL

from Leipzig, Germany

2016

Diese Arbeit wurde vom 15.10.2010 bis zum 15.01.2016 am Deutschen Rheuma-Forschungszentrum in der Arbeitsgruppe von Prof. Dr. Ria Baumgrass angefertigt.

1. Gutachter: Prof. Dr. Ria Baumgrass

2. Gutachter: Prof. Dr. Rupert Mutzel

Disputation am: 14. April 2016

Eidesstattliche Erklärung

Hiermit erkläre ich, dass ich die vorliegende Dissertation selbstständig angefertigt habe. Ausgenommen hiervon sind - wie in Kapitel 2 kenntlich gemacht - die massenspektrometrischen und bioinformatischen Analysen, die in enger Kooperation mit den genannten Wissenschaftlern durchgeführt wurden. Diese Arbeit wurde ohne unzulässige Hilfsmittel angefertigt. Ich habe keine als die hier angegebenen Hilfsmittel und Quellen verwendet. Diese Arbeit wurde in gleicher oder ähnlicher Form noch keiner anderen Prüfungsbehörde vorgelegt.

Table of Contents

1. Introduction

1.1. The Role of T Cells in the Immune System

As Stephen Jay Gould pointed out, we live in the age of bacteria, as they constitute the most successful and widespread species on our planet[1]. To survive in such a hostile world, any and every organism, especially a more complex one, needs strategies of defense against bacteria and other microbes. Mammals evolved a system of immune defense that consists of an inborn and an adaptive branch and relies on the action of specialized tissues and cells. The importance of the adaptive immune system crystallizes in cases of severe combined immunodeficiency (SCID). This syndrome is characterized by the absence of functional B- and T- cells – the major players of the adaptive branch. If untreated, patients with SCID die within the first year of life due to massive severe infections[2].

To be protective, our immune system has to fulfill two basic tasks that are diametrically opposed. On the one hand, it has to repel all threats to our body, such as viruses, bacteria, protozoan and other parasites. The failure to fulfill this integral task results in live-threatening infections[3]. On the other hand, the immune system must not become a threat itself. In other words, it must not harm our body, as an auto-aggressive immune system leads to autoimmune diseases that can be equally lethal[4,5]. The key to fulfill both parts is the system's ability to discriminate between 'foreign' (bacteria, viruses, fungi, toxins etc.) and 'own' (tissues, cells, structures etc.).

T cells are a major player when it comes to the decision between own and foreign. Every T cell has a unique T cell receptor, and its binding patterns determines the ability of the cell to become activated upon stimulation with a particular antigen[6]. The T cell receptor is a result of somatic recombination of its gene locus and is thus unique for a single T cell and its progeny (see Janeway's Immunobiology, page 155ff)[7]. Upon generation, the collectivity of T cells possesses an (in theory) unlimited diversity of antigen specificities, but is depleted of auto-reactive T cells during maturation. As a result, mature T cells should only recognize foreign antigens. In praxis, some level of self-reactivity is remaining and necessitates a further system of checks and balances to avoid undesired self-destruction[8–11].

The entity of T cells subdivides into two main branches, which can be distinguished by the selective expression of the surface molecules CD4 and CD8[12]. CD8 positive cytotoxic T cells can recognize and kill transformed cells and cells that are infected by viruses or bacteria. Thereby, cytotoxic T cells help to curtail and clear ongoing infections and cancer development

(see Janeway's Immunobiology, page 364ff)[7]. CD4 positive *T helper cells* (T_H cells) direct and modulate the action of other immune cells via direct cell-cell interaction or the secretion of soluble mediators known as cytokines[13]. Among others functions, activated T_H cells can license B cells to produce specific antibodies, or recruit and activate phagocytic cells, such as macrophages.

1.2. The Activation of T Cells.

The activation of a T cell is initiated by the binding of the T cell receptor to a specific antigen. However, to become fully activated, the T cell necessitates further signals through its co-receptor. This co-stimulation is provided by specialized antigen presenting cells (see Janeway's Immunobiology, page 343ff)[7]. In the absence of such co-stimulation, engagement of the T cell receptor does not result in activation, but in the induction of a non-responsive 'anergic' phenotype, or even clonal deletion[14].

Once activated, the cell undergoes dramatic phenotypic changes that allow for proliferation, differentiation into further T_H cell subtypes and the execution of effector functions. The particular outcome is dependent on the individual history of a T cell (e.g. naïve or antigen-experienced) as well as on signals that the cell receives from its environment (e.g. cytokines, inflammatory signals, cell-cell contacts).

Within the T cell, the information that usually arrives in the form of receptor engagement must be translated into an appropriate cellular response. As this typically involves huge qualitative and quantitative changes in protein expression, arriving signals have to be transmitted to the nucleus, where protein biosynthesis is realized. This is achieved by a network of signal transduction processes. However, these networks do not only transmit signals locally, but also integrate the presence and strength of different inputs on the background of the particular cell[15]. Defects in signal transduction can result in aberrant high or low signaling, which is a major cause for inherited immunodeficiency or cancer development[16,17].

Typically, signal transduction processes result in the activation and/or deactivation of transcription factors, which in turn reshape the transcriptional program of the cell. Three transcription factor families play a pivotal role in the course of T cell activation: *nuclear factor of activated T cells* (NFAT), *nuclear factor of κ light chain enhancer of activated B cells* (NFκB) and *activator protein-1* (AP1). The importance of these signaling pathways is highlighted when one of these pathways is interrupted by genetic mutations. This often results in more or less severe forms of primary immunodeficiency[18]. CHAPTER 1.3 will outline the

signaling pathways that govern the activation of these transcription factors upon stimulation of the T cell. The main events are illustrated in FIGURE 1.

1.2.1. T Cell Stimulation *in vitro*

In vivo, T cells are stimulated by the binding of their T cell receptor to a recognized peptide-MHC complex on antigen presenting cells. As stated above, the antigen-presenting cell also provides co-stimulation by engaging the co-receptor of the T cell. *In vitro*, antigen specific stimulation can be achieved by loading the peptide of interest on radiated antigen presenting cells and by incubation of these cells together with the T cells. Polyclonal activation of T cells is achieved by the use of anti-CD3 antibodies that bind to invariant parts of the TCR in combination with anti-CD28 antibodies that engage the co-receptor. To obtain strong and uniform T cell stimulation, the cells can be stimulated chemically by the use of *phorbol-12-myristat-13-acetate* (PMA) and ionomycin. PMA is structurally related to *diacylglyerol* (DAG) and can thereby activate *protein kinase C* (PKC) signaling in an analogue fashion (see below)[19]. As a result, NFκB and AP1 activating pathways are triggered by PMA. Ionomycin integrates into the plasma membrane, thereby evoking calcium influx into the cell that stimulates calcium dependent enzymes, such as *calcineurin* (CaN)[20]. Thus, the use of both chemicals bypasses TCR ligation, while still leading to T cell activation (FIGURE 1). However, this bypass ignores the influence of early signaling events on the outcome of T cell activation. During this work, T cells are activated either by PMA and ionomycin or by activating antibodies specific for CD3 and CD28.

1.3. T Cell Receptor Signaling

1.3.1. From T Cell Receptor Stimulation to Phospholipase-C Activation

The ability of a T cell to recognize a certain antigen is determined by the specific binding pattern of its T cell receptor, which is unique for a given T cell and its progeny. The specificity of the *T cell receptor* (TCR) is defined by the cell specific combination of the TCR α- and β-chain. Additionally, the invariant CD3γ-, CD3δ-, CD3ε- and the ζ-chain are indispensable to build up a working TCR complex (FIGURE 1)[21]. Antigen binding to the α/β-chain induces the phosphorylation of *immune receptor tyrosine-based activation motifs* (ITAM) on the CD3γ-, CD3δ-, CD3ε- and ζ-chain via the kinases *lymphocyte specific protein tyrosine kinase* (LCK) and *feline yes-related protein* (FYN)[22].

The phosphorylated ITAMs serve as a docking station for the recruitment of another kinase, *ζ-chain associated protein* (ZAP70), which binds to the phosphotyrosine motifs with its *sarc homology*-3 (SH3) domain[23]. Subsequently, ZAP70 is phosphorylated and activated by

LCK[24,25]. In turn, ZAP70 phosphorylates the scaffold protein *linker of activation in T cells* (LAT), which is associated with the plasma membrane, and *SH2 domain-containing leukocyte protein of 76 kilo Dalton* (SLP76)[26,27]. These molecules work together in order to recruit *phospholipase C-γ* (PLCγ) to the plasma membrane[28,29]. Here, PLCγ is activated through phosphorylation by the tyrosine kinase *interleukin-2 inducible T cell kinase* (ITK)[30,31].

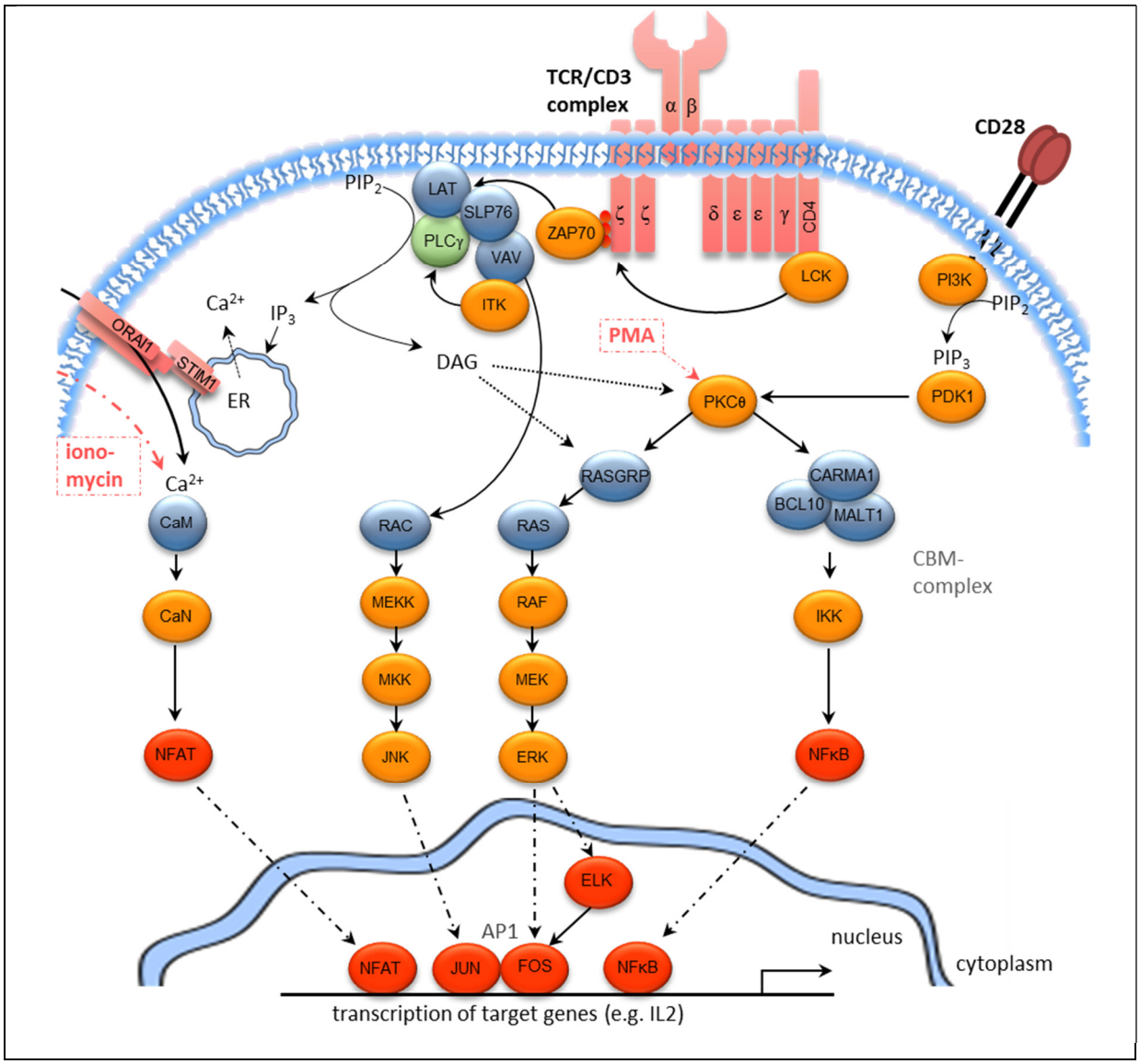

FIGURE 1. Main signal transduction pathways that lead to T cell activation. Following TCR and CD28 engagement, three main signaling pathways control the activation of the transcription factors NFAT, AP1 (JUN+FOS) and NFκB. Binding of antigen to the TCR leads to the phosphorylation of ITAM motifs on the CD3ζ chains. As a result, the kinase ZAP70 is recruited to the plasma membrane, leading to the activation of PLCγ. This enzyme generates the second messengers DAG and IP_3. Together with co-stimulation activated PDK1, DAG is responsible for the activation of PKCθ. PKCθ activates RASGRP, resulting in the triggering of MAP kinase cascades that ultimately activate AP1. PKCθ activity is also crucial for the formation of the CBM-complex that governs NFκB activation. IP_3 triggers the influx of Ca^{2+} ions into the cytoplasm. This in turn activates the phosphatase CaN via binding of CaM. CaN dephosphorylates NFAT, allowing its nuclear transition and activation. *In vitro*, T cell activation can be mimicked by incubation with PMA and ionomycin, which provokes PKC activation and calcium influx, respectively. Please refer to the text for abbreviations and further details, including cross talks between the different pathways. Adapted from www.cellsignal.com.

Phospholipase C-γ is a key molecule in the TCR induced signal transduction. It catalyzes the breakdown of the membrane phospholipid *phosphatidylinositol-4,5-bisphosphate* (PIP_2), thus generating two second messenger molecules, the phosphosugar *inositol 1,4,5-trisphosphate* (IP_3) and the membrane lipid diacylglycerol (DAG)[32]. Both molecules are essential for further signal transduction: IP_3 triggers the activation of NFAT, while DAG drives NFκB and AP1 activation, as will be highlighted during the following chapters.

1.3.2. PKCθ Activation Requires Signaling through the Co-Receptor

Following TCR engagement, activated PLCγ hydrolyses the membrane-phospholipid PIP_2 to release DAG and IP_3. DAG stays at the plasma membrane, binding and activating *protein kinase-C theta* (PKCθ)[33]. PKCθ activity in turn contributes to the activation of two main signaling cascades: the NFκB pathway and the MAP-kinase/AP-1 pathway (FIGURE 1).

However, complete activation of PKCθ also requires signaling from the co-stimulatory pathway that is triggered via the engagement of the T cell surface molecule CD28 by B7 molecules on the professional antigen-presenting cell. In brief, CD28 ligation leads to the recruitment and activation of *phosphoinositide 3-kinase* (PI3K)[34]. This kinase catalyzes the phosphorylation of PIP_2 to *phosphatidylinositol (3,4,5)-trisphosphate* (PIP_3), which in turn recruits the pleckstrin homology domain containing proteins *PIP_3 dependent kinase* (PDK1) and protein kinase B/AKT to the plasma membrane. There, both kinases contribute to the phosphorylation and activation of PKCθ[35–37]. However, recent findings draw a much more complex picture of how PKCθ is activated upon T cell stimulation[38,39].

PDK1 also physically links PKCθ to a complex that contains the proteins *caspase recruitment domain (CARD) containing membrane-associated guanylate kinase (MAGUK) protein-1* (CARMA1), *mucosa-associated lymphoid tissue lymphoma translocation protein-1* (MALT1) and *B-cell lymphoma protein 10* (BCL10, thereafter named CBM-complex) that governs the TCR induced activation of NFκB (outlined in CHAPTER 1.3.4).

1.3.3. Activation of AP1 Family Proteins through the Action of MAP Kinases

As mentioned above, the activity of PKCθ contributes to the activation of the transcription factor AP1, which is one indispensable transcription factor in the course of T cell activation (together with NFAT and NFκB). AP1 is a transcription factor that is built of a heterodimer of FOS proteins (FOS (also cFOS), FOSB, FRA1, FRA2) and JUN proteins (JUN (also c-JUN), JUNB, JUND)[40]. Different combinations of FOS and JUN proteins possess differential characteristics with respect to complex stability and preferred DNA recognition sequences[41,42]. Additionally, JUN protein can form stable homodimers, while FOS proteins

cannot[43]. Upon TCR stimulation, FOS and JUN proteins are typically activated by a *mitogen associated protein kinase* (MAPK) cascade of phosphorylation and activation (FIGURE 2, central part). While JUN is already present in resting T cells, FOS expression is dependent on stimulation.

The expression and activation of FOS is dependent on DAG. Aside of PKCθ, DAG also activates the *rat sarcoma guanyl releasing protein* (RAS-GRP)[44]. However, complete activation of RAS-GRP requires phosphorylation by PKCθ[45]. RAS-GRP in turn activates the small GTPase RAS. RAS activates the *MAP-kinase-kinase-kinase* (MAPKKK) RAF, which phosphorylates *MAPK/extracellular signal related kinase (ERK)-kinase* (MEK). MEK is responsible for the activation of the MAP-kinases ERK1 and ERK2, and activated ERKs can phosphorylate the *Ets-like transcription factor-1* (ELK1). Together with serum response factor and *cyclic adenosine monophosphate responsive element binding protein 1* (CREB1), ELK1 induces the transcription of FOS[46]. ERK-mediated phosphorylation further activates the expressed FOS protein[47].

Another cascade of MAP kinase signaling regulates the activity of JUN. The guanine nucleotide exchange factor VAV, which is activated by early signaling events, switches on the cascade of *RAS-related C3 botulinum toxin substrate-1* (RAC1), MEKK1 and MKK4/7[48]. Finally, the MAPK *JUN N-terminal kinase* (JNK) is activated. This enzyme catalyzes the phosphorylation of two serine residues in the N-terminal region of JUN, which turns on its activity as a transcription factor[49]. Thus, distinct MAP-kinase mediated pathways govern the activation of both FOS and JUN proteins, which dimerize to build the important AP1 transcription factor.

1.3.4. The CBM-Complex Governs the Activation of the Canonical NFκB Pathway in T Cells.

1.3.4.1. The CBM-Complex and IKK Activation

As we have described, TCR and co-receptor induced PKCθ activity triggers MAP-kinase cascades that lead to AP1 activation. Additionally, PKCθ also initiates a pathway that activates NFκB transcription factors, whose activity is also crucial for T cell activation and function. In general, NFκB activation can occur in response to various stimuli, such as *interleukin-1α* (IL1α), *tumor necrosis factor-α* (TNFα) or *toll-like receptor* (TLR) signaling and regulates key proliferative, anti-apoptotic and immune function genes[50]. In contrast to these other pathways, NFκB activation after TCR ligation is triggered by the PKCθ dependent formation of a complex that contains the proteins CARMA1, BCL10 and MALT1 (CBM-complex, FIGURE 2).

BCL10 was initially identified as a mutated gene in several *mucosa associated lymphoid tissue* (MALT) lymphomas[51–53]. It consists of an N-terminal *caspase recruitment domain* (CARD) and a C-terminal domain without homology to any known protein domains, which is rich in serine and threonine residues. MALT1 comprises a C-terminal *death domain* (DD) and several immunoglobulin-like domains that are important for protein-protein interactions[54]. However, the most striking feature of MALT1 is its protease domain, which is homolog to these of caspases. CARMA1 consists of several protein interaction domains: The N-terminal CARD domain is followed by a coiled-coil domain, which is connected via a linker region to the MAGUK typical C-terminus, consisting of a PDZ domain, a SH3 domain, and the GUK domain. The PDZ domain is responsible for membrane association[54].

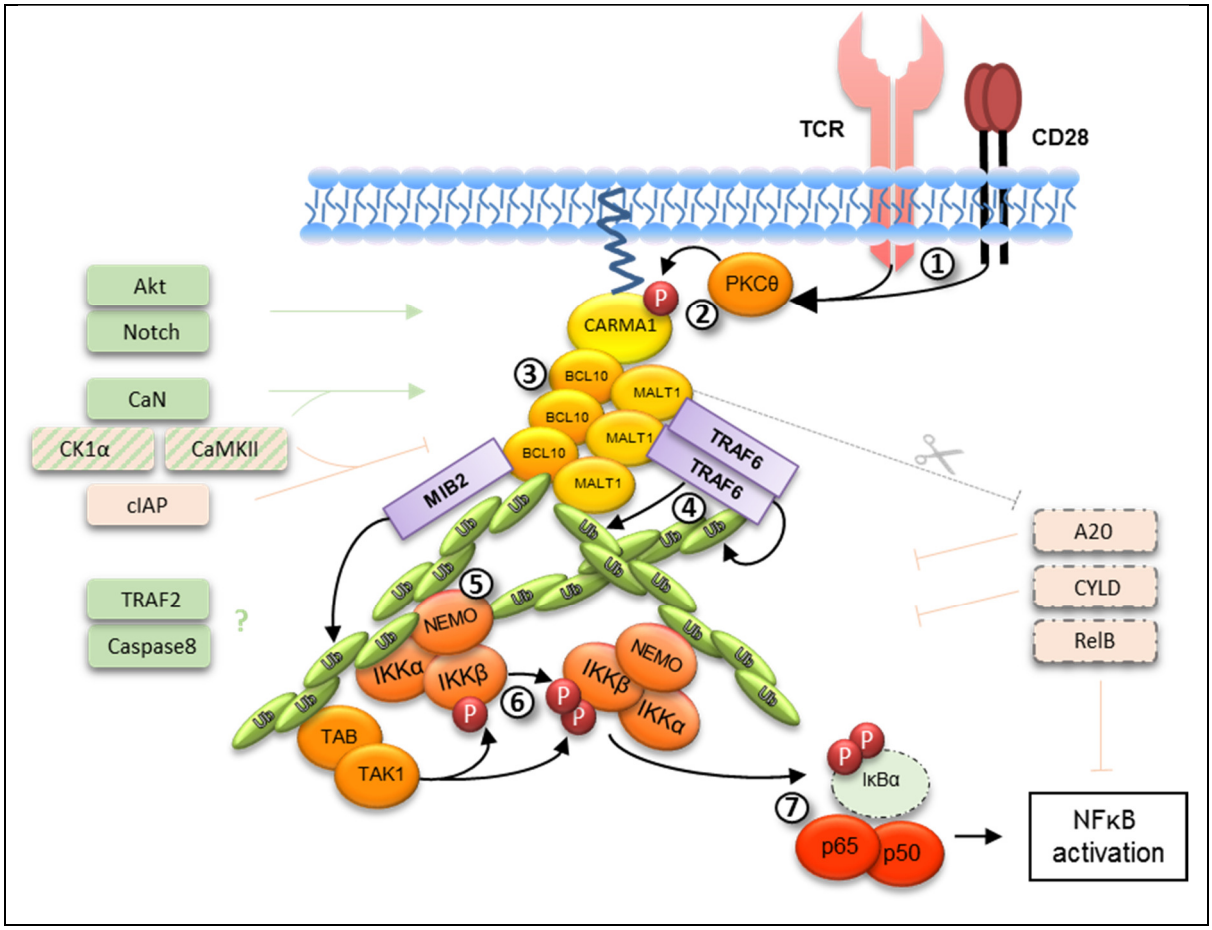

FIGURE 2. Signal transduction from TCR to NFκB. TCR and co-receptor ligation lead to the activation of PKCθ (1). CARMA1 phosphorylation by PKCθ (2) leads to a conformational change that allows binding and oligomerization of BCL10/MALT1 (3). Oligomerization of MALT-associated TRAF6 induces auto-ubiquitination/activation of TRAF6, as well as poly-ubiquitination of MALT1 and BCL10 (4). The ubiquitin network recruits the NEMO/IKK complex, which also undergoes ubiquitination, and the kinase TAK1 via TAB-proteins (5). IKKβ is activated by TAK- and trans-autophosphorylation (6). Subsequently, IKKβ phosphorylates IκBα, leading to its rapid degradation, which releases NFκB transcription factors p50/p65 from inhibition (7). Several other proteins have been shown to enhance (green) or reduce (red) CBM-complex formation and NFκB activation at different stages. For further details and abbreviations, please refer to the text. Ub: ubiquitin, P: phosphorylation.

While, in resting cells, MALT1 and BCL10 constantly associate via interaction of multiple protein domains[55–57], their interaction with CARMA1 is signal dependent. Following TCR activation, CARMA1 is phosphorylated by PKCθ, AKT and *hematopoietic progenitor kinase-1* (HPK1)[58–61]. As a result, CARMA1 undergoes a structural change from an inactive hairpin-like to an active open structure, which allows binding of BCL10 and recruitment of the BCL10-MALT1 complex to the immunological synapse. Interestingly, a putative downstream target of the CBM-complex, *inhibitor of NFκB kinase-beta* (IKKβ), is required for the induced association of BCL10-MALT1 with CARMA1, probably via phosphorylation of CARMA1[57,62]. It remains unclear, though, how IKKβ is activated initially or whether basal activity of IKKβ triggers CARMA1 phosphorylation after initial priming by other events.

The binding to CARMA1 induces oligomerization of BCL10/MALT1 in filamentous like structures, which do not only seem to activate MALT1 paracaspase activity but also facilitate further signaling[63]. MALT1 then acts as a scaffold protein that can link CBM-complex formation to IKK activation. Upon stimulation of Jurkat cells, MALT1 interacts with the ubiquitin ligase *TNF receptor-associated factor-6* (TRAF6). In turn, TRAF6 is able to attach K63 linked poly-ubiquitin chains to MALT1. These chains can be bound by the regulatory subunit of the IKK complex (IKKγ), also termed *NFκB essential modifier* (NEMO). Furthermore, binding to MALT1 also induces ubiquitination of TRAF6 itself and of NEMO, and the latter process is dependent on BCL10[64–67]. BCL10 is also poly-ubiquitinated after Jurkat cell stimulation, and only this ubiquitinated BCL10 can bind NEMO. Furthermore, caspase-8 seems to play a not completely understood role in recruiting the IKK complex to the active CBM[68–71]. The ubiquitin dependent recruitment of *TGFβ-activated kinase-1/TAK1-binding protein-1* (TAK1/TAB1) to the CBM-complex seems to be important, too, as kinase sufficient TAK1 was necessary for CBM-complex dependent IκBα phosphorylation in a reconstitution experiment[66].

The binding of NEMO to ubiquitin and/or ubiquitin induced NEMO oligomerization seems to trigger IKKβ activation, probably through TAK1 and/or auto-phosphorylation (FIGURE 2)[72–75]. In line with this, variants of NEMO, BCL10 or MALT1 that cannot be ubiquitinated or ubiquitin binding deficient NEMO all fail to induce proper IKK and NFκB activation[64,76]. While the individual knock-down of the ubiquitin-ligases TRAF6 or TRAF2 only slightly reduces NFκB activation after TCR stimulation, TRAF2/6 double knock-out has a strong synergistic effect, pointing towards functional redundancy of both TRAFs[66]. *Mind bomb homolog-2* (MIB2) is a further E3 ubiquitin ligase that was shown to interact with BCL10 upon T cell stimulation and to be important for TAK1 and IKK activation (FIGURE 2)[77].

Once activated, IKKβ phosphorylates IκBα at serine residues 32 and 36, inducing K48-linked poly-ubiquitination of IκBα that results in its rapid proteasomal degradation[78,79]. This finally releases the NFκB transcription factors p65/RELA from their former inhibitory partner, allowing translocation to the nucleus and the transcription of NFκB dependent target genes. Interestingly, while BCL10 seems indispensable for TCR induced NFκB activation, T cells from MALT1 knock-out mice still show albeit reduced IKKβ activity[80].

1.3.4.2. Post-Translational Modifications Regulate the Activity of the CBM-complex

Further signaling events were found to fine-tune the CBM-complex dependent activation of IKK and to provide negative feedback mechanisms that contribute to the transient nature of NFκB activation. *Casein kinase-1α* (CK1α) associates with the CBM-complex after stimulation via interaction with CARMA1. Although knock-down of CK1α reduces NFκB activation, it has no impact on CBM-complex formation, but slightly diminishes IKK recruitment to the complex[81]. Still, its particular function remains unclear. Interestingly, kinase deficient CK1α leads to BCL10-dependent augmented NFκB activity, pointing to the involvement of the kinase in negative feedback regulation[81]. Recent findings revealed *Notch homolog-1* (NOTCH1) as another CARMA1 interactor that contributes to CBM-complex formation[82].

BCL10 can be phosphorylated at several serine and threonine residues by a diversity of kinases, which can have diverse effects on NFκB activation. Work from Rueffli-Brasse *et al.* revealed that *receptor-interacting protein-2* (RIP2) associates with BCL10 and is important for phosphorylation of BCL10 and proper activation of NFκB following TCR ligation[83]. However, it remains unclear whether RIP2 phosphorylates BCL10 directly, and whether the phosphorylation of BCL10 is a prerequisite or result of NFκB activation. Phosphorylation of Ser48 and Thr91 by CaMKII contribute to NFκB activation, while phosphorylation of Ser138 negatively affects further signaling[84–86]. In line with that, we and others could show that the phosphatase *calcineurin* (CaN) dephosphorylates BCL10 at Ser138, and that this event is important for complete NFκB activation[87,88]. In memory T cells, but not in naïve T cells, BCL10 undergoes ubiquitination dependent degradation by autophagy after TCR stimulation, thus limiting NFκB activation. Other reports, which were mainly done on cell lines, suggested an involvement of either proteasomal or lysosomal degradation, though [85,89–93]. Among others, the E3 ligases *cellular inhibitor of apoptosis-1 and -2* (cIAP1 and cIAP2) are likely candidates to regulate the ubiquitination of BCL10[89,91,94,95]. Phosphorylation by IKK has also been linked to

BCL10 degradation as well as to decreased association with MALT1, both leading to reduced NFκB activation[57,90].

As mentioned earlier, MALT1 also possesses paracaspase activity that is crucial for optimal NFκB signaling and IL-2 production after TCR activation, however, not for initial NFκB signaling and IKK activation[66,96,97]. Several targets for MALT1 cleavage have been revealed, among them BCL10. Albeit cleavage of BCL10 is important for fibronectin adhesion of T cells after TCR engagement, it has no influence on NFκB activation[96]. Another target for MALT1 proteolysis is A20, a deubiquitinase that removes ubiquitin chains from MALT1, thus impeding interaction with the IKK complex and sustained NFκB activation. However, MALT1 cleavage only plays a minor role in A20 depletion compared to proteasomal degradation[98]. MALT1 has also been shown to cleave the NFκB protein REL-B, resulting in enhanced canonical NFκB activation[99]. Cleavage of Roquin and Regnase-1 by MALT1 promotes T cell differentiation into the TH_{17} and T_{reg} lineage[97,100].

It is not entirely understood how MALT1 proteolytic activity is regulated, but the underlying mechanism seems to depend on activated CARMA1 and CBM-complex formation[101]. BCL10 dependent mono-ubiquitination at Lys644 is indispensable for MALT1's proteolytic activity[102]. The responsible ubiquitin ligase is still to be identified, albeit TRAF6 is a likely candidate, as it is known to be involved in MALT1 poly-ubiquitination[65]. Crystal structure analyses imply that MALT1 dimerization is a prerequisite for its enzymatic activity[101]. At least in a resting state, BCL10 is needed to mediate (direct or indirect) MALT1-MALT1 interaction[64]. This points to the possibility that oligomerization of BCL10/MALT1, as it is induced by CARMA1 activation, might trigger MALT1 paracaspase activation[63].

1.3.4.3. CBM-Complex Defects Lead to Immunodeficiency or Cancer Development

Genetic defects of constituents of the CBM-complex often lead to severe immune defects, thereby underscoring the importance of this pathway in immune system function. Loss-of-function mutations of CARMA1, MALT1 or BCL10 can lead to a complete loss of NFκB activation after T cell stimulation[103]. CARMA1 deficiency causes a proliferative defect in these cells and an impaired potential for B cell help, leading to severe combined immunodeficiency. Also patients with a loss-of-function mutations in MALT1 suffer from reoccurring severe infections[103].

In contrast, aberrant activation of the CBM-complex and of downstream NFκB activation can lead to the development of malignancies. For example, chromosomal translocations that cause overexpression of MALT1 and BCL10 are commonly found in MALT

lymphomas[104]. Furthermore, CARMA1 mutations that lead to its oligomerization are found in 10 % of the activated B-cell subtype of diffuse large B cell lymphoma (ABC-DLBCL)[105]. Thus, strict regulation of the activity of the CBM-complex is crucial, as dysregulation can either compromise immune cell activity or lead to the occurrence of lymphomas.

In summary, much effort has been made to understand how the CBM-complex links antigen receptor stimulation to the activation of NFκB, and how diverse related and (seemingly) unrelated signaling events impact on this process. Albeit great advances, some processes remain elusive. Especially, the mechanisms how NEMO and the IKK complex are recruited to and activated at the CBM-complex are not entirely understood. While the importance of a complex ubiquitin network in this process became obvious, its exact role and its dynamic regulation are far from being understood. The same counts true for the contribution of TRAF2, Caspase-8 or the proteolytic activity of MALT1 to the regulation of NFκB activation. It is thus tempting to speculate that additional proteins contribute to the regulation of signal transduction at the CBM-complex. The identification of these suggested additional CBM-complex components might help to improve the understanding of the molecular mechanisms that govern immune receptor induced NFκB activation. To address this point, one part of the present work was to investigate the composition of the CBM-complex by the help of mass spectrometry (see CHAPTER 1.4).

1.3.5. Calcium Signaling Controls the Activation and Function of NFAT

1.3.5.1. Calcium Influx Triggers the Activation of Calcineurin

As mentioned above, TCR ligation leads to the activation of PLCγ, which catalyzes the breakdown of the membrane phospholipid PIP_2 into IP_3 and DAG[32]. While DAG remains at the plasma membrane to activate PKCθ, IP_3 diffuses into the cytoplasm. It binds to IP_3 receptors at the *endoplasmatic reticulum* (ER), which leads to a release of stored calcium ions from the ER into the plasma of the cell (FIGURE 1)[106]. This triggers a process called *store operated calcium entry* (SOCE), which relies on the action of the ER localized calcium sensor protein *stromal interaction molecule-1* (STIM1) and the plasma membrane pore forming protein ORAI1[107].

The depletion of calcium within the ER leads to the oligomerization of STIM1 on ER structures near the plasma membrane, where the multimeric STIM1 complexes directly interact with ORAI1, resulting in an influx of calcium from the extracellular space and to a sustained elevation of the cytoplasmic calcium level[108,109]. The protein c*almodulin* (CaM) acts as cellular calcium sensor and changes its conformation in response to the increased calcium level. In the calcium bound form, it interacts with and activates a variety of target proteins, among others

the phosphatase *calcineurin* (CaN) and members of the *Ca^{2+}/CaM-dependent protein kinase* (CaMK) family[110,111].

1.3.5.2. NFAT Proteins in Health and Disease

TCR engagement leads to an elevation of the cytoplasmic calcium concentration via a process called SOCE. When cytoplasmic calcium levels are elevated, calcium-bound CaM binds to calcineurin and activates its phosphatase activity. A major function of CaN is the activation of members of the NFAT family by dephosphorylation.

NFAT proteins play an outstanding role in the course of T cell activation and effector function. By binding to the respective promoters, NFAT promotes the transcription of a plethora of cytokines, including IL-2, IL-4, IL-5, IL-6, IL-10, IL-13, IL-17, IL-21, IL-22, TNFα, GM-CSF and IFNγ (reviewed by Kleiter *et al.*)[112]. Accordingly, abrogation of NFAT activity diminishes expression of these cytokines by T helper cells and also compromises the cytotoxic activity of CD8 positive T cells[113,114]. This shows that critical T cell effector functions, such as cytokine production and cytotoxicity, are highly dependent on NFAT transcription factors. Interestingly, NFAT is also involved in the induction of T cell tolerance, thereby preventing damage by overshooting immune responses and the development of autoimmune diseases: NFAT expression is crucial for the generation of TGFβ induced regulatory T cells, and only T cells that express NFAT are responsive to suppression by T_{reg} cells or to the induction of anergy[115–117]. Finally, aberrant expression and activation of one NFAT family member is observed in the course of tumor development. In this setting, NFAT can repress the expression of checkpoint kinases and induce the expression of the important oncogene MYC, thereby promoting cancer growth and progression[118–120].

The following chapters will focus on the family of NFAT transcription factors. Structural aspects and the regulation of NFAT activity will be highlighted. Furthermore, the crucial role that NFAT proteins play within T cells will be outlined.

1.3.5.3. The Family of NFAT Transcription Factors.

Nuclear factor of activated T cells (NFAT) was first identified as a component of an inducible nuclear factor that binds to the human IL-2 promoter in activated T cells[121]. The other component was found to be the AP1 transcription factor, which consists of a heterodimer of the basic leucine zipper proteins FOS and JUN[122]. Interest in NFAT was raised by the fact that its activation was counteracted by the widely used immunosuppressive agents *cyclosporine A* (CsA) and *tacrolimus* (FK506), indicating an important role of NFAT proteins during the immune response[123]. Since then, NFAT emerged as a key player in the activation and differentiation of lymphocytes.

The family of NFAT transcription factors consists of five isoforms, namely NFATc1 (also known as NFAT2, NFATc), NFATc2 (NFAT1, NFATp), NFATc3 (NFAT4), NFATc4 (NFAT3) and NFATc5 (FIGURE 3)[124–128]. Out of these, only NFATc1, NFATc2 and NFATc3 are expressed in lymphocytes. Except for NFATc5, which is activated by osmotic stress, all isoforms are regulated by calcium signaling. Despite the name, NFAT proteins also play a vital role in other cells of the immune system, such as B-cells, mast cells or natural killer cells[113,129–131], as well as in many non-immune cell types, such as osteoblasts, neurons and heart muscle cells[132–136].

Typically, individual knock-out of NFAT family members induces rather mild phenotypic alterations, which become more prominent upon combined knock-out of two NFATs. Albeit this points to some functional redundancy, differences in the particular knock-out phenotypes also clearly point to non-overlapping functions.

NFATc2 knock-out mice were born without any defects[137]. Surprisingly, lymphocytes from these mice are hyper-proliferative and express increased amounts of IL-4 and IL-6. All these alterations are further augmented in NFATc2/c3 double deficient T cells[138]. This suggests a high degree of redundancy in function of NFATc2 and NFATc3. In contrast to NFATc2 or NFATc3 knock-out mice, NFATc1 knock-out mice die during embryogenesis[139]. When NFATc1 is knocked out exclusively in T cells, these T cells lacking NFATc1 show reduced proliferation following stimulation. They produce normal amounts of IL-2, but less IL-4 and IL-6 than wild-type T cells[140]. These findings suggest opposing functions of NFATc1 and NFATc2/3 with regard to proliferation and the production of certain cytokines.

Finally, T cells deficient for NFATc1 and NFATc2 completely fail to produce T helper cell effector cytokines, such as the interleukins IL-2 and IL-4 or *interferon-γ* (IFNγ)[113]. The latter finding underscores the outstanding role that NFAT proteins play in the course of T cell activation. Mutations in humans that prevent NFAT from translocating into the nucleus lead to *severe combined immune defect* (SCID), thereby resembling that phenotype of the NFATc1/c2 double knock-out[141]. Thus, NFAT proteins in general are indispensable for the function of T cells and the adaptive immune system as a whole.

Most NFAT family members can be alternatively spliced to produce various isoforms with different N- and C-terminal domains, adding a further level of complexity (FIGURE 3). This was studied in great detail for NFATc1[142]. Naïve T cells mainly produce the longer isoforms NFATc1/βB and NFATc1/βC. Antigen receptor signaling initiates increased expression of NFATc1 as well as the switch to both an alternative promoter and alternative polyadenylation

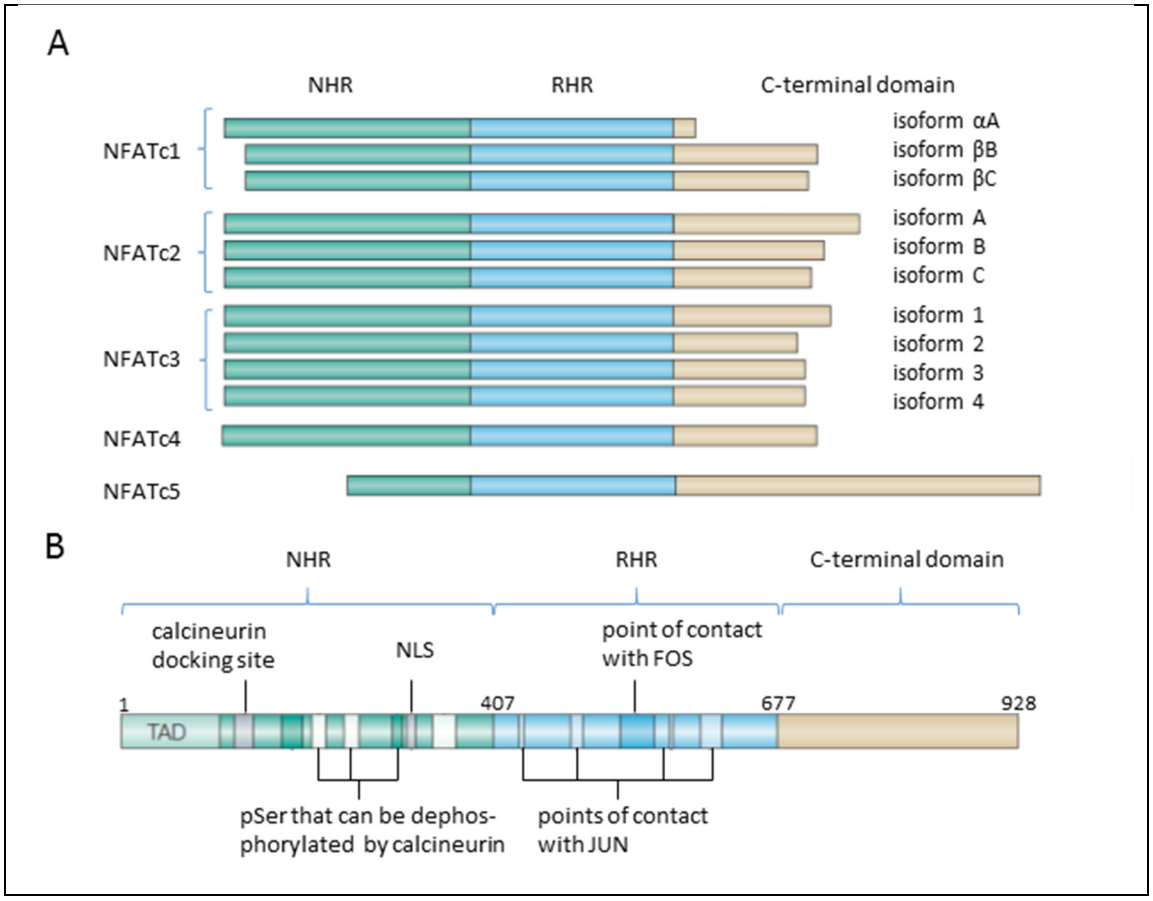

FIGURE 3. Structural and functional features of NFAT proteins. Panel A shows the most abundant isoforms of NFATc1 – NFATc5. Proteins are aligned by their Rel-homology domain (RHR) which contains the DNA binding domain. Use of alternative promoters and alternative splicing lead to differences in the N- and C-terminal regions. B: The NFAT homology region (NHR) contains the docking site for NFAT and is rich in serine residues. Phosphoserine residues that can be dephosphorylated by calcineurin are clustered in three sites. Additional to DNA binding, the RHR can form contact with JUN and FOS proteins. Adapted from Macian *et al.* [143] NLS: nuclear localization signal.

signal. This results in the predominant expression of the shorter NFATc1/αA isoform, which becomes the dominant isoform in peripheral T cells after antigen receptor engagement[144,145]. While maximum expression of NFATc1/αA occurs after 24 hours of stimulation in naïve T cells, memory cells upregulate its expression much faster with expression peaking already after 4 hours. The upregulation of NFATc1 expression is dependent on NFAT itself and, at least in B cells, on c-REL activation[146,147]. Since T cells deficient for both NFATc2 and NFATc3 express robust amounts of NFATc1/αA, NFATc1 seems sufficient to upregulate its own expression[148].

The longer NFATc1 isoforms (NFATc1/B and NFATc1/C) contain an additional transactivation domain at the C-terminus, which undergoes attachment of *small ubiquitin-like modifiers* (SUMO), so-called SUMOylation. As a result, IL-2 expression is reduced by overexpression of NFATc1/C, but enhanced by overexpression of either NFATc1/A or a SUMOylation resistant NFATc1/C variant[149]. Furthermore, the αA isoform contains an

alternative N-terminus, that is rich in serine and proline residues and seems to decrease half-life times of the protein[148]. Although the importance of the different NFATc1 isoforms is not yet completely understood, the short NFATc1/αA is believed to be the key player in NFATc1 effector functions in lymphocytes.

1.3.5.4. Structure and Regulation of NFAT Activity

All NFAT proteins consist of three structural domains: a highly conserved *REL homology domain* (RHR), a moderately conserved N-terminal *NFAT homology domain* (NHR) and a C-terminal domain (FIGURE 3). The RHR is shared by all NFAT members. It harbors the DNA binding domain which is structurally related to the REL family of transcription factors, and enables sequence specific DNA binding[150]. The NHR contains a potent transactivation domain and is rich in serine residues that are important for the regulation of NFAT activity.

In a resting state, the NHR is highly phosphorylated and NFAT is retained in the cytoplasm (FIGURE 4). Dephosphorylation by activated calcium-activated CaN induces a conformational change that exposes one or more nuclear localization sequences[123,151]. This allows the NFAT protein to enter the nucleus and to activate transcription. Mass spectrometric investigations revealed that out of 14 phosphorylated serine residues of NFATc2, 13 can be dephosphorylated by calcineurin upon stimulation[151]. Inhibition of calcineurin by CsA completely prevents NFAT activation, thereby inhibiting T cell activation. It is noteworthy, though, that inhibition by CsA also affects other targets of CaN, such as the TCR induced NFκB activation[87]. Two crucial interaction or docking sites of CaN to NFAT have been mapped to an N-terminal site with the consensus sequence PXIXIT, whereas X stands for any amino acid. This finding was supported by the fact that a high affinity peptide composed of this consensus sequence (VIVIT) was able to block NFAT dephosphorylation by calcineurin *in vitro*[114].

Once in the nucleus, NFAT can be re-phosphorylated by a couple of kinases (FIGURE 4), including *glycogen synthase kinase-3β* (GSK3β), CK1, JNK, p38 MAP kinase, *dual-specificity tyrosine-phosphorylation regulated kinase* (DYRK) and the cAMP dependent *protein kinase A* (PKA)[152–157]. PKA and/or DYRK act as priming kinases for the action of the other enzymes, and phosphorylation leads to NFAT inactivation and relocation to the cytoplasm[157]. Interestingly, several other kinases (*vaccinia-related kinase-2* (VRK2), Cot, protein kinase-Cζ, PIM1) can *activate* NFAT transcription factors by phosphorylation[158–160]. These phosphorylation sites usually are no targets of calcineurin.

NFAT localization and activation is also affected by other mechanisms (FIGURE 4). NFAT nuclear transition can be hindered by a complex which consists of the long non-coding

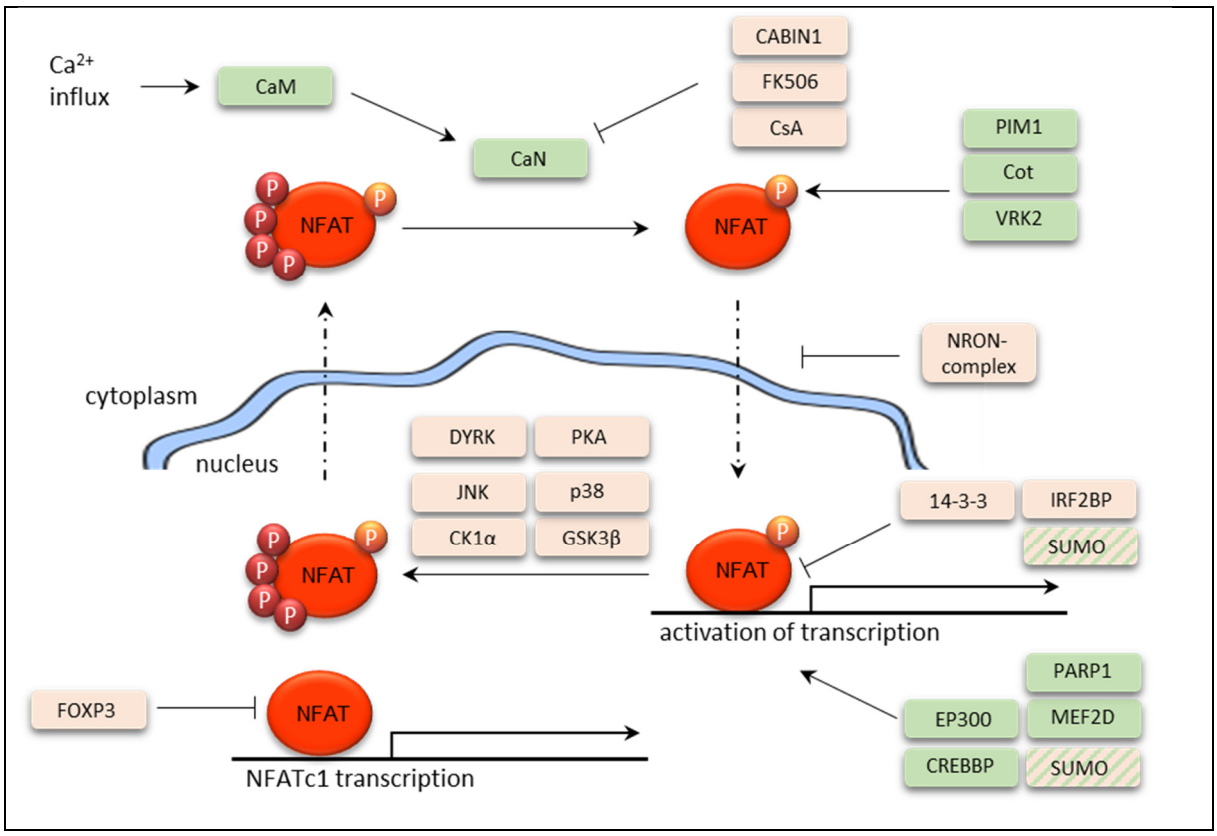

FIGURE 4. Regulation of NFAT activity. In a resting state, NFAT is highly phosphorylated by a number of kinases and retained in the cytoplasm. Elevation of cellular calcium level activates the phosphatase calcineurin (CaN) that dephosphorylates NFAT at multiple sites, allowing its nuclear transition. In the nucleus, NFAT can drive the transcription of target genes by recruitment of co-activator proteins, such as EP300 and CREBBP. Several NFAT binding proteins and posttranslational modifications increase (green) or decrease (red) the transcriptional activity of NFAT. NFAT enhances the expression of its isoform NFATc1, thus providing a positive feedback loop. FOXP3 can outcompete the binding of NFAT to this locus, thereby repressing NFATc1 transcription. Please refer to the text for abbreviations and further details.

RNA *non-coding repressor of NFAT* (NRON) and at least eleven associated proteins that binds NFAT[161,162]. Binding of 14-3-3 proteins to phosphorylated NFAT residues inhibit NFAT activity, while SUMOylation and adenosine monophosphate-ribosylation of NFATc2 can positively regulate nuclear retention and transcriptional activation[163,164].

1.3.5.5. NFAT Function and Its Interaction with the Transcription Factor AP1

In an activated state, NFAT transcription factors can bind to DNA sequences of the consensus (T/A)GGAAA[150]. Whereas NFAT exclusively exist as a monomeric form in solution, it can bind to DNA as a monomer at consensus binding sites, as a dimer on palindromic κB like sites or in combination with other transcription factors at composite binding sites[165–167]. NFAT has been shown to interact with several other transcription factors. The aforementioned interaction between NFAT and AP1 (composed of JUN and FOS proteins) is characterized in detail, including crystal structure analysis of the complex specifically bound to a composite

DNA sequence. When activated, the three transcription factors cooperatively bind to composite binding sites and many amino acid residues in the NFAT RHR contribute to the interaction interface[150].

NFAT:AP1 binding sites are found to regulate a large number of inducible, immune-related genes, including cytokines (IL-2, IL-4, IL-5, *granulocyte/macrophage-colony stimulating factor* (GM-CSF)), FAS-ligand, cyclooxygenase or the IL-2 receptor α-chain CD25[112,168]. These composite elements are often a combination of a weak or moderate binding site for one of the transcription factors with a weak to moderate binding site of the other. As a result, individual binding of one transcription factor to the composite DNA site is characterized by high dissociation rates, whereas binding of both transcription factors results in the formation of a stable complex that allows for sustained activation of transcription[122,150]. Interestingly, an engineered NFAT mutant that cannot bind to AP1 fails to induce transcription from most of these elements, confirming that the interaction between both is indeed necessary for gene activation (see below). Although the interaction of NFAT and AP1 is mainly described in the context of sequence specific DNA binding, GST-pulldown assays revealed that NFATc2, but not NFATc1 interacts with JUN homodimers, but not with JUN/FOS heterodimers, even in the absence of DNA[169]. The site of interaction was mapped to the C-terminal part of NFATc2, which was also shown to be necessary for synergistic activation of an IL-2 promoter reporter construct[169].

In the absence of AP1, NFAT can still bind as a dimer to pseudopalindromic κB like sites that comprise inverted repeats of a minimal NFAT binding site, as it was described for the TNFα promoter[167]. Stimulation via the TCR-only already provokes calcineurin activation, thus enabling NFAT dimer binding. However, co-activation is necessary to activate AP1 transcription factors and cooperative binding of NFAT and AP1 to composite binding sites.

1.3.5.6. In the Absence of AP1 Activation, NFAT Promotes T Cell Anergy

Beside engagement of its TCR, the activation of a T cell requires signaling via its co-receptor, which is usually provided by activated antigen-presenting cells and triggers (among others) AP1 activation. In contrast, binding of antigen to the TCR in the absence of co-stimulation converts T cells into a hyporeactive state, termed anergy. Anergic T cells do not proliferate or exhibit effector functions upon re-encounter of antigen, even in the presence of co-stimulation[115]. The ubiquitin ligases *gene related to anergy in lymphocytes* (GRAIL/RNF128), *E3 ubiquitin-protein ligase itchy homolog* (ITCH) and *Cbl proto-oncogene-B* (CBL-B) are upregulated in anergic T cells and counteract T cell activation by targeting important signaling molecules, such as PLCγ or PKCθ, for degradation[170–172].

There are independent lines of evidence that NFAT plays a major role in anergy induction. First, T cell anergy is induced *in vitro* by stimulus of the T cell receptor or by evoking the elevation of cellular calcium concentration via ionomycin, both conditions under which NFAT is activated[115,173]. Induction of anergy can be blocked by cyclosporine A[174]. Strikingly, T cells from NFATc2 knock-out mice are protected from anergy induction. Furthermore, overexpression of a constitutive active NFAT form also induces an anergic phenotype in T cells[115]. NFAT homodimer binding to the GRAIL promoter induces GRAIL upregulation. Furthermore, NFATc2 that is rendered incapable of dimerization does not induce unresponsiveness in T cells[170]. Finally, NFAT dependent expression of *early growth response*-2 (EGR2) and EGR3 promotes the activation of CBL-B[174].

In summary, this all points to a model in which NFAT acts as a two-edged sword, promoting both anergy induction and T cell activation. In the absence of co-stimulation, NFAT acts as a dimer to induce anergy related genes. Co-stimulation and AP1 activation allows NFAT to bind to composite NFAT:AP1 sites, starting a transcriptional program that governs T cell activation. In the latter case, several mechanisms are described to shut down anergic processes: On the one hand, NFAT dimer binding to the GRAIL promoter is diminished in fully activated T cells. The exact mode of action is not clear, but may involve concurrent binding of NFκB transcription factors, binding of AP1 to NFAT and the predominant expression of NFATc1 that does not seem to bind to the κB like sites[170]. On the other hand, the activating processes can directly counteract the anergic induction by limiting the expression and/or activation of anergy promoting proteins[174]. Altogether, this emphasizes that the interaction of NFAT with other transcription factors, such as AP1, can have a great impact on the regulation of NFAT target genes, and as such on the consequences of TCR engagement.

1.3.5.7. Interaction of NFAT with Further Transcription Factors

We have already outlined how NFAT interacts with AP1 and we have highlighted how this interaction is necessary for the activation of a T cell. In the absence of AP1 (-interaction), even properly activated NFAT does not lead to activation but to anergy induction. Thus, AP1 shapes the outcome of NFAT activation via the interaction with NFAT proteins.

Interestingly, further proteins are known to interact with NFAT proteins in a similar fashion. For example, NFAT also associates with the *forkhead-box protein-P3* (FOXP3), the master transcription factor of *regulatory T cells* (T_{reg}) that promote immune tolerance upon antigen recognition, thereby limiting T cell activation. NFAT and FOXP3 can cooperatively bind to DNA in a sequence specific manner. Crystal structures reveal intensive interactions

between NFAT and FOXP3 or the homologue FOXP2 DNA binding domain[175,176]. However, these interactions differ structurally from these between NFAT and AP1.

FOXP3-NFAT heterodimers can bind to the NFAT-AP1 binding site in the IL-2 promoter, thereby repressing IL-2 transcription[176]. Ectopic FOXP3 expression in T cells represses the activity of NFAT in a reporter gene assay, secretion of IFNγ, and proliferation in response to low dose antigen[177]. In contrast, binding of NFAT-FOXP3 to the promoters of CD25, *glucocorticoid-induced TNF receptor-related protein* (GITR) or *cytotoxic T lymphocyte-associated protein-4* (CTLA4) upregulates expression of these important T_{reg} genes. A FOXP3 mutant that is unable to interact with NFAT fails in both processes and diminishes the suppressive capacity of T_{reg}[176]. Interestingly, FOXP3 can also impede NFATc1 transcription by outcompeting the NFAT-binding to an overlapping site in the NFATc1 promoter[178]. Contrarily, NFAT is necessary for TGFβ induced FOXP3 transcription in inducible T_{reg} cells by binding to an enhancer region. While induction of such iT_{reg}s is highly dependent on NFAT, effector functions of natural and induced T_{reg} cells are less dependent on high levels of NFAT activation[116].

Beside FOXP3 and AP1 proteins, functional interaction of NFAT with numerous other transcription factors have been described. NFAT interacts with *GATA binding protein-3* (GATA3) and together, both drive transcription of IL-4 and IL-5 in T_{H2} cells[179]. Similarly, *interferon regulatory factor-4* (IRF4) strongly enhances expression of IL-4 in the presence of NFAT, and both proteins were shown to co-precipitate from primary T cells[180]. NFAT and EGR zinc finger proteins can bind to each other and can synergistically drive transcription, e.g. at the TNFα and IL-2 promoter[181]. NFAT binds to *myocyte enhancer factor-2D* (MEF2D) via its C-terminal domain and enhances MEF2D transcriptional activity even in the absence of NFAT-DNA binding. This activation is caused by increased recruitment of the co-activator EP300 via NFAT interaction[182]. The *IRF2 binding protein-2* (IRF2BP2) also binds the C-terminal domain of NFATc2, thereby repressing its transactivation potential. Consequently, IRF2BP2 overexpression leads to reduced expression of IL-2 and IL-4 in primary T cells[183].

In summary, many proteins interact with NFAT, thereby affecting its activity. The binding of NFAT to other transcription factors has a great impact on the transcriptional targets of NFAT activity. As described for the IL-2 promoter, NFAT activates IL-2 expression in concert with AP1, but represses IL-2 expression in a complex with FOXP3. In the absence of interaction partners, NFAT does not seem to bind to this locus. This guarantees that IL-2 is only produced after engagement of both TCR **and** co-receptor, which trigger NFAT and AP-1 activation, respectively. In a similar way, the interaction of NFAT with the T_{H2} lineage-specific

transcription factor GATA3 allows the lineage-specific activation of IL-4 in response to T cell activation. Thus, the interaction with other transcription factors fine-tunes the activity of NFAT to produce an appropriate, stimuli-dependent and cell-specific outcome.

Additionally, NFAT functionally cooperates with many further transcription factors, for which no direct interaction with NFAT has been reported so far. Nonetheless, these cooperation can drive differentiation and effector functions of T cells[112]. For example, both NFAT and STAT4 are necessary to drive the expression of IFNγ in T_{H1} cells. This finding is supported by the fact that the knock-out of either NFATc1 and NFATc2 or STAT4 abrogates the production of this cytokine[113,184]. Similarly, reporter gene assays and chromatin-immunoprecipitation experiments revealed that both RUNX1 and NFATc1 enhance transcription of IL-17 via binding to its promoter[185–187]. It remains unclear, yet, whether such co-regulations appear in an independent manner, as a hierarchic sequence of events, or whether direct interaction of the transcription factors contribute to these processes.

A recent *mass spectrometry* (MS)-based study on the interactome of FOXP3 revealed that this transcription factor is involved in a large network of protein-protein interactions. This study provided evidence for more than 300 (direct and indirect) interaction partners of FOXP3, including NFATc2[188]. Analogical work on RelA revealed more than 50 high confident interaction partners of this NFκB family member[189]. Since such a dataset on NFAT interactions was missing, we intended to study NFAT protein-protein interaction by an unbiased, MS based approach. Thereby, we hoped to confirm suspected NFAT interaction, but also to identify hitherto unknown NFAT interaction partners that might contribute to the diverse faces of NFAT signaling. In the following chapter, the methodical background of mass spectrometry based investigations on protein-protein interactions will be highlighted in brief.

1.4. Mass Spectrometry to Investigate Protein Complexes

1.4.1. MS in Proteomics: Isotope Labeling

Mass spectrometry (MS) is a technique that allows determining the molecular mass of atoms and molecules. In principle, the analytes are ionized, brought to gaseous phase, and separated by different interactions with electric fields (e.g. acceleration towards an electrode), which are a direct function of the mass-to-charge ratio of the analyte. The development of mild ionization methods, such as *electro-spray ionization* (ESI) or *matrix-assisted laser desorption/ionization* (MALDI), broadened the scope of application of MS towards the analysis of large biomolecules. This enabled the analysis even of protein samples and cleared the way

for MS to become a powerful method in the field of biochemistry, which was appreciated with the Nobel Prize in Chemistry for John Bennett Fenn and Koichi Tanaka in 2002[190].

During the last 20 years, MS has made its way into cell biology. With machines becoming ever more powerful and evolving methods for relative and absolute quantification, it is now possible to identify the entity of proteins within complex biological samples or compare the abundance of proteins between two or more samples. Coupling of MS to multi-dimensional orthogonal pre-separation of proteins can identify more than 10.000 different proteins from cellular extracts[191,192]. The two most common pipelines are tryptic digest-LC/LC-MS/MS and SDS-PAGE-tryptic digest-LC-MS/MS, followed by data base research to assign the identified peptides to their cognate proteins.

One drawback of mass spectrometry is its inherent lack of direct quantitative information, as signal strength depends rather on chemical properties of the analyte, such as ionization potential, than on abundance. This problem could be solved partially by introducing stable isotope labeling into MS, since the incorporation of stable isotopes into chemical compounds changes molecule mass while not affecting chemical properties[193]. Thus, when mixed and measured in one experiment, differently labeled entities of the same molecule/peptide give rise to distinguishable signals in MS, whose intensity ratio directly hints to the abundance ratio in the sample.

Beside chemical labeling methods, metabolic labeling has become state of the art in modern proteomics. *Stable isotope labeling by amino acids in cell culture* (SILAC) employs living cells for the labeling of proteins[194]. Cells were grown either in normal cell culture medium or in a modified medium, in which one or more essential amino acid (e.g. lysine, arginine, and isoleucine) are supplied only in a heavy form, i.e. it contains only ^{13}C, ^{15}N and/or ^{2}H instead of ^{12}C, ^{14}N and/or ^{1}H, respectively (FIGURE 5). These heavy amino acids are then incorporated into every single protein of every cell while the cells grow and divide. Thus, proteins and all derived peptides from the two cultures are distinguishable in mass spectrometry by a characteristic mass shift, while chemical properties remain unaffected[194]. This allows tracing differences in the whole proteome of the cells or within a given subset.

A huge advantage of metabolic labeling is that samples can be mixed very early during preparation, which minimizes variations derived from handling. However, since metabolic labeling necessitates complete protein turnover, it is limited to cells that readily divide several times in culture medium (mostly cell lines) or cells from animals that are given a – rather expensive – isotope labeled diet over several generations[195]. It is noteworthy that newly

developed label free quantification methods are recently on the rise in the field of MS based proteomics[196–198].

1.4.2. Analysis of Protein Complexes by CoIP-MS

Western blot analysis of protein co-purification experiments can be used to confirm and study protein-protein interactions. Hereby, a protein of interest (the so-called 'bait') is isolated from a cellular extract and the presence of co-purified, interacting proteins (the so-called 'prey') is probed by immunoblotting. However, this approach is usually limited to the investigation of already known or suspected interactions.

Semi-quantitative tandem MS can be combined with co-immunopurification to investigate the (dynamic) composition of protein complexes in an unbiased manner (FIGURE 5). In recent years, the combination of protein co-purification with mass spectrometric read-out proved to be a powerful tool to identify protein-protein interaction in an unbiased – and hitherto unseen comprehensive – manner. Especially, MS based investigations of large protein complexes revealed multiple new and often unsuspected components. Among others, MS based protein complex analyses greatly enhanced our understanding of the function and regulation of the TNFα receptor complex, of a cytoplasmic signaling module containing SLP-65 or of FOXP3 centered transcription factor complexes[188,199,200].

As with all co-purification experiments, proper control experiments are a prerequisite for the production of reliable data. In CoIP-WB experiments, specific antibodies are usually exchanged for isotype matched control antibodies to show that a potentially interacting protein is not enriched by unspecific binding. This approach is not recommendable for CoIP-MS. The main reason is that the specific and the control antibody will always bind non-specifically to a non-overlapping spectrum of proteins. Since in CoIP-MS all bound and eluted proteins are analyzed in an unbiased way, the use of a control antibody would lead to a large amount of false-positive hits. Therefore, it is indispensable that the control experiment is done with the same purification system. The conditions have to be chosen in a way that the complex is isolated in the actual experiment but not in the control experiment (FIGURE 5). In most cases, this is realized by overexpression of an epitope-tagged form of the bait protein in the bait cells, but not in the control cells. Thus, complex-isolation using a tag-specific antibody will yield the complex of interest only from the bait cells, while non-specific binding should be equal in both experiments. Overexpression of a tagged control-protein (such as GFP) in the control cells can be used to preclude tag-binding proteins from enrichment. The overexpression of a non-tagged bait protein in the control cells is a good strategy to obtain high similarity between bait and control cells with regard to protein expression.

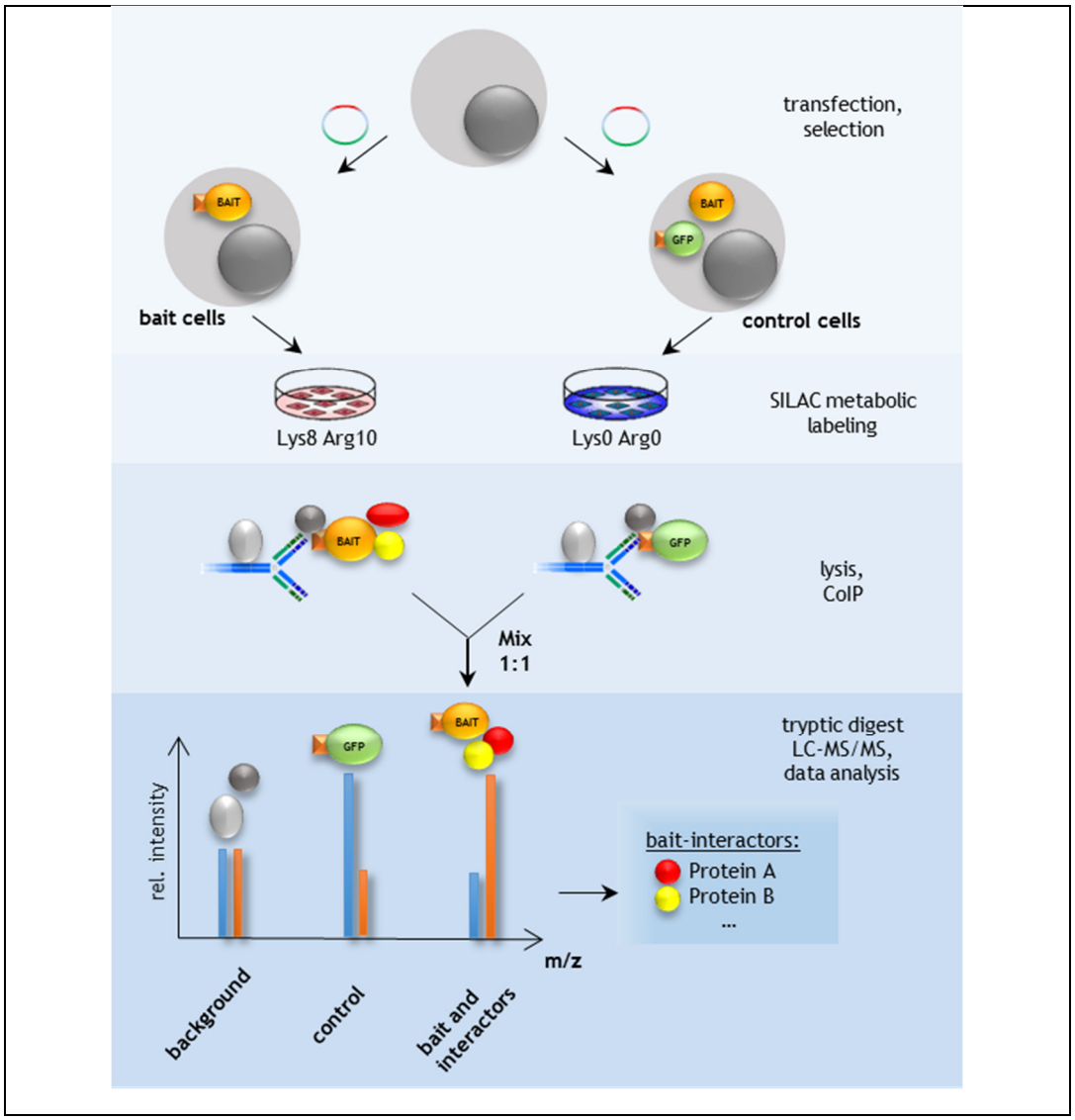

FIGURE 5. Basic principle of protein complex analysis by CoIP-MS. An epitope-tagged form of the bait protein is stably transfected into bait cells (left side). Control cells (right side) are transfected with a non-tagged form of the bait protein or with an epitope-tagged form of a control protein, such as GFP. Bait and control cells are grown in `light' or `heavy' SILAC medium to achieve metabolic labeling of all proteins with light or heavy arginine and lysine, respectively. CoIP is done from both cell populations using the same protocol and reagents. Bait and control proteins are mixed at a 1:1 ratio, either before or after elution from the affinity matrix. Proteins are digested by trypsin and peptides are analyzed by LC-MS/MS. Bait-specific interactors are identified by high heavy-to-light ratios, whereas nonspecific interactors appear in a ratio of near 1:1.

To summarize, CoIP in combination with mass spectrometry permits the analysis of protein complexes in an unbiased and hitherto unseen comprehensive manner. The use of SILAC labeling facilitates the quantification of MS data, thereby contributing to high reproducibility and reliability of the acquired data. However, proper controls are indispensable to avoid false-positive results and require careful considerations.

1.5. The Jurkat Cell Line

The choice of an experimental system is always a compromise of advantages and drawbacks. We decided to perform MS experiments in a cell line and not in primary cells for several reasons: First, our preferred strategy involved overexpression of an epitope-tagged protein in the cells (see CHAPTER 1.4.2). While transfection/transduction of primary T cells is, at least, challenging, effective protocols exist for most cell lines. Second, expansion and maintenance of stably transfected cells are much less time and money consuming for cell lines. Since we needed large amounts of cells for every single experiment, an easy access to high numbers of cells constituted an imported point for this consideration. Third, we wanted to take advantage of the high reproducibility of the SILAC approach (see CHAPTER 1.4.1), which from our experience is not compatible with primary T cells.

In detail, we chose to employ the Jurkat cell line for our purposes. This T cell line was established in 1977 from a 14 year old boy with acute T cell leukemia[201]. Since then, the Jurkat cell line has evolved to a widely used model system in T cell biology with more than 16.400 quotations in the PubMed database to date. However, the transformed nature of cell lines should always be considered when interpreting results[202]. Especially, functional findings from cell line experiments should be challenged for whether they prove true in primary cells or living organisms, too.

1.6. Goals of this Thesis

Signaling complexes integrate complex input signals on an individual cellular background to produce an adequate outcome. After an individual T cell binds its specific antigen via its T cell receptor, different signaling cascades act in concert to realize T cell activation. The goal of the present thesis was to advance the understanding of two important integrational processes in T cell receptor induced signaling. This concerned, first, how the cytoplasmic CBM-complex induces the activation of NFκB transcription factors in response to TCR ligation; and second, how the interactions of NFAT family members with other transcription factors influence NFAT activity and function.

Therefore, the CBM-complex and NFAT-containing protein complexes should be isolated and analyzed by mass spectrometry to identify yet unknown interaction partners. The approach for the analysis of both complexes was similar and consisted of:

(1) Establishment and evaluation of Jurkat cell lines that stably express epitope-tagged bait proteins (BCL10 for the CBM-complex, or NFAT isoforms)
(2) Optimization of protocols for the isolation of BCL10- or NFAT- containing protein complexes
(3) Isolation of BCL10- or NFAT-containing protein complexes by an optimized protocol
(4) Identification of so far unknown interaction partners by CoIP-mass spectrometry
(5) Verification of the interactions in follow-up experiments

Depending on the results, the significance of these interactions on the activation of T cells should be determined during further investigations.

The identification of so far unknown players and interdependencies in T cell receptor signaling will enhance our understanding of T cell biology. Ultimately, this may reveal new targets to modulate T cell activation and might inspire the development of more effective and specific treatment options for immunodeficiencies, autoimmune diseases or T cell derived lymphomas.

2. Material and Methods

2.1. Material

2.1.1. Cells

Jurkat E6 cells were purchased from ATCC and cultivated in complete RPMI. Cells were sub-cultured by dilution with new medium to not exceed a cell density of 10^6 cells/ml. For the isolation of Primary human $CD4^+$ T cells, PBMCs were isolated from healthy donor blood (Blutspende Charité Berlin) using Percoll density gradient and $CD4^+$ cells were positively selected by CD4 MACS beads. Purity was checked by CD4-staining followed by flow cytometry analysis and was between 95-99 %. Cells rested overnight in supplemented RPMI at 4 °C and were incubated for at least 1 hour at 37 °C before any experiment. HEK 293FT cells were cultured in complete DMEM and cells were sub-cultured by trypsination before reaching confluency.

2.1.2. SILAC Media

SILAC media were prepared from RPMI without arginine and lysine by addition of 10 % dialyzed FCS, 2 mM L-glutamine, 100 u/ml penicillin, 100 µg/ml streptomycin, 0.115 mM light (standard $^{12}C_6{}^{1}H_{14}{}^{14}N_4{}^{16}O_2$) or heavy arginine ($^{13}C_6{}^{1}H_{14}{}^{15}N_4{}^{16}O_2$) and 0.275 mM light (standard $^{12}C_6{}^{1}H_{14}{}^{14}N_2{}^{16}O_2$) or heavy lysine ($^{13}C_6{}^{1}H_{14}{}^{15}N_2{}^{16}O_2$), respectively. 2.6 mM of light L-proline were added to all media to avoid arginine-to-proline conversion[203].

2.1.3. Vectors and Constructs

The retroviral auxiliary plasmids pVSVG and pCPG, the pQCXIX vector and the pMIG vector were a kind gift from the research group of Andreas Radbruch, DRFZ, Berlin. Human *NFATC2* protein coding sequence was amplified from human cDNA. The sequence was verified by Sanger sequencing and corresponds to NM_173091.3 with the silent mutation A1723C. Human *NFATC1/αA* sequence (herein referred to as *NFATC1S* [short]) was sub-cloned from pREP-NFAT2, which was a gift from Anjana Rao (Addgene Plasmid #11788, sequence originates from Northrop *et al.*[125] and corresponds to NM_172390.2 with the mutation G1157A [P255Q] and the silent mutation C1980T). Human *NFATC1/*βC (NM_172387) sequence (herein referred to as *NFATC1L* [long]) was synthesized and sub-cloned by Genescript into the pUC57 vector.

The pMIG (pMSCV-IRES-GFP) vector backbone was prepared for the expression of proteins with an attached tag consisting of a BirA-biotin-ligase site (AVI-tag) and a Tobacco Etch virus cleavage (TEV) site either at the N-terminus (pMIG-N-AVITEV) or the C-terminus

(pMIG-C-AVITEV, FIGURE 6). The three NFAT sequences were sub-cloned into the N-AVITEV, the C-AVITEV, and into the core vector without any tag. *NFATC1L* was cloned into pMIG-N-AVI without initial methionine residue to avoid translation without tag.

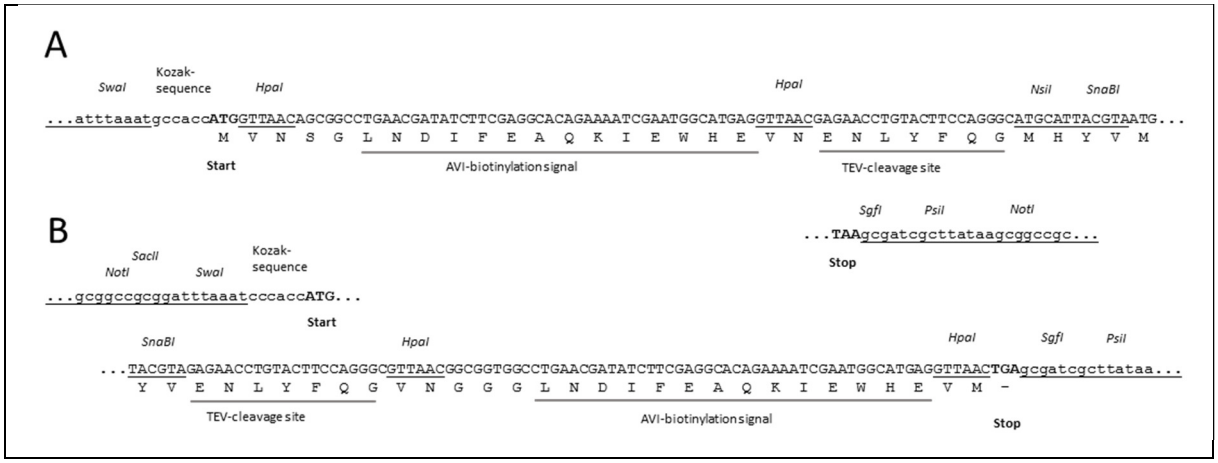

FIGURE 6. Cloning sites of pMIG-N-AVI (A) and pMIG-C-AVI (B). Both vectors allow the expression of AVITEV-Fusion proteins, if respective protein coding sequences are inserted in-frame. Start- and stop-codon are marked in bold letters. Selected restriction enzyme cleavage sites are underlined. The corresponding amino acid sequences of the tag are depicted below the nucleotide sequence.

The pBY2982, containing the E.*coli* biotin ligase *birA*-mCherry fusion protein sequence was a gift from Ralf Baumeister (Addgene plasmid # 23220)[204]. The construct was sub-cloned into the pMSCV vector without GFP. The human EF1a promoter was cloned prior to the BirA open reading frame to enhance expression, and the linker sequence between BirA and mCherry was exchanged for the P2A self-cleaving peptide[205] by overlap extension PCR.

The sequence of human *BCL10* open reading frame (NM003921.4) was obtained from Imagenes clone IOH29004-pdEYFP-C1amp and sub-cloned into the pEXPR-IBA 103 vector to obtain a BCL10 fusion protein with C-terminal StrepOne tag (BCL10-SO). This construct was further sub-cloned into the retroviral pMIG vector. To obtain higher expression rates, the sequence of the human EF1α promoter was amplified from pQCXIX vector and inserted in front of the open reading frame.

The CRISPR/Cas9 vector pSpCas9(BB)-2A-GFP (PX458) was a gift from Feng Zhang (Addgene plasmid # 48138)[206]. The plasmid allows expression of a self-cleaving Cas9-2A-GFP fusion protein under the control of the CBH promoter and expression of a gRNA under the control of the human U6 promoter. The CBH promoter was cut out and replaced by the hEF1α promoter to allow stronger transgene expression in Jurkat cells. Guide RNAs were designed by the help of the website http://crispr.mit.edu to target early exons expressed by all isoforms of the respective protein. To minimize off-target effects, only gRNAs that possess at least three

mismatches to known human DNA sequences were used. Two non-matching guanidine nucleotides were added to the 5' end of the guide to further enhance specificity[207]. Another online tool was used to identify potential highly active gRNA sequences[208]. The gRNA sequences were synthetized with overhangs and inserted into the vector as described by Ran *et al*[206]. The coding sequences of all used vector constructs were confirmed by Sanger sequencing.

TABLE 1. Target sequences of the used CRISPR gRNAs.

Targeted protein	gRNA sequence	target
NFATc2	ggGCCGCAGAAGTTTCTGAGCG	Sense strand of second exon
Ikaros	ggTCTGGAGTATCGCTTACAGG	Anti-sense strand of second exon

2.1.4. Chemicals, Including Peptides and Proteins

Designation (used concentration if applicable)	Distributor
Acetic acid	Biozym, Hamburg, Germany
Acetonitrile	Carl Roth, Karlsruhe, Germany
Agarose	Biozym, Hamburg, Germany
Ammonium hydrogen carbonate	Carl Roth, Karlsruhe, Germany
APS	Bio-Rad Laboratories, Hercules, USA
ATP	Thermo Fisher Scientific, Waltham, USA
Boric acid	Carl Roth, Karlsruhe, Germany
Bromophenol blue	Sigma-Aldrich, St. Louis, USA
$CaCl_2$	Carl Roth, Karlsruhe, Germany
CsA	AWD, Dresden, Germany
DAPI	Sigma-Aldrich, St. Louis, USA
Disodium phosphate	Carl Roth, Karlsruhe, Germany
DMSO	New England Biolabs, Ipswich, USA
DTT	Applichem, Darmstadt, Germany
EDTA	Merck-Millipore, Darmstadt, Germany
Ellegic Acid (10 µM)	Biaffin, Kassel, Germany
Ethanol	Merck-Millipore, Darmstadt, Germany
Glutathion (oxidized)	Applichem, Darmstadt, Germany
Glutathion (reduced)	Applichem, Darmstadt, Germany
Glycerol	Carl Roth, Karlsruhe, Germany
Glycine	Carl Roth, Karlsruhe, Germany
HEPES	Carl Roth, Karlsruhe, Germany
IGEPAL-Ca630	Sigma-Aldrich, St. Louis, USA
Ionomycin	Merck-Millipore, Darmstadt, Germany
Isopropanol	Carl Roth, Karlsruhe, Germany
JNK inhibitor VII (2 µM)	Biaffin, Kassel, Germany
Kenpaullone (2 µM)	Biaffin, Kassel, Germany
L-Arginine	Sigma-Aldrich, St. Louis, USA
L-Arginine $^{13}C_6$, $^{15}N_4$	Thermo Fisher Scientific, Waltham, USA

L-Lysine	Sigma-Aldrich, St. Louis, USA
L-Lysine-$^{13}C_6$,$^{15}N_2$	Cambridge Isotope Laboratories, Tewskbury, USA
L-Prolin	Applichem, Darmstadt, Germany
Methanol	Carl Roth, Karlsruhe, Germany
Monopotassium phosphate	Carl Roth, Karlsruhe, Germany
Orange-dye	Sigma-Aldrich, St. Louis, USA
PD169-316 (2 µM)	Biaffin, Kassel, Germany
PMA	Sigma-Aldrich, St. Louis, USA
Potassium bicarbonate	Merck-Millipore, Darmstadt, Germany
Potassium chloride	Carl Roth, Karlsruhe, Germany
SDS	Sigma-Aldrich, St. Louis, USA
Sodium chloride	Carl Roth, Karlsruhe, Germany
Sodium glycerol phosphate (1 µM)	Sigma-Aldrich, St. Louis, USA
Sodium *orto*-vanadate (1 µM)	Sigma-Aldrich, St. Louis, USA
Sodium pyrophosphate (2.5 µM)	Sigma-Aldrich, St. Louis, USA
Strep-tag® II peptide	IBA GmbH, Göttingen, Germany
TEMED	Sigma-Aldrich, St. Louis, USA
Thio-urea	Sigma-Aldrich, St. Louis, USA
Trifluoroacetic acid	Carl Roth, Karlsruhe, Germany
Tris	Carl Roth, Karlsruhe, Germany
Triton X-100	Sigma-Aldrich, St. Louis, USA
Tween 20	Sigma-Aldrich, St. Louis, USA
Urea	Sigma-Aldrich, St. Louis, USA
β-Mercaptoethanol	Thermo Fisher Scientific, Waltham, USA

2.1.5. Pre-made Buffers, Solutions and Stocks

Designation	Distributor
2 X YT medium	Carl Roth, Karlsruhe, Germany
Acrylamide/Bis-Acrylamide (Rotiphorese)	Carl Roth, Karlsruhe, Germany
Ampicillin solution	Bioline, Luckenwalde, Germany
BSA 10 mM	New England Biolabs, Ipswich, USA
CD4 MACS beads	Miltenyi Biotec, Bergisch Gladbach, Germany
Complete protease inhibitor	Roche, Rotkreuz, Switzerland
Cutsmart buffer	New England Biolabs, Ipswich, USA
Dialyzed FCS	Thermo Fisher Scientific, Waltham, USA
DMEM with Glutamax (GIBCO)	Thermo Fisher Scientific, Waltham, USA
DNA loading buffer	Thermo Fisher Scientific, Waltham, USA
dNTP solution mix	New England Biolabs, Ipswich, USA
FastDigest buffer	Thermo Fisher Scientific, Waltham, USA
Fetal calf serum (Biochrom), LOT 0587B	Merck-Millipore, Darmstadt, Germany
Fixation/permeabilization buffer	eBioscience, San Diego, USA
GelRed nucleic acid gel stain 10.000x	Biotium, Hayward, USA
Genruler DNA Ladder Mix	Life Technologies, Carlsbad, USA
LB-medium capsules	MP Biomedicals, Santa Ana, USA
NEB buffer 1-4	New England Biolabs, Ipswich, USA
Non-essential amino acids 100x	Sigma-Aldrich, St. Louis, USA
Odyssey molecular weight marker	LI-COR Bioscience, Lincoln, USA
Odyssey non-vertebrate blocking buffer	LI-COR Bioscience, Lincoln, USA

Pacific orange-NHS live/dead stain	Sigma-Aldrich, St. Louis, USA
Penicillin/Streptomycin 100x	Life Technologies, Carlsbad, USA
Percoll	VWR International; Radnor, USA
Permeabilization buffer	eBioscience, San Diego, USA
Protein A agarose	Thermo Fisher Scientific, Waltham, USA
Protein G µMACS beads	Miltenyi Biotec, Bergisch Gladbach, Germany
Protein G agarose	Thermo Fisher Scientific, Waltham, USA
Pyruvate	GE Healthcare, Little Chalfont, UK
RPMI Media for SILAC (Perbio)	Thermo Fisher Scientific, Waltham, USA
RPMI with Glutamax (GIBCO)	Thermo Fisher Scientific, Waltham, USA
Strep-Tactin Superflow	IBA GmbH, Göttingen, Germany
Streptavidin agarose	Sigma-Aldrich, St. Louis, USA
T cell activator beads DYNA	Life Technologies, Carlsbad, USA

2.1.6. Home-made Buffers and Media

Buffer	Composition
2x HBS	274 mM NaCl 10 mM KCl 1.4 mM Na_2PO_4 42 mM HEPES pH 7.05
ABC buffer	50 mM NH_4HCO_3 in 50 % (V/V) ACN pH 7.8
Ammonium hydrogen carbonate buffer	50 mM NH_4HCO_3 pH 7.8
Blotting buffer	16 mM tris-HCl 120 mM glycine 10 % (v/v) methanol
Cytolysis buffer (NFAT-CoIP)	25 mM HEPES 25 mM NaCl 2 mM EDTA 0.1 % (V/V) Tween 20 pH 7.6
Dilution buffer (NFAT-CoIP)	25 mM HEPES pH 7.6
DMEM medium, complete	90 % (V/V) DMEM with Glutamax 10% (V/V) FCS 100 u/ml penicillin 100 µg/ml streptomycin 1x non-essential amino acids 1 mM sodium pyruvate
Elution buffer EB-1 (BCL10-CoIP)	20 mM tris/HCl 4 mM EDTA 0.01 % (W/V) SDS 0.5 mM strep-tag peptide (SAWSHPQFEK) pH 8.0
Laemmli buffer, 6x, reducing	12 % (W/V) SDS 60 % (V/V) glycerol 350 mM tris 0.6 M DTT 0.02 % (W/V) bromophenol blue pH 6.8
Lysis buffer LB-1 (BCL-10 CoIP)	200 mM tris/HCl 150 mM NaCl 1 % (V/V) Igepal-Ca630 1 % (V/V) Triton X-100 pH 8.0

Nucleolysis buffer LB-2 (NFAT-CoIP)	25 mM 500 mM 0.5 % (V/V) pH	HEPES NaCl Tween20 7.6
PBS	137 mM 2.7 mM 4.3 mM 1.4 mM pH	NaCl KCl Na_2HPO_4 KH_2PO_4 7.4
PBS/BSA	 0,5% (W/V) pH	PBS BSA 7.4
RPMI medium, complete	90 % (V/V) 10% (V/V) 100 u/ml 100 µg/ml 10 µg/ml	RPMI with Glutamax FCS penicillin streptomycin β-mercaptoethanol.
SDS-PAGE buffer	25 mM 190 mM 10 % (W/V)	tris-HCl glycine SDS
Separating gel buffer	1.5 M pH	tris-HCl 8.8
SILAC medium, complete,	90 % (V/V) 10% (V/V) 100 u/ml 100 µg/ml 0.115 mM 0.275 mM 2.6 mM	RPMI for SILAC w/o lysine and arginine dialyzed FCS penicillin streptomycin arginine (light or heavy) lysine (light or heavy) proline (light)
Stacking gel buffer	0.5 M pH	tris-HCl 6.8
TAE	20 mM 1 mM 0.11 % (V/V)	tris-HCl Titriplex III acetic acid
TEV RB buffer	50 mM 5 mM 3 mM 0.3 mM 0.1 % (V/V) pH	tris/ HCl citrate glutathione oxidized glutathione Igepal-Ca630 8.0
Urea buffer	6 M 2 M 20 mM pH	urea thio urea HEPES 8.0
Wash buffer WBU-1 (BCL10-CoIP)	20 mM pH	tris/HCl 8.0
Wash buffer WBU-2 (NFAT-CoIP)	25 mM 150 mM 0.1 % (V/V) pH	HEPES NaCl Igepal-Ca630 7.6

2.1.7. Enzymes

Designation	Distributor
DNase 2x10.000 U recombinant	Roche, Rotkreuz, Switzerland
MobiTEV protease. recombinant	MoBiTec GmbH, Göttingen, Germany
Phusion	New England Biolabs, Ipswich, USA
T4 ligase 1000 U	Thermo Fisher Scientific, Waltham, USA
T4 polynucleotide kinase 500 U	Thermo Fisher Scientific, Waltham, USA
Trypsin	Promega, Madison, USA

2.1.8. Kits

Designation	Distributor
µMACS streptavidin kit	Miltenyi Biotec, Bergisch Gladbach, Germany
BCA protein assay	Thermo Fisher Scientific, Waltham, USA
Cell Line Nucleofector kit V	Lonza, Basel, Switzerland
DNeasy tissue kit (50)	Qiagen, Hilden, Germany
Duolink PLA starter kit mouse-rabbit, red	Sigma-Aldrich, St. Louis, USA
NucleoBond Xtra Midi Plus EF (50)	Machery Nagel, Düren, Germany
NucleoSpin Plasmid Easy	Machery Nagel, Düren, Germany
QIAquick gel extraction kit (50)	Qiagen, Hilden, Germany
RNase-free DNase set (50)	Qiagen, Hilden, Germany
SuperScript first-strand synthesis system for RT	Life Technologies, Carlsbad, USA

2.1.9. Antibodies

Specificity	Distributer	Clone/ Batch	Species	Clonality	Dilution
BCL10	Santa Cruz, Dallas, USA	331.1	mouse	monoclonal	WB: 1:200
BCL10	Santa Cruz, Dallas, USA	H197	rabbit	polyclonal	WB: 1:200
BCL10	Santa Cruz, Dallas, USA	C-17	goat	polyclonal	WB: 1:200
Calcineurin	Becton Dickinson, Franklin Lakes, USA	G182-1847	mouse	monoclonal	WB: 1:500
CARMA1	New England Biolabs, Ipswich, USA	1D12	rabbit	monoclonal	WB: 1:1000
CHEK1	Acris, Herford, Germany	AM20031AF-N	mouse	monoclonal	WB: 1:1000
CIAP 1/2	R&D Systems, Minneapolis, USA	315301	mouse	monoclonal	WB: 1:500
CREB1	New England Biolabs, Ipswich, USA	48H2	rabbit	monoclonal	WB: 1:1000
EP300	Santa Cruz, Dallas, USA	C20	rabbit	polyclonal	WB: 1:200
Flag	New England Biolabs, Ipswich, USA		rabbit	polyclonal	WB: 1:1000
Flag-tag	Sigma-Aldrich, St. Louis, USA	F3165	mouse	monoclonal	WB: 1:1000
FOS	New England Biolabs, Ipswich, USA	9F6	rabbit	monoclonal	WB: 1:500
GFP, coupled to IR DYE700	Rockland, Limerick, USA	600-130-215	goat	polyclonal	WB: 1:10000
GSK3β	New England Biolabs, Ipswich, USA		rabbit	polyclonal	WB: 1:1000
Helios	Santa Cruz, Dallas, USA	M20	goat	polyclonal	WB: 1:500
Ikaros	Santa Cruz, Dallas, USA	H100-x	rabbit	polyclonal	WB: 1:2000
IκBα	New England Biolabs, Ipswich, USA	44D4	rabbit	monoclonal	WB: 1:1000
IκBα(pSer)	New England Biolabs, Ipswich, USA	14D4	rabbit	monoclonal	WB: 1:1000
JUN	New England Biolabs, Ipswich, USA	60A8	rabbit	monoclonal	WB: 1:500
JUNB	New England Biolabs, Ipswich, USA	C37F9	rabbit	monoclonal	WB: 1:500
LAMIN-B	Santa Cruz, Dallas, USA	sc-6217	goat	polyclonal	WB: 1:500
MALT	Abcam, Cambridge, UK	EP603Y	rabbit	monoclonal	WB: 1:1000
MIB2	Bethyl Laboratories, Montgomery,	A301-414A	rabbit	polyclonal	WB: 1:2000
NFATc1	Becton Dickinson, Franklin Lakes, USA	7A6	mouse	monoclonal	WB: 1:500
NFATc2	Becton Dickinson, Franklin Lakes, USA	NFAT1	mouse	monoclonal	PLA: 1:200
NFATc2	DRFZ		rabbit	polyclonal	WB: 1:500
NFκB p105/50	Abcam, Cambridge, UK	E381	rabbit	monoclonal	WB: 1:1000
NFκB p65	Abcam, Cambridge, UK	E379	rabbit	monoclonal	WB: 1:10000

NFκB p65	New England Biolabs, Ipswich, USA	93H1	rabbit	monoclonal	WB: 1:1000
RBCK1	Antikörper Online	ABIN310424	rabbit	polyclonal	WB: 1:1000
RNF31	Abcam, Cambridge, UK	ab85294	rabbit	polyclonal	WB: 1:250
RPTOR	New England Biolabs, Ipswich, USA	2280	rabbit	monoclonal	WB: 1:500
RUNX1	Santa Cruz, Dallas, USA	C19	goat	polyclonal	WB: 1:200
SATB1	Becton Dickinson, Franklin Lakes, USA	14/SATB1	mouse	monoclonal	WB: 1:1000
SCAI	New England Biolabs, Ipswich, USA	12892	rabbit	monoclonal	WB: 1:500
StrepMAB-	Biotrend, Köln, Germany	2-1517-001	mouse	monoclonal	IP: 10 µg/ml
Strep-tag	IBA GmbH, Göttingen, Germany		mouse	monoclonal	WB: 1:200
TRAF2	Santa Cruz, Dallas, USA	N19	rabbit	polyclonal	WB: 1:200
TRAF2	Abnova	PAB6989	goat	polyclonal	WB: 1:1000
WDR48	Abcam, Cambridge, UK	ab122473	rabbit	polyclonal	WB: 1:500
α-TUBULIN	New England Biolabs, Ipswich, USA	DM1a	mouse	monoclonal	WB: 1:1000
β-ACTIN	Santa Cruz, Dallas, USA	C4	mouse	monoclonal	WB: 1:10000

2.1.10. Disposables

Designation	Distributor
Amicon Ultra-0.5 Centrifugal Filter	Merck-Millipore, Darmstadt, Germany
Amicon Ultra-4 Centrifugal Filter Unit	Merck-Millipore, Darmstadt, Germany
BA85 Protran 0.45 µm blotting membrane	VWR International, Radnor, USA
Chromatography paper 3MM CHR.150x200mm	VWR International, Radnor, USA
Cover slip 24x60 mm	Carl Roth, Karlsruhe, Germany
Culture-inserts Stem Cell	Ibidi, München, Germany
Glass slide Menzel Gläser, Superfrost Ultra Plus	Thermo Fisher Scientific, Waltham, USA
Gradient SDS PAGE 4-20 %	Biorad, Hercules, USA
Multi-8 Columns molecular (12×8)	Miltenyi Biotec, Bergisch Gladbach, Germany
Sterile filters, 45 µM and 25 µM	VWR International, Radnor, USA

2.1.11. Hardware

Designation	Distributor	Purpose
BD FACSAria™ II Cell Sorter	BD Biosciences, San Jose, USA	fluorescence activated cell sorting
Biorevo BZ-9000	Keyence	fluorescence imaging
LI-COR Scanner	LI-COR Bioscience, Lincoln, USA	western blot detection
MACSQuant® VYB	Miltenyi Biotec, Bergisch Gladbach, Germany	FACS analysis
Mini Trans-Blot cell	Bio-Rad Laboratories, Hercules, USA	western blot
Minigel-Twin	Biometra, Göttingen, Germany	SDS-PAGE
NanoDrop 2000 UV-Vis spectrophotometer	Thermo Fisher Scientific, Waltham, USA	DNA and RNA Quantification
Nucleofector IIb Device	Lonza, Basel, Switzerland	transfection
PerfectBlue Maxi Gel System M	Peqlab, Erlangen, Germany	agarose gel electrophoresis
PTC 200 Thermal Gradient Cycler	MJ Research, St. Bruno, Canada	thermocycler, PCR
Sigma 4K15C centrifuge	Qiagen, Hilden, Germany	centrifugation
SpectraMax Plus 384	Molecular Devices, Sunnyvale, USA	microplate reader
Thermomixer compact	Eppendorf, Hamburg, Germany	block heater
Universal Hood II Gel Imager	Bio-Rad Laboratories, Hercules, USA	gel documentation

MultiMacs M96 Separator	Miltenyi Biotec, Bergisch Gladbach, Germany	CoIP (BCL10)
MacsMix	Miltenyi Biotec, Bergisch Gladbach, Germany	CoIP

2.1.12. Software

Designation	Author/Distributor
ApE (A plasmid Editor) 2.0.45 M	Wayne Davis
cobindR (Bioconductor)	M. Benary *et al*.
FlowJo 7.6.5	Tree Star Inc., Ashland, USA
GraphPad Prism 5.02	GraphPad Software Inc., La Jolla, USA
Image Lab 5.1	Bio-Rad Laboratories, Hercules, USA
MxPro3005P 4.10 Agilent Technologies	Santa Clara, USA
Odyssey Application Software 2.1	LI-COR Bioscience, Lincoln, USA
oPOSSUM 3.0	W.W. Wassermann *et al.*

2.2. Methods

2.2.1. Methods in Cell Biology

2.2.1.1. Cell Stimulation

For chemical stimulation, cells were incubated in RPMI that was supplemented with 1 mM $CaCl_2$ and PMA and ionomycin were added directly to the medium. For stimulation with CD3/28 specific antibodies, Jurkat cells were resuspended at a density of 10^7 cells/ml and incubated for 30 min with 5 µg/ml anti-CD3 antibody and 10 µg/ml anti-CD28 antibody for 30 min on ice. 20 µg/ml anti-mouse IgG were added to crosslink the antibodies and cells were incubated for further 15 min on ice. Cells were stimulated for the designated time by incubation at 37 °C in a water bath. Primary T cells were stimulated with T cell activator beads that were added to the cells in a bead-to-cell ratio of 1:1.

2.2.1.2. SILAC Labeling of Jurkat Cells

For SILAC experiments, cells grew in heavy or light SILAC medium for at least 10 days. On day zero, cells were washed with PBS and put into the respective SILAC medium. On day two, cells were again pelleted, washed with PBS and put into new medium. Cells were again put in new medium on day 4 or 5. Subsequently, cells were expanded and new medium was added to the existing medium to dilute the cells to the intended cell density

2.2.1.3. Nucleofection

Jurkat cells were transfected by nucleofection using an AMAXA nucelofector IIb device and cell line nucleofection kit V. One million cells were spun down and resuspended in nucleofection mix and 2-5 µg respective vector DNA. Cells were nucleofected by using program X-001 and diluted in 4 ml cell culture medium.

2.2.1.4. Virus Production

For production of retrovirus, $4*10^6$ HEK293FT cells were seeded in 10 ml complete DMEM onto a 10 cm culture dish. The next day, cells were transfected with pCGP (10 µg), pVSVG (5 µg) and a plasmid of interest (20 µg) by calcium precipitation. Briefly, the plasmids were diluted in 500 µl *aqua dest.* containing 210 mM $CaCl_2$. 500 µl 2xHBS were added drop-wise while mixing the solution with air bubbles using a pipette boy. After further 20 s mixing and 60 s incubation, the mixture was added drop-wise onto the cultured cells, and cells were incubated for 5 h in an incubator before medium was exchanged to complete DMEM supplemented with 20 mM HEPES, pH 7.05. The virus supernatant was harvested after 24 h, passed through a 45 nm filter, and if necessary, stored in aliquots at -80 °C.

2.2.1.5. Establishment of Stably Transduced Cell Lines by Retroviral Transduction

Cells were spun in a culture plate, resuspended in viral supernatant and spun for 90 min at 32 °C and 1000 g. Cells were incubated for at least 2 h or overnight in the virus supernatant. Afterwards, the supernatant was removed; the cells were washed two times and were resuspended in culture medium. Marker gene expression was checked 2 days after transfection. The cells were sorted (two to three times) on a FACS for high expression of fluorescence surrogate marker and subsequently expanded for several days. The purity of marker positive cells was typically >99 %. For cells stably expressing two transgenes with different surrogate markers, sorted cells were subject to a second round of transduction and sorted for marker double positive cells. Transgene expression was monitored by western blot analysis. Aliquots of the cells were frozen in 90 % FCS/10 % DMSO (V/V) in liquid nitrogen.

2.2.1.6. Establishment of Stable Transduced Cell Lines by Nucleofection/Selection

Cells were transfected with linearized plasmids by nucleofection as described in chapter 2.2.1.1 and cultivated for at least seven days. After that time, only cells that have integrated the transfected DNA into the host genome still express the surrogate fluorescence marker. Thus, stably transfected, fluorescence positive cells (>1 %) were sorted on a FACS, expanded and sorted again to increase purity. Transgene expression was monitored by western blot analysis. Aliquots of the cells were frozen in 90 % FCS/10 % DMSO (V/V) in liquid nitrogen.

2.2.1.7. Establishment of Knock-out Cell Lines by CRISPR/CAS9

Jurkat cells were transfected with 2 µg of the CRISPR/Cas9 plasmids bearing the target gene specific gRNA by nucleofection. One day post transfection, transfected cells were sorted for GFP expression by FACS. Two days later, single cells were distributed into individual wells

of a 96-well plate by a FACS machine. Single cell clones were expanded and screened for phenotypic knock-out by western blot analysis. Aliquots of the cells were frozen in 90 % FCS/10 % DMSO (V/V) in liquid nitrogen.

2.2.1.8. Proximity Ligation Assay

During the Proximity Ligation Assay (PLA), the recognition of two proximate proteins by differently labeled antibodies results in signals that can be detected by fluorescence microscopy (FIGURE 7). The cells are probed with two antibodies (primary or secondary) that contain short oligo-nucleotides. In the case that both antibodies bind in close proximity, they can be ligated to an added DNA oligo-nucleotide with complementary sequences to both probes, thus forming a circular DNA molecule. Subsequently, rolling circle amplification is used to amplify this circular DNA. The amplified DNA is still attached to the antibody and as such to the interacting molecules. Detection is done via fluorophore-coupled complementary DNA oligo-nucleotides that bind to the amplified DNA sequence. Owing to the strong signal amplification, a single ligation of the proximity probes results in a detectable signal, and each signal refers to a single interaction.

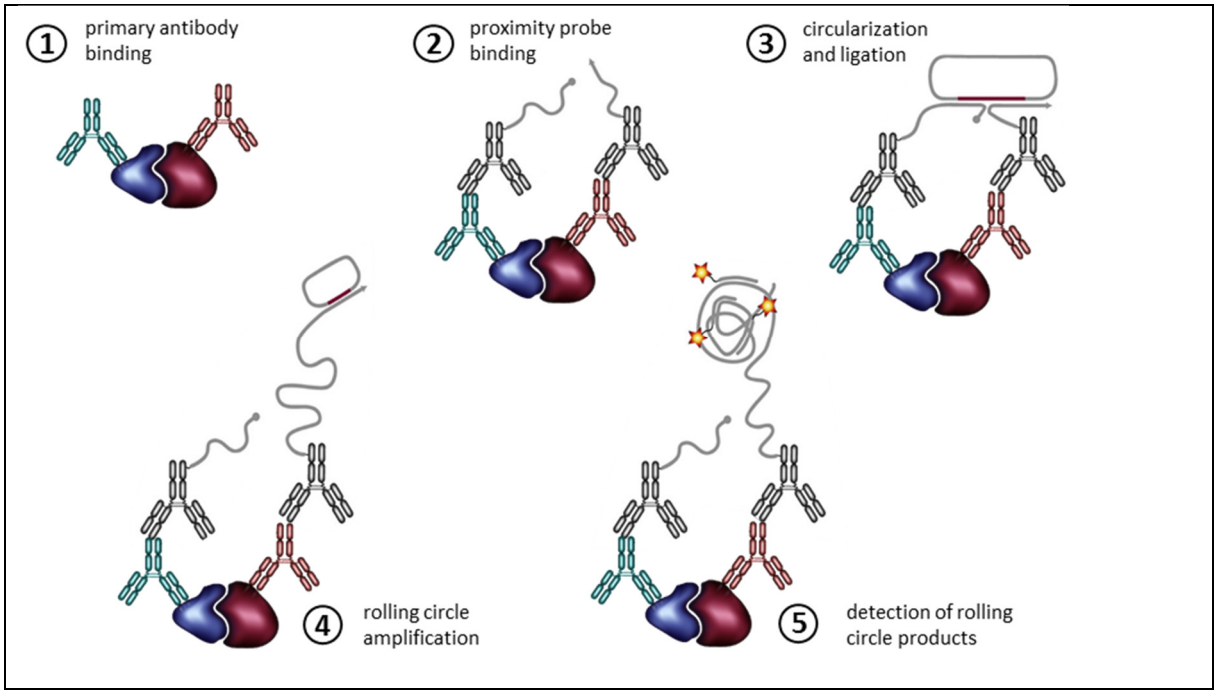

FIGURE 7. Principle of proximity ligation assay. Primary antibodies raised in different species bind to their target proteins (1) and subsequently are recognized by the proximity probes, which consist of oligo-nucleotide coupled secondary antibodies (2). If the probes bind in close proximity, they can be ligated to a DNA oligo-nucleotide with complementary sequences to both probes, forming a circular DNA molecule (3) which is amplified by rolling circle amplification (4). The amplified DNA consists of multiple sequence copies. It can be visualized by fluorophore-coupled complementary oligo-nucleotides. Image adopted from Söderberg *et al.*[209]

The proximity ligation protocol was adopted from Leuchowius *et al.*[210], using reagents from the Duolink Starter Kit (TABLE 2). Fixation and permeabilization steps were done in 1.5 ml microtubes, while all further steps were executed in a 96-well micro titer plate with conic bottom. Jurkat cells were stimulated with 20 µg/ml PMA and 1000 µg/ml ionomycin for 60 min, washed in PBS and resuspended in fixation/permeabilization buffer at a concentration of $5*10^6$ cells/ml. After 2 h of incubation at 4 °C, the cells were washed with PBS/BSA and permeabilization buffer, followed by incubation with the primary antibodies overnight at 4 °C in 100 µl permeabilization buffer. Primary human $CD4^+$ T cells were stimulated with 20 µg/ml PMA and 1000 µg/ml or with human T cell activator beads at a bead-to-cell ratio of 1:1 for 60 min. Beads and cells were separated with a magnet. The cells were incubated with Pacific-Orange-NHS live/dead stain for 20 min on ice, and washed two times with PBS. The cells were resuspended in fixation/permeabilization buffer at a concentration of $2*10^7$ cells/ml. After 2 h of incubation at 4 °C, the cells were washed with PBS/BSA and sorted on a FACS for Pacific-Orange negative cells to exclude cells that were dead before fixation. The cells were washed with PBS/BSA and permeabilization buffer and $1*10^6$ cells were incubated with primary antibody overnight at 4 °C in 100 µl permeabilization buffer.

Next day, the cells were washed two times with PBS/BSA and one time with permeabilization buffer. An aliquot for the staining control was taken at this step, incubated with fluorophore coupled secondary antibody for 1 h at 4 °C, washed three times with PBS/BSA and prepared for imaging the same way as the PLA samples. The remaining cells were incubated with 23 µL PLA probe mix and incubated for 1 h at 37 °C and 95 rpm in a shaking incubator. The cells were washed four times with wash buffer A and incubated with 23 µl ligation mix for 30 min at 37 °C and 95 rpm, washed twice with wash buffer A and incubated with 23 µl amplification mix for 2 h at 37 °C and 95 rpm. Then, the cells were washed four times in wash buffer B and one time in 0.01 x wash buffer B.

The cells were prepared for imaging by an adjusted cyto-spin protocol. The cell concentration was adjusted to a maximum of $5*10^5$ cells/ml. 10 µl of cell suspension was given onto a latex culture insert on a glass slide. The slides were spun for 3 min with 300 g at 20 °C. The supernatant was removed and PLA mounting medium containing DAPI was added onto the cells before topping with a coverslip. Image acquisition was done on a Keyence Biorevo. Images from Jurkat cells for PLA signal quantification were acquired with 20x objective, all other images with 100-x objective using oil immersion. PLA signals were acquired in the TritC channel. PLA signals were quantified using BlobFinder[211]. All parameters were adjusted to the image properties, but remained unchanged within one experiment.

The following cells were manually excluded from the statistical analysis: Jurkat cells with a nuclear size of less than 400 pixels or more than 1000 pixels, CD4+ T cells with a nuclear size of less than 3500 or more than 10000 pixel, cells that are cut by the image boarder, other cells that were incorrectly recognized by the program, as judged by visual inspection. Significance was probed using Kruskal-Wallis test, because the data were not normal distributed.

TABLE 2. Reaction conditions during PLA.

PLA probe mix (25 µl)	Ligation mix (25 µl)
5 µl PLA probe PLUS	5 µl 5x ligation mix
5 µl PLA probe MINUS	19.45 µl H_2O
15 µl permeabilization buffer	0.55 µl T4 ligase
2.5 µg/ml sonicated salmon sperm DNA	
Amplification mix (25 µl)	
5 µl 5x amplification mix	
19.73 µl H_2O	
0.27 µl T4 ligase	

2.2.2. Methods in Protein Biochemistry

2.2.2.1. SDS-PAGE/ Western Blot

For western blot analysis of complete cell extracts, cells were lysed in 1x lysis buffer LB-1 supplemented with protease inhibitors, incubated on ice for 10 min and sonicated. The lysates were cleared by centrifugation. All samples were supplemented with 1x reducing Laemmli buffer. Proteins were separated according to their size on a discontinuous SDS-PAGE, with an acrylamide/bis-acrylamide concentration of 4 % in the stacking gel and 7.5 % to 16 % in the resolving gel. The SDS-PAGE was either stained in Commassie-Brilliant-Blue staining solution and de-stained with 10 % (V/V) acetic acid/50 % (V/V) methanol, or subjected to western blotting. For the latter, the gel was put in a sandwich consisting of a sponge, two layers of filter paper, the SDS-PAGE gel, nitrocellulose membrane, two layers of filter paper and a sponge. Proteins were transferred to the membrane by tank blotting in a chilled Biorad Mini Transblot Cell, using blotting buffer with 10 % (V/V) methanol. Typically, blotting lasted 60 min at a constant voltage of 100 V while stirring. The membrane was blocked for at least 30 min in blocking solution and incubated with primary antibodies for 1.5 h at room temperature or overnight at 4 °C on a rocking platform. The membrane was washed three times for 5 min with PBS-T, incubated for further 45 min with fluorophore coupled secondary antibody and washed again three times. Imaging was done on a Licor Odyssey machine. Subsequently, further proteins were detected with analogue incubation in primary and

subsequently secondary antibody dilutions. If necessary, fluorophores were quenched by incubation of the membrane with 1x striping buffer. GFP was detected with a fluorophore-coupled primary antibody and biotin was detected with a fluorophore-coupled streptavidin conjugate.

2.2.2.2. Co-Immunopurification

BCL10 Experiments

For co-immunopurification of BCL10-SO-complexes, stably transfected Jurkat cells were stimulated for the indicated time with PMA (300 ng/ml) and ionomycin (200 ng/ml). The cells immediately were put on ice, spun down, resuspended in PBS and spun down again. The cell pellets were resuspended in 200 µl lysis buffer LB-1 supplemented with 1x complete protease and phosphatase inhibitors, incubated on ice for 30 min, sonicated in an ultra-sound bath for 20 s at 100 % intensity and incubated again for 20 min on ice. The resulting lysates were cleared by centrifugation for 10 min at 17000 g. 1 µg of biotinylated anti-strep-tag antibody was added to each 200 µl of lysate followed by overnight incubation at 4 °C in a MacsMix device. Next day, 50 µl of magnetic streptavidin-coupled microbeads were added, followed by 1 h incubation at 4 °C in a MacsMix device. For the collection of the beads, the suspensions were given onto µMacs columns, which were put in a magnet separator and equilibrated with 100 µl biotin equilibration buffer (protein) and 200 µl lysis buffer LB-1. The columns were washed twice with 200 µl lysis buffer LB-1 and three times with 100 µl washing buffer WBU-1. The columns were incubated in 20 µl elution buffer EB-1 (pre-warmed to 95 °C) for 5 min and proteins were eluted with 4x 20 µl of hot elution buffer EB-1 in intervals of 3 min. The eluates were combined. BCL10 complexes from primary cells were isolated by an analogue protocol. For this purpose, cell lysates were incubated with a mouse-monoclonal antibody against human BCL10 (5 µg/ml) and immuncomplexes were collected using magnetic protein-G beads.

For MS analysis, eluates from six to eight samples were pooled and buffer was exchanged to urea buffer in an Amicon centrifugal filter with a cutoff of 4 kDa. To eliminate SDS and strep-peptide, subsequent rounds of concentration/dilution were executed to reach a final dilution factor of 3000 in a volume of 60 µl. Tryptic digestion, two-dimensional LC-MS/MS measurement and data analysis were done in the laboratory of Prof. Dr. Eberhard Krause at the Leibnitz Institut für Molekulare Pharmazie in Berlin-Buch as described. See section 2.2.2.3 for further details.

NFAT Experiments

For co-immunopurification of NFAT containing complexes, stably transfected Jurkat cells were stimulated for the indicated time with PMA (20 ng/ml) and ionomycin (1000 ng/ml). The cells were then put on ice immediately, spun down, resuspended in PBS and spun down again. $3*10^7$ cells per 1.5 ml tube were resuspended in hypotonic cytolysis buffer and put on ice for 10 min. The suspension was spun for 1 min at 8000 g and the supernatant containing the cytoplasmic fraction was discarded. High salt nucleolysis buffer LB-2 (40-60 µl) was added to the pelleted nuclei and the suspension was incubated on ice for 30 min, subjected to ultra sound (4 times 10 s at 25 % intensity) and incubated again on ice for 30 min. The nuclear lysates were diluted with 2 volumes of dilution buffer and cleared by 10 min centrifugation at 13000 g. Supernatants were collected and combined.

To isolate the NFAT containing complexes, equilibrated streptavidin agarose beads were added and the suspension was incubated at 4 °C while rotating in a MacsMix device. Beads were pelleted by centrifugation and washed two times with washing buffer WBU-2 and four times in TEV reaction buffer for subsequent elution by TEV protease; or washed two times in LB-2 and four times with WBU-2 prior to elution by Laemmli buffer.

Bound proteins were eluted either by incubation in 2x reducing Laemmli buffer for 10 min at 95 °C or by incubation in TEV protease buffer containing TEV for 2 h at room temperature. For the MS experiments, the procedure in general followed the same protocol. For each experiment, 200 – 300 Mio of respective cells were stimulated for 2 h with PMA and ionomycin; nuclear extracts were prepared, and protein concentration was determined by BCA assay. For each sample pair, equal amounts and concentrations of proteins were incubated with streptavidin coated agarose beads. Beads from corresponding pairs of heavy and light cells were mixed after the first washing step.

The TEV eluates were supplemented with 1/6 6x Laemmli buffer. 20 µl of the sample were separated on a gradient SDS Page (4-20 %) for 1 hour at constant voltage of 200 V. The gel was fixed, stained by Commassie staining overnight and de-stained for 5 h. Each lane was cut by hand into 16 slices. The slices were washed 1x in 200 µl ABC buffer for 10 min, 1x in 200 µl ammonium hydrogen carbonate buffer for 10 min, 1 time in 50 µl ACN for 3 min, and tried in a vacuum centrifuge. For tryptic digestion, 0.5 µl trypsin in 35 µl ABC were added to each slice. The digest was performed overnight at 37 °C in a covered thermomixer. Next day, 35 µl of stop solution were added and the supernatant was collected. The slices were shrunk in 30 µl ACN for 5 min at RT and the supernatant was collected. The dilution agent of the combined supernatants was removed by centrifugation in a vacuum centrifuge at 50 °C, the

precipitate was dissolved in 5 % ACN/0.1 % TFA (V/V) and put into an ultra sound bath for 3 min. The samples were stored at -20 °C until they were measured.

2.2.2.3. MS Measurement

After in-gel tryptic digestion or in solution digestion of the proteins, the detection and analysis of the complex peptide mixtures was done by nanoLC-ESI-MS/MS. Measurement and data analysis was done in the laboratory of Prof. Dr. Eberhard Krause at the Leibnitz Institut für Molekulare Pharmazie in Berlin-Buch. The experimental procedures and data processing were executed as decribed[212]. In brief, the peptides were desalted in a trap column and separated on a C18 nanoLC in an Eksigent 2D Nanoflow LC-System that was coupled to a LTQ-orbitrap XL-mass spectrometer via a nanospray source. Mass spectra were acquired in a data-dependent mode with one MS survey scan in the orbitrap and MS/MS scans of the five most intense precursor ions in the LTQ. The MS survey range was m/z 350-1500. Identification and quantitation of proteins was done by the open source software MaxQuant. In brief, generated peak lists were submitted to the MASCOT search engine and searched against a human protein database. For identification, at least two peptides, including one unique peptide, was obligatory.

2.2.3. Bioinformatic Methods

2.2.3.1. Identification of Peak Regions from Public ChIP-Seq Datasets

Public ChIP-Seq data were re-analyzed by the company Microdiscovery, Berlin. In brief, experiments were downloaded from Gene Expression Omnibus (GEO Accession GSM157075) with corresponding controls. Bases with quality below 20 were trimmed and only reads with existing barcodes, as defined by the original authors, were used[213]. Remaining reads were mapped against MM10 using Bowtie with parameters: -v, --best, --strata and -C if color-coded. Mapped reads were filtered for duplicates using Picards Mark Duplicates function. Peaks were identified using MACS2 with default options for mouse genomes.

2.2.3.2. Identification of Transcription Factor Binding Site Enrichment

The extracted peak regions were employed for the identification of enriched transcription factor binding sites. Analyses were done by Fridolin Gross, Humboldt University, Berlin, using the web-based program oPOSSUM (‘single site analysis’ and ‘sequence based’). A GC-matched background was generated by the help of the tool ‘background/foreground GC composition matching’ from the same website. The background was modulated to match the length distribution of the input sequences. The background was increased by a factor of three to increase significance. Binding motifs were obtained from the public JASPAR database (jaspar.binf.ku.dk, JASPAR core vertebrate profile) and additional motifs from TRANSFAC

(genexplain.com/transfac-1) and Swissregulon (www.swissregulon.unibas.ch). The motif V$NFAT_Q4_01_NFAT (TRANSFAC) was used as the NFAT binding motif.

2.2.3.3. Identification of Pairs of Transcription Factor Binding Sites

Analysis was done by Fridolin Gross, Humboldt University, Berlin, using the BioconducteR package cobindR[214]. As before, the genomic regions from 2.2.3.1 were used as input data.

3. Results

3.1. Characterization of the CBM-complex by Mass Spectrometry

In earlier projects, we and others had identified BCL10 and the CBM-complex as an important signaling module that integrates signals and strength from different TCR induced signaling pathways into the strength of NFκB activation[87,88]. We hypothesized that this complex bears additional, so far unknown components that modulate NFκB activation in response to T cell activation. We decided to use BCL10 as a bait protein to isolate the CBM-complex and to identify its components by mass spectrometry. This should be done by the design and cloning of *BCL10*-cDNA constructs that code for epitope-tagged BCL10 proteins, introduction of this DNA into the genome of a cell line to induce stable expression of these proteins, immunopurification of the CBM-complex by the help of the epitope-tagged BCL10, and analysis of the composition of this complex by semi-quantitative mass spectrometry.

3.1.1. Generation of a Cell Line that Stably Expresses Epitope-Tagged BCL10

A common way to isolate protein complexes is to overexpress one component of the complex fused to an epitope-tag, which is then incorporated into the complex. The epitope-tag, and thereby the whole complex, can be bound by an affinity-matrix and, thus, can be separated from other proteins. To generate an expression vector for epitope-tagged BCL10, we sub-cloned the human *BCL10*-cDNA sequence into the pEXPR-Iba-103 vector to obtain BCL10 with a C-terminal StrepOne tag (BCL10-SO, FIGURE 8). The StrepOne tag is a tandem repeat of the short strep-tag, which can be isolated via its strong interaction with Streptactin. The *BCL10* open reading frame was transferred into the pMIG vector, creating the BCL10-SO-IRES-GFP expression construct. The IRES-GFP-reporter enables the identification of transgene expressing cells by fluorescence and allows positive selection by *fluorescence activated cell sorting* (FACS). For enhanced expression, the human *elongation factor-1α* (EF1α) promoter was sub-cloned upstream of the transgene.

The linearized expression cassette was introduced into Jurkat cells by nucleofection. Although this method allows only for transient transgene expression, a small subset of cells randomly integrates the transferred DNA into its genome. These stably transfected cells were sorted for high GFP expression on a cell sorter after two weeks. The sorted polyclonal fraction expressed BCL10-SO at a level 5-10 times higher than endogenous BCL10, as confirmed by western blot (FIGURE 9).

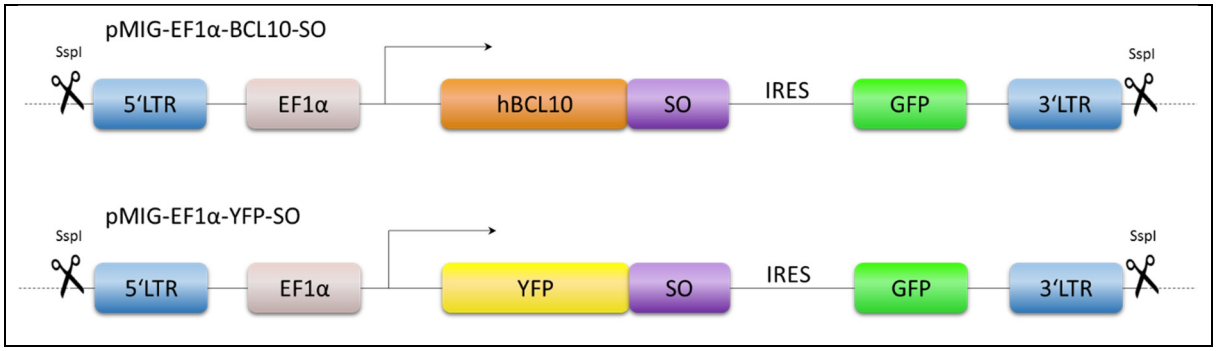

FIGURE 8. Design of the BCL10-SO and YFP-SO expression cassettes. BCL10- or YFP- StrepOne tag fusion proteins were expressed as IRES-GFP constructs under the control of MSCV-LTR and the human EF1α promoter. MSCV: murine stem cell virus, LTR: long terminal repeats, SO: StrepOne tag, IRES: internal ribosomal entry site.

Similarly, an YFP-SO construct in an analogue expression vector was introduced into Jurkat cells (FIGURE 8). Stably transduced cells were sorted into different fractions based on GFP expression. For control experiments, we chose a fraction expressing similar amounts of SO-tagged transgene compared to the BCL10-SO cells, as probed by western blot with an antibody against the strep-tag (data not shown).

3.1.2. Isolation of the CBM-Complex via Epitope-Tagged BCL10

We had successfully established Jurkat cell lines that stably express SO-tagged BCL10. Since we wanted to take use of these cell lines to isolate and characterize the CBM-complex, we intended to evaluate whether we could use the cells for this purpose. Wild-type (i.e. non-tagged) BCL10 constitutively interacts with MALT1 and associates, among others, with CARMA1 and MIB2 upon TCR stimulation[56,77,215]. Thus, we attempted to reproduce these interactions with our BCL10 constructs to (a) test whether the epitope-tagged BCL10 integrates into the CBM-complex as well and (b) to optimize our co-purification conditions.

First, we used Streptactin coupled agarose beads to isolate BCL10-SO and BCL10-SO containing protein complexes from cell lysates of BCL10-SO expressing Jurkat cells that were stimulated with PMA and ionomycin for 15 minutes. The eluates were analyzed by western blot for the presence of BCL10 and its interactors MALT1, CARMA1 and MIB2. Wild-type Jurkat cells served as a negative control. As expected, we detected BCL10 and MALT1 in the eluates of the transfected cells, but not in these of the wild-type cells (FIGURE 9A). In contrast, we did not observe any co-purification of CARMA1 or MIB2 after stimulation of the cells, albeit both are known to interact with BCL10 in a stimulation dependent manner[77,216].

We speculated that the absence of the inducible interactors might be due to sterical hindrance, which denies the interaction of the macroscopic beads and the tag once BCL10 is integrated into larger complexes. In this way, we would only catch pairs of BCL10-MALT1

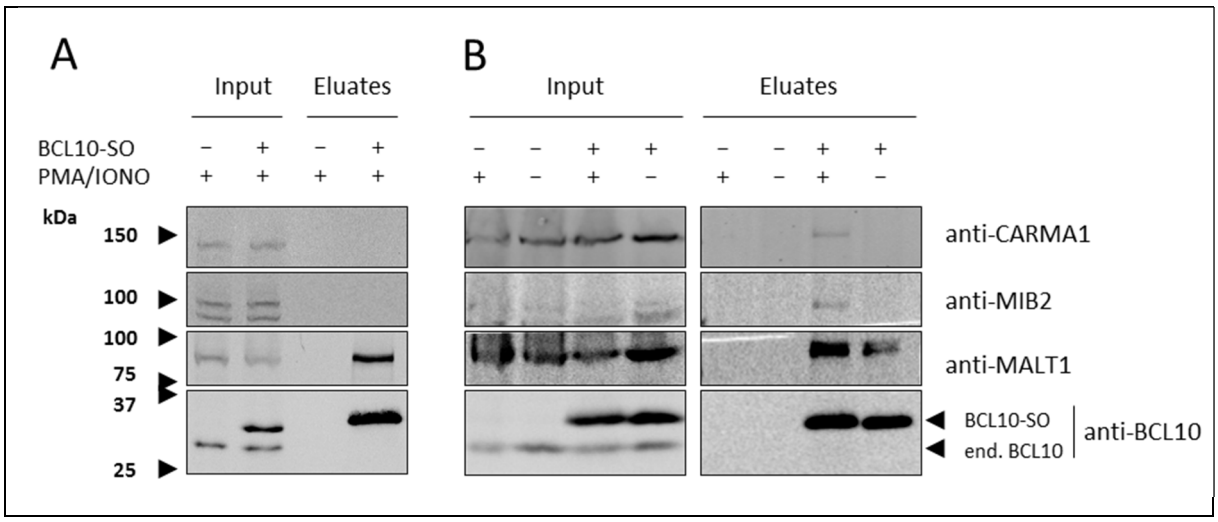

FIGURE 9. Co-purification of CBM-complex proteins with StrepOne tagged BCL10. Wild-type or BCL10-SO expressing Jurkat cells were stimulated for 15 min with PMA/ionomycin or left untreated. Cellular extracts were probed with streptactin beads (A) or biotinylated anti-strep-tag antibodies and magnetic streptavidin beads (B), respectively. The eluates were analyzed by immunoblot. The shown images are representative for two (A) or five (B) individual experiments.

that are not (yet) recruited to CARMA1. To circumvent this caveat, we tried to isolate the complexes by the use of a biotinylated anti-strep-tag antibody. The extracts were incubated with the antibody, followed by capture of the immune-complexes by magnetic streptavidin beads. Indeed, we observed co-purification of CARMA1 and MIB2 together with BCL10 and MALT1 after stimulation of the cells when we captured BCL10 via anti-strep-tag antibodies (FIGURE 9B). None of the proteins was detected in the eluates originating from wild-type cells, which confirms the specificity of the results.

Thus, we had established a protocol that enables the isolation of the CBM-complex from stimulated Jurkat cells by the help of epitope-tagged BCL10. In further experiments, this protocol was employed to analyze the composition of the CBM-complex.

3.1.3. Isotope Labeling of Jurkat Cells using SILAC

In the previous experiments, we had successfully isolated the CBM-complex from BCL10-SO overexpressing Jurkat cells, as indicated by the specific enrichment of CARMA1, MALT1 and MIB2. To identify further proteins that interact with BCL10 after stimulation, we aimed to analyze the purified BCL10-containing complexes by SILAC based semi-quantitative mass spectrometry. During this approach, the abundance of proteins from two CoIPs is compared in one measurement (as shown in FIGURE 5). The experimental setup is shown in FIGURE 10A. A pre-requisite for this type of experiment is the labeling of the cellular proteins with stable isotopes. For this isotope labeling, cells were cultivated for several days in special media that either contain only heavy or only light forms of the amino acids lysine and arginine.

These then become incorporated into all proteins of the respective cells. By this, proteins of these cells become distinguishable in mass spectrometric measurements even from a mixture (see SECTION 1.4.1).

Since pure heavy amino acids are rather expensive, we titrated the amount of arginine that is needed for proper growth of Jurkat cells in RPMI medium. Therefore, cells were grown in RPMI with arginine concentrations between 0 and 200 mg/l (as present in standard RPMI) and the proliferation of the cells was monitored over one week. While those cells that were grown in the absence of arginine almost stopped proliferation after day five, no major difference in cell numbers was observed for arginine concentrations between 20 and 200 mg/l on day seven (data not shown). Thus, we chose 20 mg/l arginine as the standard concentration for the SILAC media.

3.1.4. Mass Spectrometric Analysis of BCL10 Containing Protein Complexes

In order to identify further components of the CBM-complex we performed CoIP-MS experiments using BCL10-SO as a bait protein. For these CoIP-MS experiment, Jurkat cells were grown for ten days in the particular media to achieve a comprehensive isotope labeling of the cells. The labeling efficiency was checked by MS and was above 98 %. We then isolated BCL10 containing complexes from differently labeled BCL10-SO expressing Jurkat cells that were either stimulated for 15 minutes with PMA and ionomycin or left untreated. The proteins were trypsin digested in solution. The resulting peptides were separated and analyzed by a two dimensional RP-HPLC coupled to an ESI-MS/MS device.

The Identification of precursor proteins and quantification was done by MaxQuant software[217]. This software quantifies the heavy-to-light ratio of each detected peptide and assigns the detected peptides to their precursor proteins. By averaging several heavy-to-light peptide-ratios for a given precursor protein, a heavy-to-light ratio for the protein is generated by the software. This ratio can be interpreted as an enrichment value between the paired experiments (in this case, CoIP from unstimulated or stimulated cells). The experiment was done twice including a label swap. This means that while in the first run, stimulated cells were grown in light medium and unstimulated in heavy medium, labeling was reversed in the second run. To show up in the results, we demanded a protein to be present in both individual MS runs, and to be identified by at least two unique peptides in each of these runs.

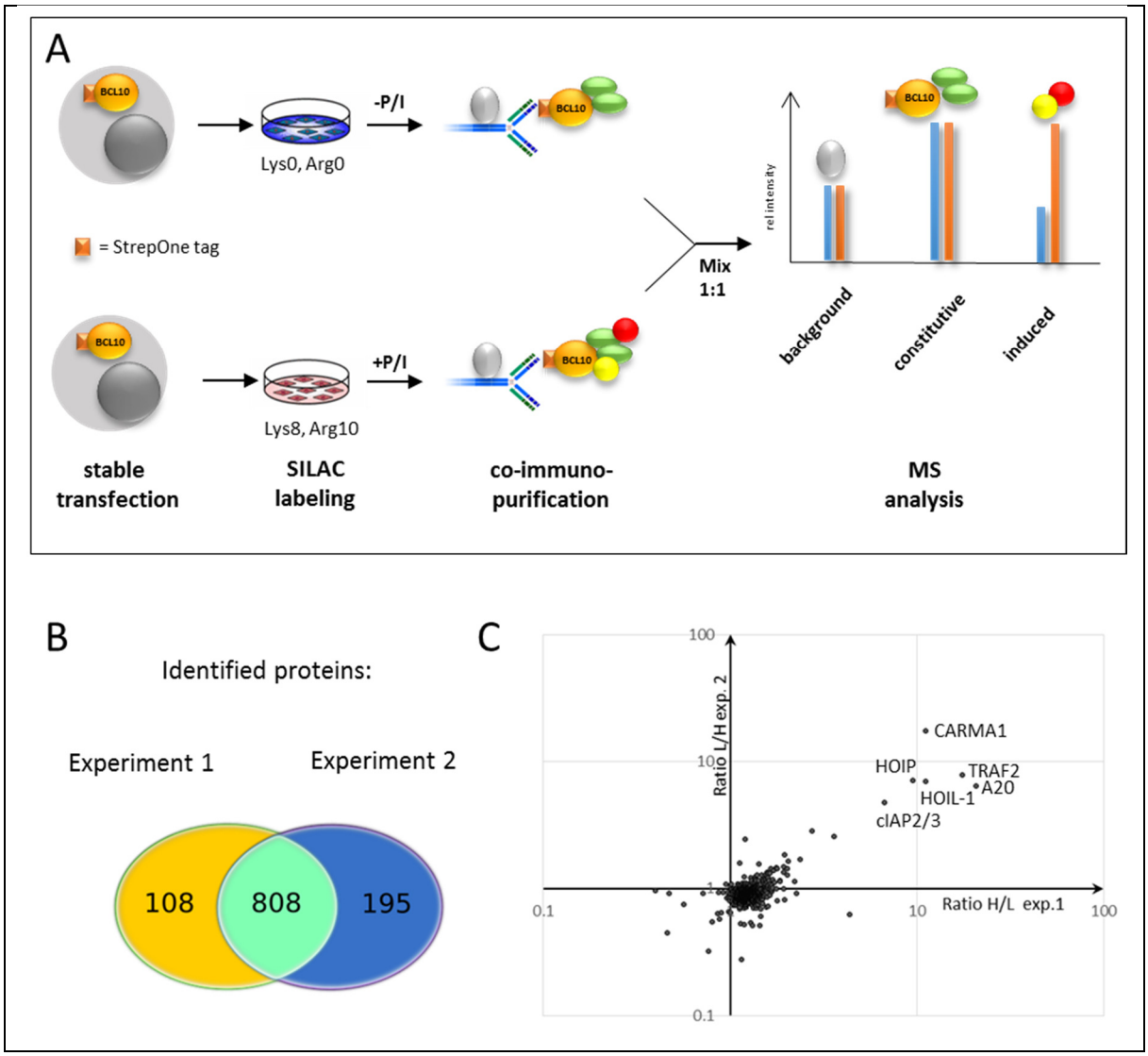

FIGURE 10. Experimental setup and results of the mass spectrometric analysis of the BCL10 CoIPs. A: Experimental setup of experiment 1. BCL10-SO expressing Jurkat cells were differently labeled by SILAC. "Light"-labeled cells (blue) were left untreated, while "heavy"-labeled cells (red) were stimulated with PMA and ionomycin. After co-immunopurification, eluates were mixed 1:1 and analyzed together by LC-MS/MS. Stimulation-induced interactors are identified by high heavy-to-light ratios. For the second experiment, SILAC labeling was switched, while other parameters remained unchanged. B: Quantity of proteins that were identified in one or both experiments. C: Combined distribution of heavy-to-light or light-to-heavy ratios, respectively, over both experiments. High values indicate that proteins were predominantly co-purified from stimulated cells. Logarithmic scale. P/I: PMA/ionomycin. MS: mass spectrometry.

Overall, 808 proteins were identified and quantified in both runs (FIGURE 10B), while 303 further proteins were identified in one run only. Most proteins appeared in a ratio near 1 (FIGURE 10C). A ratio of 1 means that a protein originates from unstimulated and stimulated cells in the same quantity, or in other words, it is not enriched or depleted by the stimulation. On the one hand, these can be proteins that were co-purified nonspecifically in both experiments, resulting from unspecific binding to the beads and/or the antibody. On the other hand, proteins that interact constitutively with BCL10 also are co-purified with BCL10 under both conditions, resulting in a ratio near 1. Indeed, BCL10 itself appeared in ratios of 1.0 and

0.6, respectively. The same is true for the constant BCL10 interactor MALT1 (1.1, 1.0). It is not possible to distinguish between constant interactors and background from this kind of experiment, though.

In contrast, proteins that interact with BCL10 exclusively after stimulation should appear in higher abundance from CoIPs from stimulated cells, resulting in higher ratios. Indeed, to our contentment, this was seen for CARMA1 (CARD11), a known stimulation dependent interactor of BCL10. The fact that CARMA1 was enriched in the dataset demonstrated that the CoIP had worked as intended and encouraged us to have a closer look at other enriched proteins. A further group of five proteins was enriched by a ratio of >4 in both experiments and can be found in TABLE 3.

Out of these, *baculoviral IAP repeat-containing protein-2/3* (BIRC2/3, also known as cIAP1/2), and *TNFα induced protein-3* (TNFAIP3/A20) have already been shown to associate with the CBM-complex[66,69,91,94,95,98,218] and regulate NFκB activation, so we laid our focus on the remaining proteins. Albeit interaction between TRAF2 and BCL10 as well as CARMA1 and TRAF2 have been described, the role of TRAF2 in immune receptor signaling to NFκB remains extremely vague[66,95,218,219]. Finally, the proteins *RanBP-type and C3HC4-type zinc finger-containing protein-1* (RBCK1) and *ring finger protein-31* (RNF31) had not been assigned a role in TCR induced signaling. The proteins are better known as *heme-oxidized IRP2 ubiquitin ligase-1* (HOIL1) and *HOIL1 interacting protein* (HOIP), respectively. Together with *SHANK-associated RH domain interacting protein* (SHARPIN), they form the liner ubiquitin assembly complex, that can attach head-to-tail linked ubiquitin chains to target proteins[220–222].

TABLE 3. Results of the MS analysis for selected proteins. Proteins marked with * were not known previously to interact with BCL10.

Gene ID (alias)	Average number of unique peptides	Sequence coverage [%]	Ratio count H/L	Ratio H/L exp. 1	Ratio L/H exp. 2
BCL10	25.0	60.1	105	1.0	0.6
MALT1	23.5	30.0	67	1.1	1.0
CARD11 (CARMA1)	3.0	5.5	4	11.2	17.3
RNF31 (HOIP)*	4.0	7.6	10	9.6	7.1
TRAF2	4.0	13.4	7	17.6	7.7
BIRC2;BIRC3 (cIAP 1/2)	3.0	9.5	6	6.7	4.7
TNFAIP3 (A20)	2.5	5.8	5	20.8	6.3
RBCK1 (HOIL1)*	2.0	5.3	4	11.2	6.9

3.1.5. TRAF2 and HOIP Interact with BCL10 after TCR Stimulation

Previously, we had isolated BCL10 containing complexes from stimulated and unstimulated Jurkat cells and compared their composition by mass spectrometry. As expected, the interaction of BCL10 and CARMA1 was highly augmented by stimulation, referring to the formation of the CBM-complex. Interestingly, we identified further inducible interactors of BCL10 in this experiment: TRAF2, HOIP, and HOIL, as well as the known CBM-complex modulators cIAP and A20.

In order to verify the interactions between BCL10, HOIP, HOIL1 and TRAF2 in stimulated Jurkat cells, we again isolated BCL10 containing complexes from BCL10-SO expressing Jurkat cells that were either stimulated for 15 minutes with PMA and ionomycin or left untreated. For the isolation of the CBM-complex, we employed the same protocol as for the CoIP-MS experiments. The eluates were analyzed by western blot for the presence of the mentioned proteins (FIGURE 11 A). Indeed, TRAF2 and HOIP only co-purified with BCL10-SO after stimulation with PMA/ionomycin, but not with YFP-SO which served as a negative control. Thus, we confirmed the interaction of BCL10 with these two proteins. However, we did not detect HOIL-1 interaction with BCL10 in any CoIP-WB experiment (data not shown).

So far, we proved that BCL10 interacts with HOIP and TRAF2 in PMA/ionomycin stimulated Jurkat cells. However, T cell stimulation with PMA and ionomycin is a rather artificial stimulation as it bypasses early T cell signaling events by direct stimulation of PKC and calcium influx (see SECTION 1.2.1). In order to test whether HOIP and TRAF2 also interact with BCL10 after antigen receptor engagement, we stimulated BCL10-SO or YFP-SO expressing Jurkat cells with agonistic antibodies against CD3 and CD28 for different periods of time and subsequently isolated the formed complexes with anti-strep-tag antibodies. The eluates were analyzed by western blot (FIGURE 11B). Along with Bcl10, we detected HOIP and TRAF2 as well as MIB2 and CARMA1 in the eluates from antigen-receptor stimulated BCL10-SO expressing Jurkat cells. In contrast, none of these proteins was detected in eluates from unstimulated cells or from stimulated control cells. Minor signals are seen for CARMA1 and HOIP in the control CoIPs from unstimulated cells, which are most likely artefacts, as they do not appear in stimulated cells in this experiment. Thus, analogue to the stimulation with PMA and ionomycin, the stimulation of T cell receptor and CD28 co-receptor induced the interaction of BCL10 with TRAF2 and HOIP in Jurkat cells.

Since its establishment, the Jurkat cell line has been a useful model system to study T cell biology and T cell receptor signaling. However, due to their altered genotype, cell lines

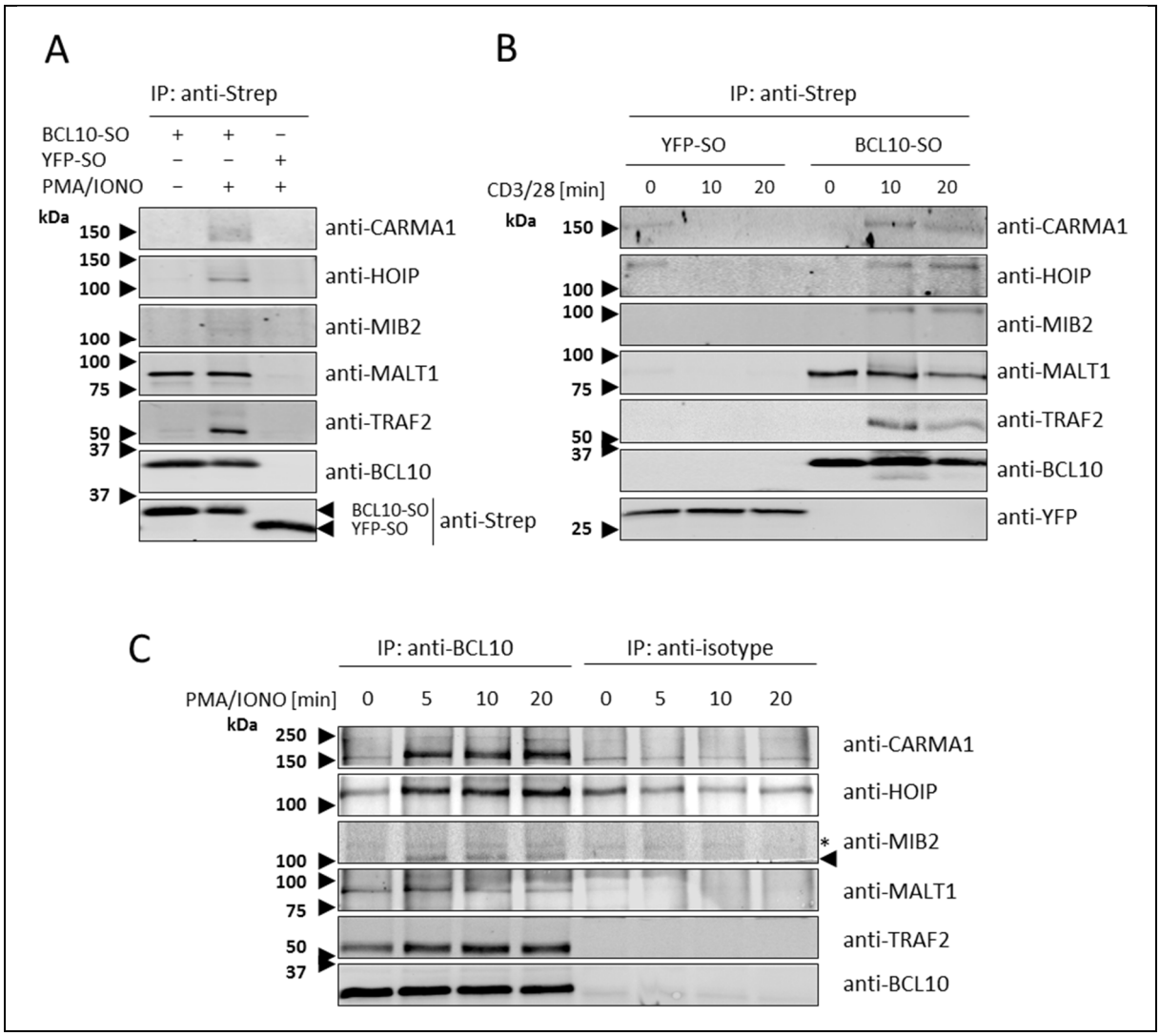

FIGURE 11. BCL10 interacts with HOIP and TRAF2 after T cell stimulation. (A and B) BCL10-SO or YFP-SO expressing Jurkat cells were stimulated for 15 min with PMA/ionomycin or with anti-CD3/CD28 agonistic antibodies for the indicated time. Complexes were isolated using anti-strep-tag antibody and eluates were analyzed by western blot. (C) Primary human CD4-positive T cells were stimulated with PMA/ionomycin for the indicated time. CoIP was performed with a BCL10 specific antibody or with an isotype-matched control antibody. Eluates were analyzed by western blot. * indicates a non-specific band. Images are representative for five (A) or two (B and C) independent experiments.

do not always resemble the phenotype of primary cells. Because of this, results from cell line experiments should be interpreted cautiously[202]. Therefore, we wanted to investigate whether the observed interaction of BCL10 with HOIP and TRAF2 in Jurkat cells also occurs in primary T cells.

To examine the respective BCL10 interactions in primary T cells, we isolated CD4-positive T cells from healthy blood donors. Cells were either stimulated with PMA and ionomycin or left untreated. Using a monoclonal antibody against BCL10, we isolated BCL10 containing complexes and analyzed them by western blot (FIGURE 11C). A similar experiment was performed using an isotype-matched antibody to control for unspecific binding. BCL10 was isolated from primary human T cells with the specific antibody, but not with the isotype

control antibody. TRAF2 is already co-purified along with BCL10 from unstimulated cells, though this interaction is enhanced after stimulation. In contrast, no TRAF2 protein was detected in the control experiment's eluates. HOIP was present in low amounts in all the eluates from the isotype control experiments. The signal strength is comparable to the signal obtained from unstimulated cells with the BCL10 specific antibody, indicating unspecific binding of HOIP under the applied conditions. However, in contrast to the control experiment, larger amounts of HOIP were co-purified with BCL10 after stimulation of the cells, which indicates an induced direct or indirect binding of HOIP to BCL10. Thus, we could show that BCL10 interacts with HOIP and TRAF2 in primary human T cells after PMA/ionomycin stimulation. Furthermore, this experiment demonstrates that the wild-type form of BCL10 interacts with both proteins, and that these interactions occur at endogenous expression levels of BCL10.

To summarize, we identified and confirmed TRAF2 and HOIP as inducible components of the CBM-complex. We showed that these interactions are dependent on TCR stimulation and occur in primary human T helper cells. Since the CBM-complex governs the activation of NFκB transcription factors after TCR engagement, this finding suggested that TRAF2 and HOIP might contribute in one or another way to this process. To examine this hypothesis, we intended to knock-down TRAF2 and HOIP to investigate whether these proteins contribute to the CBM-complex formation, IKK activation, IκBα degradation and NFκB transcriptional activity following T cell stimulation.

However, at this stage, the group of Nicolas Bidère published a report on the involvement of the LUBAC in TCR induced NFκB signaling[223]. In this report, the authors showed on different levels that HOIP and SHARPIN are essential for complete NFκB activation after TCR stimulation. Interestingly, E3 ligase activity of HOIP seems dispensable for this process (please see CHAPTER 4.1.3, (page 87ff) for a more comprehensive analysis of this report). The authors also demonstrated an involvement of the LUBAC in CARMA1 dependent constitutive NFκB activation in ABC-DLBCL tumor cells. This observation was also published by Yibin Yang *et al.* at the same time[224].

Thus, these reports confirmed our findings that the LUBAC complex associates with the CBM-complex following TCR stimulation. Furthermore, they proved our hypothesis that this interaction has an impact on subsequent NFκB activation. After intense and careful considerations, we concluded that our research on this topic was not likely to shed further light on the regulation of the TCR induced NFκB pathway. Thus, we decided to terminate our efforts towards this topic.

3.2. Identification of NFAT Interaction Partners

The activation of NFAT family transcription factors is a hallmark of T cell activation, and NFAT proteins in general are indispensable for the function of T cells and the adaptive immune system as a whole. NFAT proteins form complexes with other transcription factors (e.g. FOXP3, AP1 or GATA3), and these interaction strongly influence NFAT DNA binding sites and target gene activation[176,179,225]. While recent MS based studies revealed multiple novel binding partners of the transcription factors FOXP3 and RelA, a comprehensive study of NFAT interaction partners was missing[188,189].

To fill this gap, the aim of the second part of the present thesis was to identify hitherto unknown interaction partners of human NFAT proteins. This should be done by design and cloning of *NFAT*-cDNA constructs that code for epitope-tagged NFAT proteins, introduction of this DNA into the genome of a cell line to induce stable expression of these proteins, immunopurification of NFAT-containing protein complexes by the help of the epitope tag, and, finally, analysis of these complexes by semi-quantitative mass spectrometry

3.2.1. Establishment of Cell Lines that Stably Express Biotin-Tagged NFAT Proteins

3.2.1.1. Choice of Epitope-Tag and Vector System

During the first part of this thesis, we successfully employed epitope-tagged BCL10 to isolate the CBM-complex from activated Jurkat cells. By employing MS to analyze the isolated complex, we identified TRAF2 and HOIP as so far unknown constituents of this signaling module (see CHAPTER 3.1.4). In an analogous fashion, we intended to overexpress epitope-tagged NFAT isoforms to isolate NFAT containing protein complexes, which can by analyzed by MS subsequently. Several epitope tag systems are available, which allow the (co-) purification of proteins, all bearing certain advantages and drawbacks. For the isolation of NFAT proteins, we decided to employ a peptide tag that is readily biotinylated by the co-expressed *E.coli* biotin ligase BirA (AVI tag)[226,227]. This allows taking advantage of the very high affinity of the biotin-streptavidin interaction for complex isolation and avoids the use of antibodies during this process (FIGURE 12). From our experience, the last point is extremely useful especially when dealing with DNA containing nuclear extracts.

However, at the same time, the strong binding to streptavidin requires harsh elution conditions to release the biotinylated proteins from the affinity matrix. To circumvent this drawback, we inserted a *tobacco etch virus* (TEV) protease cleavage site between the NFAT protein and the tag[228]. This allows the release of the protein complexes by proteolytic digestion, which is not only mild but also more specific: It mainly releases proteins that are bound to the

streptavidin matrix via the biotinylated tag, while non-specifically bound proteins and other biotinylated proteins remain unaffected. Furthermore, the major part of the tag including the biotin moiety, as well as proteins that interact with the tag, are not eluted from the matrix (FIGURE 12C). The combination of TEV cleavage site and AVI tag is hereafter referred to as AVITEV.

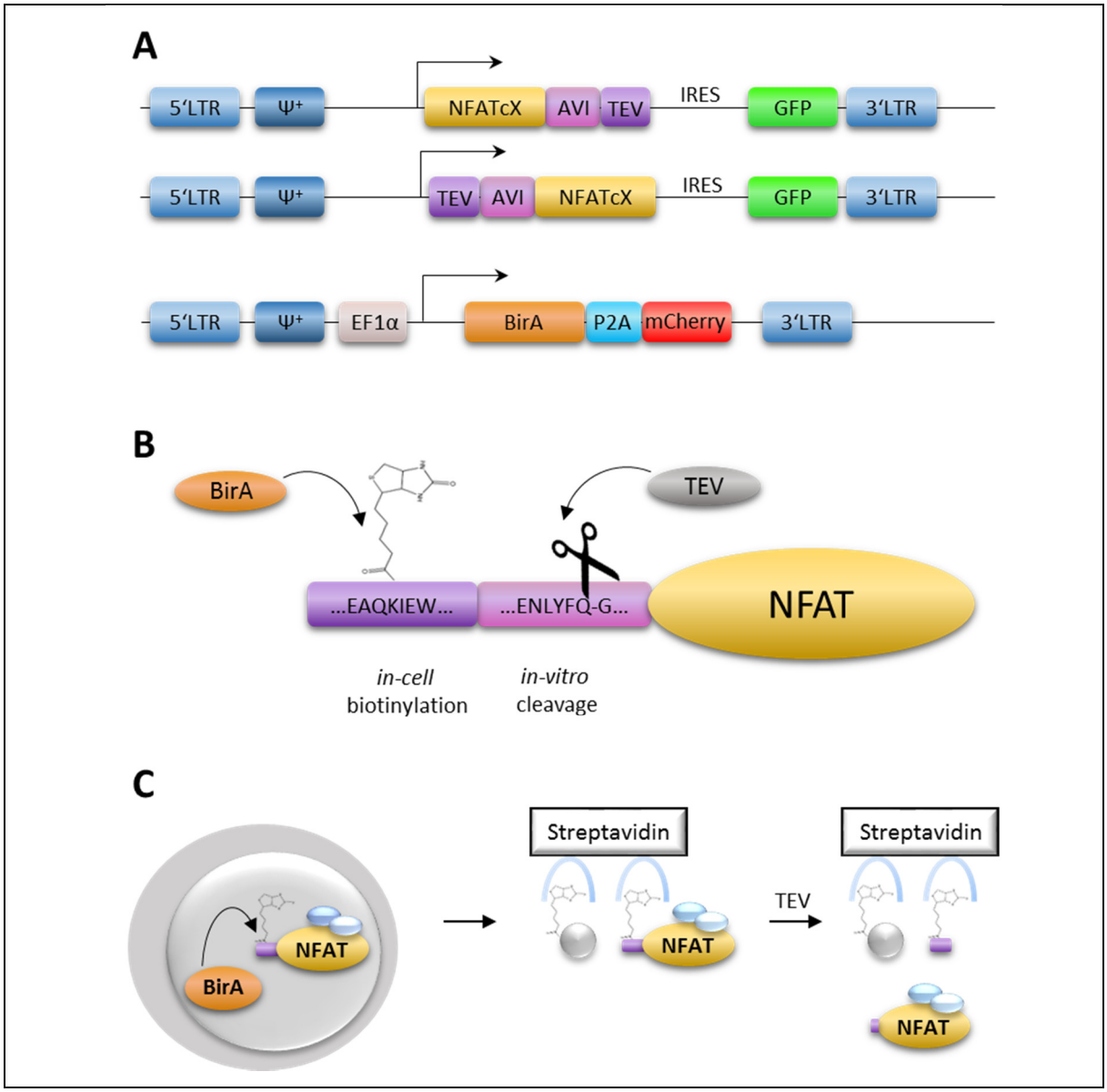

FIGURE 12. Design and function of the NFAT-AVITEV constructs. A: Vector design. Retroviral vectors were generated that allow the expression of NFAT-proteins fused to an N- or C-terminal AVITEV-tag. Expression can be monitored through the co-expression of GFP via an IRES-GFP site. Similarly, a vector that drives expression of a self-cleaving biotin ligase BirA-mCherry fusion protein was established. B: Function of the AVITEV-tag: A biotinylation signal sequence (AVI) is recognized and biotinylated by the co-expressed E.coli protein biotin ligase BirA. A cleavage site for tobacco etch virus protease (TEV) allows cleavage of NFAT from the biotinylated peptide-tag. C: Principle of protein isolation: NFAT-AVITEV is biotinylated in living cells. NFAT and interacting proteins can be isolated via binding to streptavidin-beads. TEV protease treatment releases NFAT and interactors, but not other biotinylated proteins from the streptavidin matrix. LTR: long terminal repeat, Ψ+: extended packaging signal, TEV: tobacco etch virus (cleavage site), EF1α: elongation factor 1α promoter, IRES: internal ribosome entry site.

As a basic plasmid, we chose the retroviral pMIG (pMSCV-IRES-GFP). This plasmid allows the production of retroviruses, which can be used as a vector to stably integrate a chosen transgene into the host's genome. Since transgene expressing cells co-express GFP, the selection of transfected / transduced cells can be done via FACS. We created variants of pMIG that are primed for the C-terminal or N-terminal expression of AVITEV-tagged proteins, respectively (FIGURE 12A). Next, we inserted the sequence of human *NFATc2*, *NFATc1/αA* (herein referred to as *NFATc1S* [short]), and *NFATc1/βC* (herein referred to as *NFATc1L* [long]) into these vectors. We also generated a retroviral vector that allows for the expression of a BirA-P2A-mCherry fusion protein. The P2A peptide moiety induces self-splicing of the expressed protein and releases untagged BirA and mCherry proteins[205].

Altogether, the generated retroviral vectors coded for three different human NFAT isoforms (NFATc1S, NFATc1L and NFATc2), each fused either to an N- or C-terminal AVITEV-tag. The co-expression of the biotin-ligase BirA should lead to the biotinylation of the tag. Consequently, biotinylated AVITEV-containing proteins can be isolated via binding to a streptavidin-coupled matrix.

3.2.1.2. Stable Transfection of Jurkat Cells with Epitope-Tagged NFAT Isoforms

We utilized the aforementioned plasmids to produce corresponding retroviruses in HEK-293T cells and transduced Jurkat cells with one of the NFAT-fusion proteins and the BirA ligase by the help of these viruses. The cells were sorted three times for high, stable expression of GFP and/or mCherry to obtain polyclonal populations of Jurkat cells that express high levels of one or both fluorophores.

The coding sequences of the fluorophores and the transgenes are connected via an *internal ribosome entry site* (IRES). Thus, both proteins are coded on a single mRNA and, hence, transcribed simultaneously. Therefore, the presence of the fluorophore (GFP or mCherry) indicates the transcription of the corresponding transgene (NFAT or BirA). However, since the translation of the surrogate marker and the transgene occur independently, the protein expression of the corresponding transgene has to be checked separately. We performed western blot analysis of cell lysates from GFP positive or GFP-mCherry double positive cells to evaluate the level of transgene expression and biotinylation of the AVITEV-tag within these cells (FIGURE 13).

As seen from the western blot, **NFATc1S** overexpression was only detected in cells transduced with the vector for the N-terminal tagged protein, which also showed a high level of biotinylation (FIGURE 13, top panel). In contrast, we did not detect any expression of C-terminal tagged NFATc1S protein.

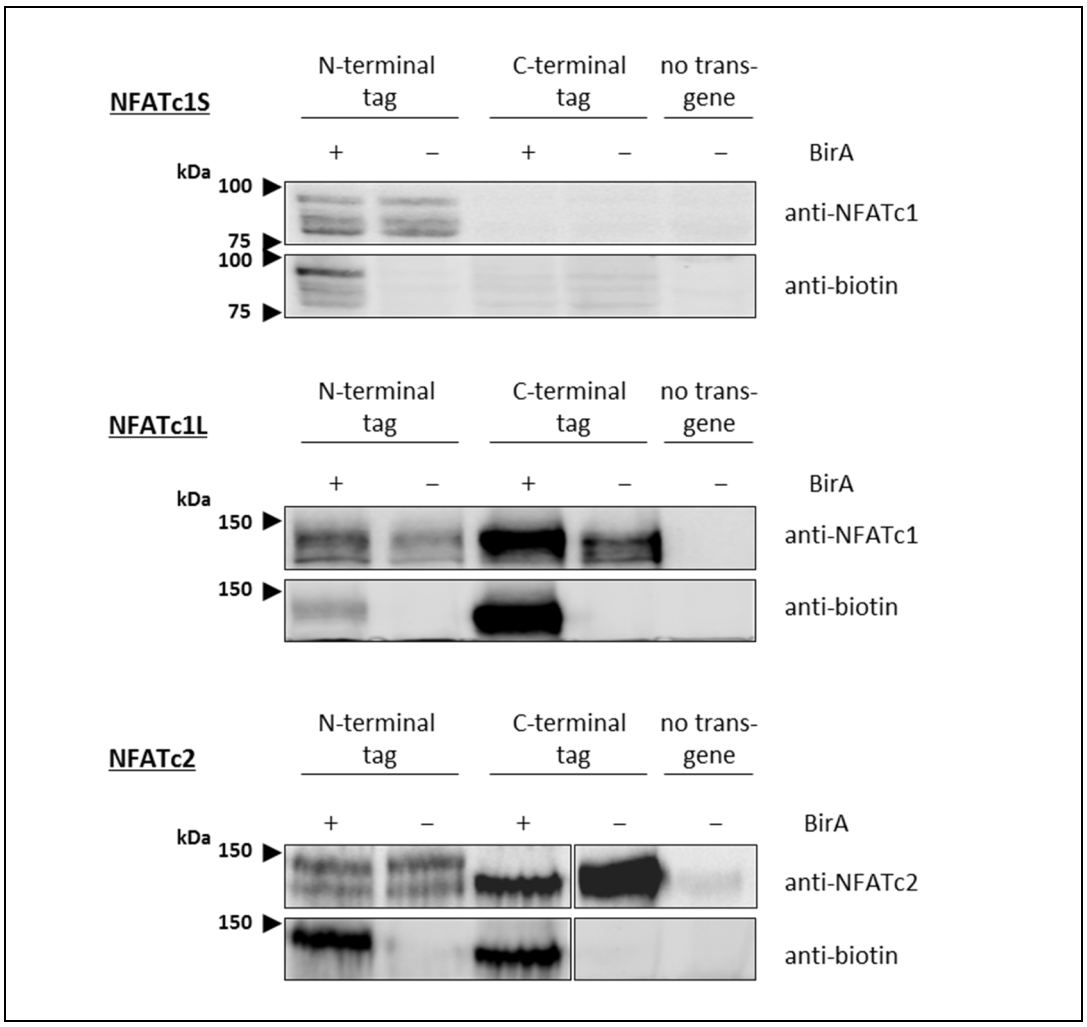

FIGURE 13. Evaluation of expression and biotinylation of NFAT-AVITEV fusion proteins in stably transduced Jurkat cells. Jurkat cells were transduced with either C-terminal or N-terminal tagged forms of NFATc1S (top), NFATc1L (middle) or NFATc2 (bottom). Cellular lysates were analyzed by immunoblot with antibodies against the indicated NFAT isoforms. The extent of biotinylation by the co-expressed BirA biotin ligase was monitored with a fluorophore-coupled streptavidin conjugate. Images are representative for two independent experiments.

NFATc1L, the long variant of NFATc1, was expressed as an N-terminal and a C-terminal fusion protein (FIGURE 13, central panel). However, while the C-terminal tag was readily biotinylated when the biotin ligase BirA was co-expressed, only a weak biotin signal was detectable from the N-terminal tagged protein, which indicates that *in-cell* biotinylation of the latter fusion protein was less efficient.

Regarding **NFATc2**, both the C- and N-terminal AVITEV fusion proteins were detected in the transduced Jurkat cells. When the biotin ligase BirA was co-expressed, strong biotinylation was seen for both tagged proteins (FIGURE 13, bottom panel). The N-terminal tagged NFATc2 showed up in the western blot as two distinct bands of equal intensity, of which only the upper one was biotinylated. This points towards the possibility that roughly half of the protein is translated without the tag using an alternative AUG as translation start point.

Overall, we generated Jurkat cell lines that stably express the three employed NFAT isoforms that are N- or C-terminal fused to an AVITEV-tag, with the exception of C-terminal tagged NFATc1S, whose expression was not detectable. Out of the expressed AVITEV fusion proteins, all but the N-terminal tagged NFATc1L proteins are readily biotinylated by the co-expressed biotin ligase. In general, NFATc1S showed a lower expression level than NFATc1L.

3.2.2. Characterization of NFAT Overexpressing Cell Lines

To evaluate whether the epitope-tagged NFAT forms are a valid model to investigate NFAT interactions, we analyzed the translocation and phosphorylation patterns of the biotinylated NFAT forms in Jurkat cells and compared it to the patterns known from primary cells. In resting primary T cells, NFAT proteins are heavily phosphorylated and thereby kept in the cytoplasm of the cells. After T cell stimulation, NFAT is dephosphorylated by *calcineurin* (CaN), causing a translocation of NFAT into the nucleus (FIGURE 4). The latter process can be prevented by blocking calcineurin activity with *cyclosporine A* (CsA).

In order to test whether NFAT phosphorylation and translocation are affected by the AVITEV tag, we stimulated the NFAT-AVITEV overexpressing cell lines for 30 minutes with PMA and ionomycin in the presence or absence of CsA. For comparison, we also included Jurkat cells that overexpress untagged, i.e. wild-type forms of the corresponding NFAT proteins into this experiment. We then isolated cytoplasmic and nuclear fractions of the cells and checked the localization and phosphorylation of NFAT proteins by western blot (FIGURE 14). Noteworthy, NFAT proteins appear in several bands, which represent differently phosphorylated forms of the same protein (see below). The endogenous NFAT proteins, while still expressed, are not seen on the blots. This is due to their much lower expression level compared to the overexpressed forms (also compare the right lane in FIGURE 13 to the other lanes).

3.2.2.1. Cellular Localization of Epitope-Tagged NFAT Proteins

First, we had a look at the distribution of the epitope-tagged NFAT proteins between nucleus and cytoplasm. In contrast to our expectations, we could already detect all NFAT proteins in the nuclear fraction without stimulation. On the one hand, this might be explained by the transformed nature of the Jurkat cell line[202]. Indeed, non-transduced (i.e. wild-type) Jurkat cells show low to medium levels (20-40 %) of nuclear NFATc1 and NFATc2 in the absence of stimulation (data not shown). On the other hand, overexpression of NFAT proteins might *per se* affect their sub-cellular location, e.g. by overstraining NFAT export processes. This is supported by reports from another group, which observed nuclear NFATc1 in primary murine T helper cells after viral overexpression of either the long or short isoforms[146].

In detail, the overexpressed **NFATc1L** protein was evenly distributed between the nuclear and cytoplasmic fraction prior to the stimulation, as judged by the western blot signals (FIGURE 14, middle panel). As expected, treatment with PMA and ionomycin increased the amount of nuclear NFAT at the expense of the cytoplasmic fraction, indicating a stimulation-induced translocation to the nucleus. When calcineurin activity was blocked with CsA, again an even distribution of NFATc1L between cytoplasm and nucleus – as seen in unstimulated cells – was observed. We did not observe any influence of the AVITEV tag on NFATc1L translocation, as both epitope-tagged and the wild-type NFATc1L showed the same sub-cellular localization pattern.

NFATc1S was found preferentially in the nucleus of unstimulated cells (FIGURE 14, lower panel). Stimulation alone did not affect the localization ratio of the protein, while stimulation in the presence of CsA led to a slight increase in cytoplasmic NFATc1S. As seen for NFATc1L, the presence of the AVITEV tag did not alter the localization of NFATc1S.
Like NFATc1S, most of the over-expressed **NFATc2** protein was already nuclear without stimulation (FIGURE 14, upper panel). The wild-type and the C-terminal tagged NFATc2 showed a further increase in nuclear NFAT and a decrease of cytoplasmic NFAT upon stimulation with PMA and ionomycin. This is in line with the expected nuclear translocation in response to stimulation. A divergent pattern was seen for the N-terminal tagged NFATc2 (FIGURE 14, upper panel, left side). Here, the upper band, which corresponds to the biotin-tagged protein (see also FIGURE 13), did not show an increased nuclear localization in response to the stimulus.

In general, all variants of the over-expressed NFAT isoforms were found in the nucleus of unstimulated Jurkat cells, which might be caused by the overexpression *per se* and/or by anomalous signaling processes of the Jurkat cells. Importantly, the AVITEV tag itself did not alter the localization pattern of most NFAT isoforms, as the epitope-tagged variants resembled the translocation patterns of the over-expressed wild-type forms. One exception from this was seen for the N-terminal tagged NFATc2, which did not translocate to the nucleus after stimulation.

3.2.2.2. Phosphorylation of Epitope-Tagged NFAT Proteins

Having analyzed the localization of the epitope-tagged NFAT proteins, we had a look at the phosphorylation status. Due to a nominal decrease in net charge, the phosphorylation of proteins usually leads to a slower migration in SDS-PAGE, which results in distinguishable bands in western blots for differentially phosphorylated proteins of the same species. Following

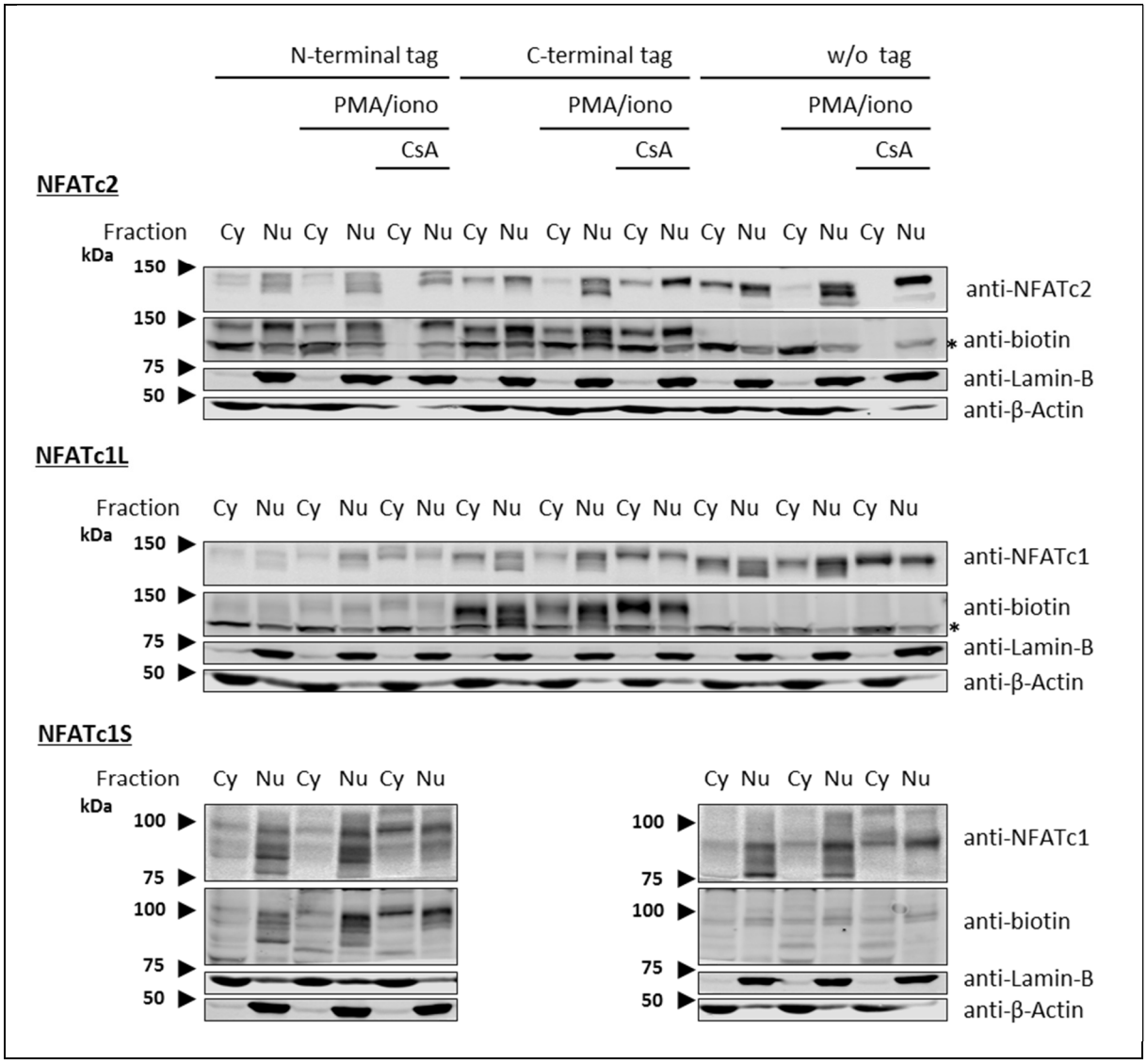

FIGURE 14. Translocation and phosphorylation pattern of NFAT-AVITEV fusion proteins. Cells overexpressing wild-type, N-terminal or C-terminal epitope-tagged forms of NFATc2 (top panel), NFATc1L (middle panel) or NFATc1S (bottom panel) were stimulated with PMA and ionomycin in the presence or absence of 50 mM cyclosporine A. Cytosolic and nuclear extracts were analyzed by immunoblotting. Lamin-B and β-Actin served as loading controls for the nuclear and the cytosolic extracts, respectively. NFAT proteins appear in several bands, which represent differently phosphorylated forms of the same protein. Cy: cytosolic fraction, Nu: nuclear fraction. * marks a biotin band that does not originate from NFAT. Images are representative for two independent experiments.

T cell activation, CaN dependent dephosphorylation of NFAT proteins leads to a vast increase of faster migrating NFAT species, which can be monitored by western blot analysis[87].

This expected pattern was observed for all overexpressed **NFATc2** proteins (Figure 14, upper panel). Stimulation led to an increase in faster migrating NFATc2 species, corresponding to a lower state of NFAT phosphorylation. In the presence of CsA, only the slowly migrating (phosphorylated) species appeared. Thus, the overexpressed NFATc2 resembled the expected phosphorylation pattern for NFAT proteins (FIGURE 4).

In contrast, the phosphorylation of both overexpressed **NFATc1** forms followed a different pattern in Jurkat cells (FIGURE 14, middle and lower panel). NFATc1 was dephosphorylated to a large extend in unstimulated cells. Stimulation led to an increase in phosphorylated NFATc1 species, which weas further augmented by the addition of CsA.

To explain the differences to the expected pattern, it is important to remember that not only the NFAT phosphatase calcineurin, but also counteracting NFAT kinase are activated by the stimulation, such as p38 and JNK (FIGURE 4). As discussed above, the overexpression of NFAT proteins might overstrain the phosphorylation potential of NFAT kinases under resting conditions, resulting in incompletely phosphorylated NFAT species. Stimulation then overcomes this limitation by activation of NFAT kinases, and blocking calcineurin with CsA further shifts the reversible process of phosphorylation/dephosphorylation towards the former one. Differences in the regulation of NFATc1 and NFATc2 might be explained by the fact that some NFAT kinases discriminate between both isoforms and can phosphorylate only one or the other isoform (as reviewed by Okamura *et al.*[153]). Thus, while the overexpressed NFATc2 proteins showed the expected phosphorylation pattern following stimulation, some aberrations were observed for NFATc1 proteins.

Remarkably, as observed for the translocation, the AVITEV tag did not have any influence on NFAT phosphorylation, since all tagged NFAT proteins also resemble the phosphorylation patterns of the corresponding untagged forms. This point is important, for it shows that the AVITEV fusion proteins of NFAT are recognized and regulated by the cellular machinery just as the wild-type variants. This made us confident that the tag would not disturb the majority of other protein-protein interactions that involve NFAT either, and that, hence, these AVITEV-NFAT fusion proteins would serve as a valid tool to reveal and study these interactions.

Most of the following experiments were performed with N-terminal tagged NFATc1S, C-terminal tagged NFATc1L and C-terminal tagged NFATc2, as the other forms were either poorly expressed (C-terminal tagged NFATc1S, see FIGURE 13), poorly biotinylated (N-terminal tagged NFATc1L, see FIGURE 13) or poorly translocated in response to stimuli (N-terminal tagged NFATc2, see FIGURE 14). For convenience reasons, the text will refer to these employed isoforms unless stated otherwise. It is noteworthy that the expression level of the NFATc1S-fusion protein was much lower than it was for the other two employed isoforms (FIGURE 13).

3.2.3. Purification of NFAT Proteins by the Help of the AVITEV Tag

In our preliminary work, we had successfully established Jurkat cell lines that stably express biotin-tagged forms of NFATc1S, NFATc1L and NFATc2 (FIGURE 13). Furthermore, we could show that the presence of the tag did not influence the translocation and phosphorylation patterns of the NFAT fusion proteins (at least, not for the employed constructs; see above). Thus, we were confident that these cell lines would serve us to isolate NFAT containing protein complexes and to identify NFAT interaction partners.

In order to yield NFAT containing protein complexes, we attempted to isolate the biotinylated NFAT proteins using the features of the AVITEV tag. As the tag is biotinylated within the living cell by the co-expressed biotin ligase, the extracted fusion proteins should bind tightly to streptavidin beads. Subsequently, the attached TEV protease cleavage site should allow mild and specific elution from the beads by proteolytic cleavage (FIGURE 12).

To prove this, we incubated cleared nuclear lysates of wild-type or NFAT-AVITEV overexpressing Jurkat cells with streptavidin-coupled agarose beads and collected the supernatants. TEV-protease was added to the washed beads to cleave off the NFAT protein from the beads, and the eluate was collected. Afterwards, the beads were stripped of remaining proteins by incubation in Laemmli buffer at 95 °C, which was then collected as 'post-eluate'. The success of protein isolation and elution was tested by western blot, which is shown exemplarily for NFATc2 in FIGURE 15. Similar experiments with the NFATc1S and NFATc1L constructs showed comparable pictures (data not shown).

As intended, the collected supernatant contained only minimal amounts of tagged NFATc2 (FIGURE 15, upper right panel), compared to the nuclear extract ('input'). This indicates that most of the biotinylated protein was bound by the streptavidin beads and thereby

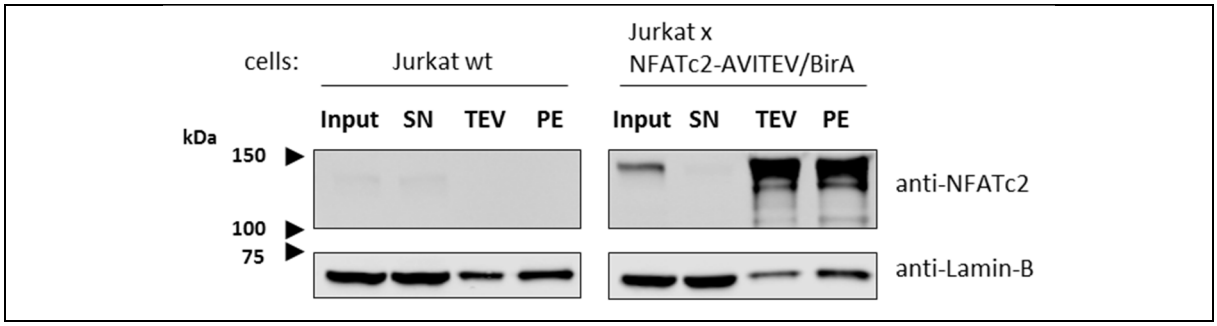

FIGURE 15. Isolation and elution of biotin tagged NFAT proteins. Nuclear lysates from wild-type or NFATc2-AVITEV expressing Jurkat cells were incubated with streptavidin coupled agarose beads. Beads were separated from the supernatant (SN), washed, and proteins were eluted by TEV protease cleavage. Remaining proteins were stripped off the beads by boiling in Laemmli buffer and collected as post eluates (PE). Images are representative for three independent experiments.

removed from the supernatant. Contrarily, wild-type NFATc2 (upper left panel) and the nuclear structure protein Lamin-B (lower panels) were hardly removed from the nuclear extract by the beads. This finding suggests a relative specific binding of biotinylated proteins to the streptavidin beads.

In contrast to the supernatant, both the eluate and the post eluate contained large amounts of the overexpressed NFATc2. Incubation with TEV protease released approximately half of the NFATc2 protein from the beads into the eluate fraction, while the other half was only released from the beads by boiling in Laemmli buffer (post eluate). Although the eluate and post eluate contained residues of Lamin-B, no enrichment as seen for NFATc2 was detectable. Furthermore, TEV protease activity releases only a minor part of the Lamin-B from the beads, which shows that the use of the TEV protease mediated cleavage leads to a further depletion of unspecific binding proteins from the eluate (FIGURE 15). Taken together, we observed a strong and specific enrichment of NFATc2 protein via binding to streptavidin-coupled agarose beads and a substantial release of the bound protein by TEV protease.

3.2.4. Co-Purification of Known NFAT Interacting Proteins

By the help of the AVITEV tag, we were able to purify NFAT proteins from NFAT overexpressing Jurkat cells. Motivated by these results, we tested whether known NFAT interacting proteins would be co-purified together with our NFAT constructs. We stimulated NFAT overexpressing Jurkat cells for 2 h with PMA/ionomycin to allow stimulation induced upregulation of known NFAT transcriptional partners such as FOS and JUN. We employed the same protocol as before to isolate NFAT and NFAT containing protein complexes and tested the eluates for the presence of JUN, JUNB, FOS and EP300, which are described to interact with NFAT proteins[123,168,169,229,230]. Nuclear extracts from Jurkat cells that express the biotin ligase BirA but no further transgene were also probed with beads in the same way, and the eluate served as a negative control.

The results from the co-purification experiments with NFATc1L and NFATc2 overexpressing cells are shown in FIGURE 16. The eluates from the cells expressing epitope-tagged NFATc1L or NFATc2 showed large amount of the respective proteins compared to those from the control cells. Furthermore, they also contained FOS, JUNB and EP300, which served us as positive controls. In contrast to what we had expected, we did not detect any JUN protein in the eluates (see SECTION 4.2.1.2 for a probable explanation why JUN was not detected here). In contrast, the eluate from the control cells did not contain detectable amounts of these proteins, which indicates a specific co-purification together with both NFAT proteins.

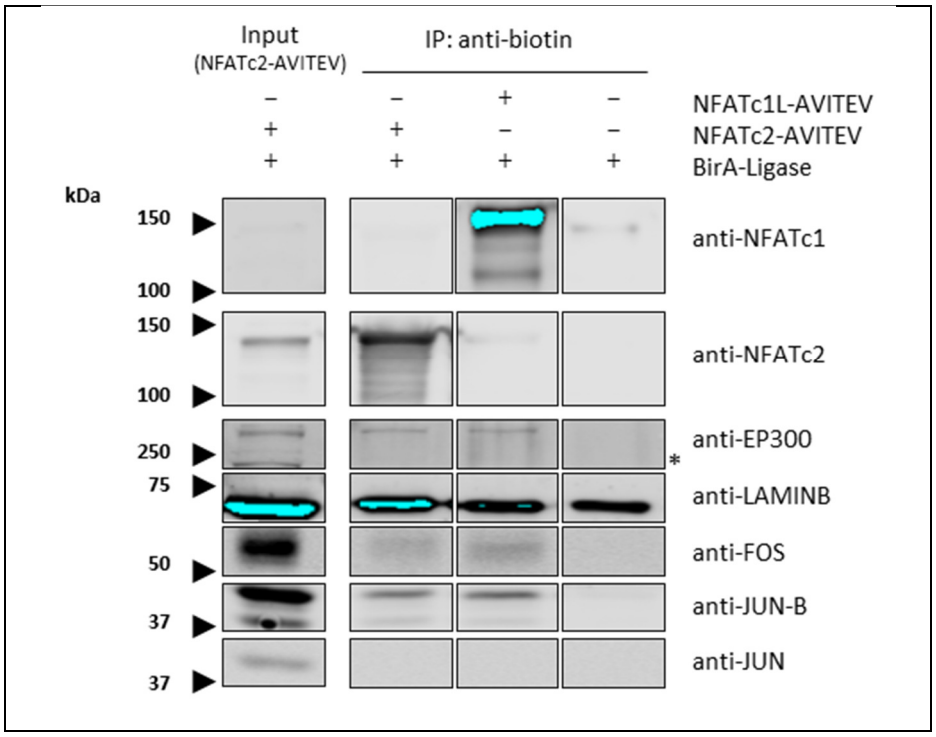

FIGURE 16. Co-immunopurification of known NFAT interacting proteins. Jurkat cells expressing the indicated transgenes were stimulated with PMA/ionomycin for 2 h. NFATc1L-AVITEV or NFATc2-AVITEV containing complexes were isolated from nuclear extracts with streptavidin-coupled agarose beads and eluted by TEV protease cleavage and the eluates were analyzed by immunoblotting. Cells expressing only BirA-ligase were used as control cells. * marks a non-specific band of the EP300 antibody. Only the input sample from NFATc2-AVITEV overexpressing cells is shown. Images are representative for two individual experiments.

The level of enrichment of FOS, JUNB and EP300 was lower than that observed for the NFAT proteins. It is a common observation in CoIP experiments that the bait proteins are by far more enriched than the prey proteins, resulting from a weaker and more transient nature of most protein-protein interaction compared to the strong interaction of epitope-tag systems. As we had expected, the structure protein Lamin-B was not specifically enriched with NFAT, since it was detectable also in the negative control's eluates in comparable amounts.

In addition, we performed similar experiments with NFATc1S overexpressing cells (data not shown). Analogously to the other isoforms, NFATc1S was specifically enriched by the use of the biotin beads and was subsequently eluted from the beads by TEV protease cleavage. In general, all detected protein signals from the eluates were much weaker than in the experiments using NFATc2 or NFATc1L as bait proteins, probably due to the lower level of over-expression of NFATc1S (data not shown). However, we observed specific co-purification of FOS together with NFATc1S, which was clearly over background (data not shown). Altogether, these experiments showed that our system could be used to confirm already described interactions of NFATc1 and NFATc2 with other proteins. Thus, we were confident

that this experimental setup could serve us to uncover so far unknown NFAT protein interactions.

3.2.5. Mass Spectrometric Analyses of NFAT Containing Protein Complexes

As shown in the previous chapters, we had successfully established Jurkat cells lines that overexpress epitope-tagged forms of human NFAT proteins. Furthermore, we were able to isolate NFAT containing protein complexes from these cells by the help of the AVITEV tag. Finally, we confirmed selected known NFAT protein-interactions when we analyzed these isolated protein complexes by western blot.

Western blot analysis of protein co-purification experiments can be used to confirm and study protein interactions. However, this is in most cases limited to the investigation of already known or suspected interactions, because specific antibodies are used for the detection of interacting proteins. In recent years, the combination of protein co-purification with mass spectrometric read-out proved to be a powerful tool to identify protein-protein interaction in an unbiased – and hitherto unseen comprehensive – manner (see SECTION 1.4.2). We intended to use this powerful method to identify so far unknown NFAT interacting proteins. Therefore, we aimed to analyze the purified, NFAT containing protein complexes by SILAC based semi-quantitative mass spectrometry. A pre-requisite for this type of experiment is the labeling of the cellular proteins with stable isotopes (see CHAPTER 1.4 and 3.1.3)

3.2.5.1. Design of CoIP-MS Experiments to Identify Proteins that Interact with NFAT

In order to use mass spectrometric technology to identify NFAT interactors, we differentially labeled pairs of NFAT-AVITEV expressing bait cells and corresponding control cells with stable isotopes (TABLE 4). To this end, the cells were grown in heavy or light SILAC medium, respectively, for ten days to achieve comprehensive labeling. The labeling allows distinguishing signals from both samples even out of one mixture, as well as easy semi-quantitative quantification of protein abundance between the samples (FIGURE 5, page 23).

For experiments with NFATc2 and NFATc1L, we used control cells that overexpress a tag-less (i.e. wild-type) form of the respective proteins additional to the biotin ligase BirA (TABLE 4). This was done to exclude that NFAT induced differences in protein expression between bait and control cells introduce an artificial bias into the experiments. However, a recent report from another group indicated that in general, transgene induced alterations in protein expression should not compromise the results from MS-based protein interaction[189]. For

technical reasons, control cells overexpressing only the biotin ligase were used in the experiments with NFATc1S.

All cells were stimulated for 2 h with PMA and ionomycin. Subsequently, NFAT complexes were isolated as before (see CHAPTER 3.2.4), with the only exception that beads with bound protein complexes from the control and bait experiments were mixed after the first washing step and thereafter treated as one sample.

TABLE 4. Labeling approach of bait and control cells for the mass spectrometric analyses of NFAT containing protein complexes.

		Bait cells		Control cells	
Experiment		Transgenes	SILAC label	Transgene(s)	SILAC label
NFATc2	(1)	BirA + NFATc2-AVITEV	Light	BirA + NFATc2	Heavy
	(2)		Heavy		Light
NFATc1S	(1)	BirA + AVITEV-NFATc1S	Light	BirA	Heavy
	(2)		Heavy		Light
NFATc1L	(1)	BirA + NFATc1L-AVITEV	Light	BirA + NFATc1L	Heavy
	(2)		Heavy		Light
	(3)		Heavy		Light

After elution by TEV cleavage, the eluates were separated on a SDS-PAGE and each lane was cut into 16 slices, followed by in-gel tryptic digest. The peptides were analyzed by RP-HPLC coupled to an ESI-orbitrap-MS/MS device, and identification and quantification was done by MaxQuant software[217]. This software quantifies the heavy-to-light ratio of each detected peptide and assigns the detected peptides to their precursor proteins. By averaging several heavy-to-light peptide-ratios for a given precursor protein, a heavy-to-light ratio for the protein is generated. This ratio can be interpreted as an enrichment value between the paired experiments (in this case, bait- versus control-CoIP, TABLE 4). All experiments were performed twice including a label swap, i.e., bait cells were grown in light medium in the first run and in heavy medium in the second run, while control cells were labeled vice versa (TABLE 4). A third run was performed for NFATc1L with heavy-labeled bait cells. To show up in the results, we demanded a protein to be identified by at least two unique peptides in an individual MS run.

3.2.5.2. Overview of MS Analyses of NFAT Containing Protein Complexes

With the aim of identifying so far unknown NFAT interaction partners, we had isolated protein complexes using either NFATc1S, NFATc1L or NFATc2 as a bait protein. Subsequently, these protein complexes were analyzed by semi-quantitative mass spectrometry. The experiments were run in duplicate for NFATc1S and NFATc2 or in triplicate for NFATc1L.

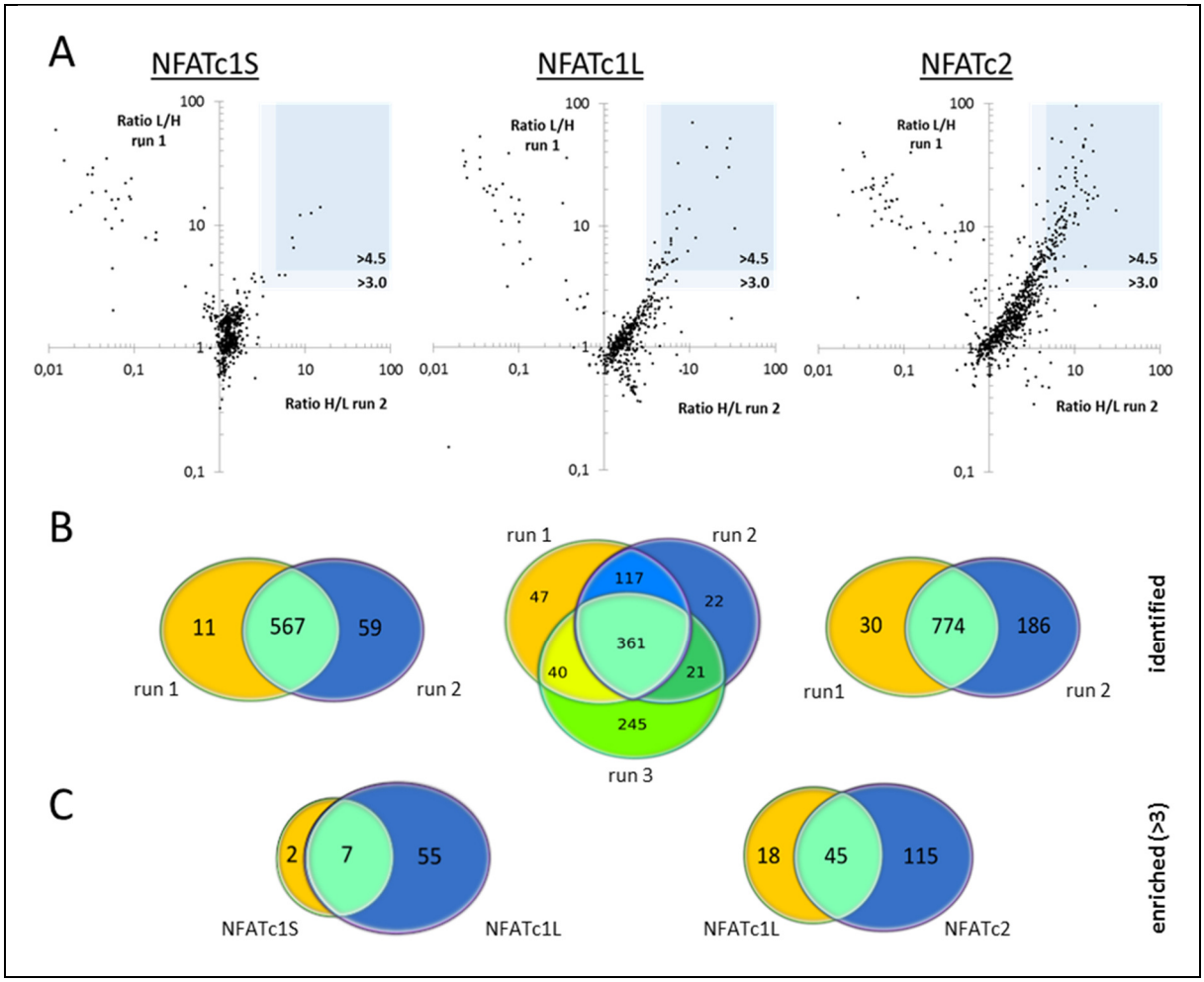

FIGURE 17. Overview of the MS analyses of NFAT co-immunopurifications. A: The charts show the combined heavy-to-light or light-to-heavy ratios, respectively, over two experiments. High values indicate proteins that were enriched together with the NFAT proteins. Blue squares mark enrichment factors of 3 or 4.5, respectively. Logarithmic scale. B: Venn diagrams that show the overlap of identified proteins from experimental duplicates or triplicates. Left: NFATc1S, center: NFATc1L, right: NFATc2. C: Venn diagrams that show the overlap of enriched proteins (factor >3) between NFATc1S and NFATc1L (left) or NFATc1L and NFATc2 (right), respectively.

TABLE 5. Overview of quantified proteins by co-immunopurification/mass spectrometry.

Experiment	Quantified proteins				Enriched by factor		Enrichment of bait		
(bait)	Run1	Run2	Run3	in 2 runs	>3	>4.5	Run1	Run2	Run3
NFATc1S	578	626		567	9	5	5.8	19.3	
NFATc1L	565	521	667	539	63	39	9.5	>20	15
NFATc2	804	960		774	160	91	>20	10.5	

Overall, between 500 and 800 proteins were identified and quantified in each experimental run (FIGURE 17B and TABLE 5). Most proteins (82-98 %) that were identified in one run of one experiment were also identified in a second run (FIGURE 17B), which points towards a high reproducibility of the MS measurement and data interpretation. The third run for NFATc1L, which originated from a separate sample preparation, showed a slightly decreased, but still substantial overlap with the two other runs (58-78 %). For further analyses, we regarded only those proteins that were identified in at least two individual MS runs.

In FIGURE 17A, the combined heavy-to-light and light-to-heavy ratios from paired experiments were blotted to visualize the specific enrichment of proteins. A ratio near 1 means that a protein originates from the paired CoIPs (CoIPs using bait or control cells) in the same quantity, or in other words, it is not enriched over background together with the NFAT bait-protein. In contrast, higher ratios indicate that a protein is enriched together with the bait protein in one of the CoIPs (FIGURE 5).

Generally, values below 2 were mostly regarded as non-significant. However, the definition of a certain cut-off value that divides potential interactors from background proteins remains arbitrary. Depending on the experiment, enrichment factor cut-offs of as low as 2 have been used to divide background from potential interactors by others[231,232]. In principle, higher enrichment values raise the confidence of a detected interaction. For our experiments, we considered proteins with a ratio of at least 3 in both experiments as enriched, i.e. as potential interactors. We set a further cut-off at a ratio of 4.5 and regarded proteins above this threshold as potential interactors with increased confidence (TABLE 5 and FIGURE 17A). For a more comprehensive consideration of these cut-offs, please refer to CHAPTER 4.2.1.4.

In order to get a first insight into the quality of the datasets, we looked whether our bait proteins were enriched in the MS data. Indeed, all bait proteins were enriched between 5.8 fold and more than 20 fold in each single run (TABLE 5). Since we saw an enrichment of the bait proteins, we were confident that the experiments had worked in general. Thus, we took a closer look at the other proteins that were enriched in the dataset (TABLE 6 and FIGURE 17). A selection of the enriched proteins from all experiments is listed in TABLE 6. Complete lists of all enriched proteins from the individual experiments, including counts of unique peptides and enrichment ratios can be found in the appendix (TABLE A 1-A3, page VII). The data from the three experiments will be highlighted separately in the following sections. For enriched proteins, enrichment ratios will be given in brackets.

TABLE 6. **Overview of selected potential NFAT interactors as identified by mass spectrometric analysis.** The listed gene products were identified by at least two unique peptides and were enriched by a factor of >4.5 (++) or >3 (+) in at least two experiments, or in only one experiment ([+]), respectively. Proteins depicted in bold are previously known interactors of NFAT proteins, interaction of proteins marked with * was confirmed by CoIP-WB in the present study.

Gene ID	Enrichment with			Gene ID	Enrichment with		
	NFATc1L	NFATc1S	NFATc2		NFATc1L	NFATc1S	NFATc2
Bait				**SWI/SNF-complex (continued)**			
NFATc1	++	++		SMARCA4	+		+
NFATc2	++		++	SMARCA5			+
Transcription factors				SMARCB1	+		
Basic leucine zipper				SMARCC1	+		+
ATF7	++		++	SMARCC2	++		+
CREB1 *	++	+	++	SMARCD1	+		+
FOS *	[+]		++	SMARCD2	++		+
JUN *			++	SMARCE1	++		+
JUNB *	++		++	**14-3-3 proteins**			
MAFG			++	YWHAB			++
MAFK			++	YWHAE			++
Zinc finger				YWHAG			++
BCL11B	+		++	**YWHAQ**			++
EGR1			++	**YWHAZ**			++
EP300 *	++		++	**Ser/Thr kinases**			
GATAD2A			++	CHEK1 *	++		++
IKZF1 *	++	+	++	**CSNK1D**	++	++	++
IKZF2 *	++		++	**GSK3B ***	++	++	++
POGZ			++	NEK6/NEK7	++		[+]
PRDM15			++	PLK1	[+]		++
UHRF1			++	**Response to DNA damage**			
YY1	++		+	LIG3	+		++
ZBTB40	++		(+)	**PARP1**			++
ZNF131			++	POLG			++
ZNF148			++	PRKDC			++
ZNF217	[+]		++	RFC2	++		++
ZNF384			++	RFC3			++
Other				RFC4	+		++
BTAF1			++	RFC5		+	++
CBFB	+		[+]	RPA1	+		++
CTBP1	+		++	RPA2			++
ETV6	[+]		++	RPA3			++
FOXK1	++		++	XRCC1			++
FOXK2	++		[+]	XRCC5	+		++
HIRA			++	XRCC6	++		++
IFI16	+		++	**Miscellaneous**			
LEF1	++		++	ALDH18A1			++
NFYB			++	CABIN1			++
NFYC	[+]		++	CACYBP			++
RUNX1 *	+		++	CAD	[+]	+	++
SATB1 *	+		++	CHAMP1	+		++
SUPT6H			++	ERAL1			++
TFAM			++	FXR	++		
TFCP2			++	HSPA1A			++
Regulation of transcription				HSPA5	+	[+]	++
CBX5			++	HSPA9	+		+
CHAF1B			++	KIF2C	[+]		++
CREBBP	++			KIF4A			++
DEK			++	LRRC47	+		++
ERCC3			++	MOSPD1	++		
HLTF	++		++	MRPL39			++
IRF2BP1			++	MTHFD2	++		++
IRF2BP2			++	RANBP9	++		++
SCAI *	++	++	++	RPTOR *	++		++
SSRP1			++	SSBP1			++
TP53BP1			++	SUCLA2			++
TRRAP	++		++	TUFM	+		++
UHRF1			++	UBE2S			++
SWI/SNF-complex				VAPA	++		+
ACTL6A	+		+	WDR26	[+]		++
ARID1A	++		++	WDR48 *	++	++	++
DPF2	++		++				

3.2.5.3. Protein-Protein Interactions Involving NFATc1S and NFATc1L

In order to identify interaction partners of NFATc1, we had performed CoIP-MS experiments using either epitope-tagged NFATc1S or NFATc1L as a bait protein. Two parallel CoIP-MS runs were performed using the short variant of NFATc1 as a bait. For the second run, the SILAC labeling was switched (TABLE 4). Out of the 567 proteins that were quantified in both runs, nine proteins were enriched together with NFTAc1S by a factor of at least three in both runs (FIGURE 17A and TABLE 5). Of these proteins, casein kinase-1 (isoforms α and isoform δ/ε), GSK3β (enrichment factors of 8.6 and 12.1) and *cyclic AMP response element binding protein-1* (CREB1, 5.9, 3.9) are already described to interact with NFATc1[152,233]. The enrichment of these known NFAT interacting proteins showed that our experimental setup was capable of producing valid data. Interestingly, the transcription factor Ikaros (IKZF1, 5.1, 3.9) was also enriched, as were the proteins *WD repeat domain 48* (WDR48, 7.4, 6.5), *suppressor of tumor cell invasion protein* (SCAI, 15.2, 13.9), the aspartate carbamoyl transferase CAD (3.3, 3.5) and the *replication factor C subunit 5* (RFC5, 3.1, 3.8).

For the analysis of NFATc1L containing protein complexes, three CoIP experiments were done with NFATc1L as a bait protein: two runs with switched labels that were performed in parallel and one standalone experiment (TABLE 4). In total, 539 proteins were identified and quantified in at least two runs. Out of these, 63 proteins were enriched by a factor of >3 and 39 by a factor of >4.5 in at least two experimental runs (FIGURE 17 and TABLE 5). Almost all proteins that were found to co-purify with the short isoform of NFATc1 were enriched with the long isoform, too (FIGURE 17C). This includes the known NFAT interacting proteins GSK3β (enriched by factors of 15.9, 44.4, 27.9), CK1 (27.2, 42.6) and CREB1 (28.5, 30.4, 3.5). The only exceptions were CAD and RFC5, which were enriched together with the short, but not with the long variant of NFATc1. Contrarily, the known NFAT interaction partners EP300 (32.5, 24.5) and JUNB (7.5, 14.5) were found to be enriched with NFATc1L only. Again, the enrichment of known NFAT interacting proteins enhanced the status of the dataset.

In addition to the known NFAT interactors, our CoIP-MS elements revealed a large set of yet unknown, potential interaction partners of NFATc1L (TABLE 6). To get an insight into the functional implications of our datasets, the enriched proteins were functionally annotated using Database for Annotation, Visualization and Integrated Discovery (DAVID 6.7) software package (http://david.abcc.ncifcrf.gov/home.jsp). The analysis revealed that 15 out of the 63 enriched proteins were transcription factors, including Ikaros (enriched by factors of 7.0, 9.6, and 7.0), Helios (9.8, 13.8), CREB1, JUNB, RUNX1 (3.9, 4.7, 3.0), LEF1 (5.7, 6.1, 3.8), SATB1 (4.0, 3.5, 3.2), ATF7 (5.4, 12.5), FOXK1 (3.9, 7.3, 6.1) and FOXK2 (8.2, 6.0) (TABLE

6). Further 17 enriched proteins were assigned to the regulation of transcription, e.g. the protein SCAI (21.1, 25.2, 19.9), or several members of the SWI/SNF chromatin-remodeling complex. Thus, roughly half of the enriched proteins is related to transcriptional regulation. Additionally, a group of nine enriched proteins is known to be involved in the repair of DNA damage.

We performed experiments to confirm some of the protein interactions with the different NFATc1 isoforms by CoIP with western blot read-out. Specifically, we intended to verify the interaction of NFATc1 with selected known NFAT partners as controls (JUN, CREB1, EP300 and GSK3β) and with some of the newly identified, potential NFAT interacting transcription factors (*special AT-rich sequence binding homeobox 1* (SATB1), Helios, Ikaros). We also included the proteins WDR48 and SCAI into the analysis, which were co-purified with both NFATc1 isoforms, as well as the mTOR complex-1 member r*egulatory associated protein of mTOR* (RPTOR, enriched by factors of 31.0, 1.8 and 19.5 together with NFATc1L). To this end, we stimulated Jurkat cells overexpressing either NFATc1S-AVITEV or NFATc1L-AVITEV along with BirA for different periods of time. Cells that overexpress wild-type NFATc1L and BirA were used as a negative control and treated analogously. Afterwards, we performed CoIPs just as before and analyzed the eluates by immunoblot (FIGURE 18).

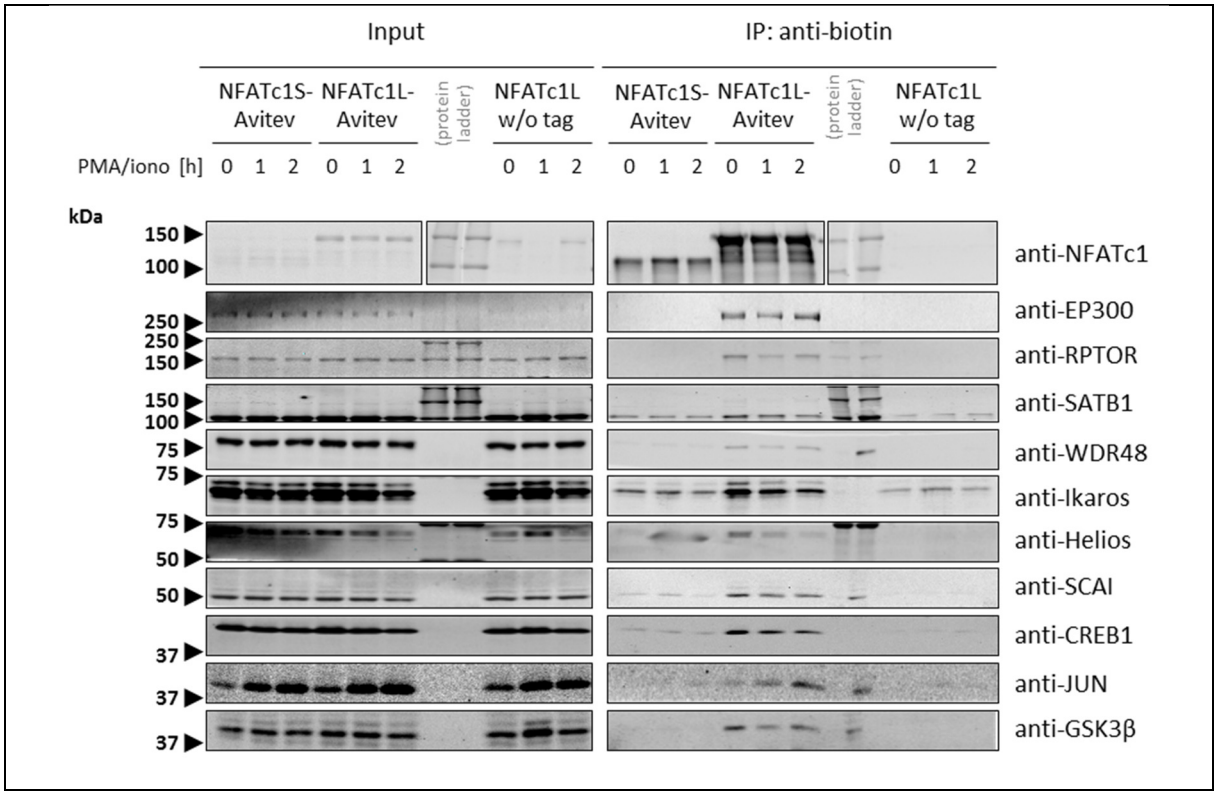

FIGURE 18. Co-immunopurification of NFATc1 complexes. Jurkat cells expressing the indicated variants of NFATc1 along with BirA were stimulated with PMA/ionomycin. NFATc1-AVITEV containing complexes were isolated from nuclear extracts with streptavidin-coupled agarose beads and eluted by boiling in Laemmli buffer. The eluates were analyzed by immunoblotting. Cells over-expressing wild-type NFATc1L (without tag) and BirA-ligase were used as control cells. Images are representative for two independent experiments.

As seen before (FIGURE 14), overexpressed NFATc1 was already present in the nucleus of unstimulated cells and the amount of isolated bait proteins did not differ between unstimulated and stimulated cells. In line with earlier experiments (FIGURE 16), EP300 and JUN proteins were co-purified with NFATc1L. These interactions were specific, because clearly minor amounts of both proteins were detected in the eluates of the control experiment. The interactions of NFAT with EP300 and JUN are well described and served us as a positive control in this experiment[169,230]. Moreover, we observed co-purification of the NFAT kinase GSK3β and of the transcription factor CREB1 along with NFATc1L; both were known NFATc1 interacting proteins[152,233].

To our contentment, we also observed specific enrichment of those proteins whose interaction with NFATc1L had not been described, but was suggested by the MS results. The proteins RPTOR, SATB1 WDR48, SCAI, Ikaros (IKZF1), and Helios (IKZF2) all were specifically enriched together with the long variant of NFATc1 (FIGURE 16). The detected interactions were not altered by the stimulation of the cells. For these proteins, whose western blot signal intensity increased (e.g. JUN) or decreased (e.g. Helios and Ikaros) over stimulation time, the alterations clearly correlated with the altered expression levels as seen in the input samples. Thus, we did not observe any alterations in the interaction between NFATc1L and the tested proteins within 2 hours of stimulation.

For the short variant of NFATc1, the results were less clear. Owing to the minor level of overexpression of the bait protein, the levels of all co-purified proteins were considerably lower and only slightly (if at all) increased compared to the control experiment. Therefore, it was not possible to confirm or exclude the interactions between NFATc1S and other proteins from this kind of experiment.

To summarize, by performing CoIP-MS experiments, we identified five proteins as potential and so far unknown interaction partners of NFATc1S, and more than 50 potential interaction partners of NFATc1L. Out of these, we exemplarily confirmed the interactions of SATB1, RPTOR, WDR48, Ikaros, Helios, and SCAI with the long variant of NFATc1 by CoIP-WB, underscoring the validity of our approach.

3.2.5.4. Protein-Protein Interactions Involving NFATc2

Analogously to the experiments that we had performed with NFATc1, we performed two parallel CoIP-MS runs using NFATc2 as a bait protein. For the second run, the SILAC labeling was switched (TABLE 4). In total, 774 proteins were identified and quantified in both MS runs with NFATc2-AVI as a bait (FIGURE 17). Out of these, 160 proteins were enriched by a factor of >3 and 91 proteins by a factor of >4.5 in comparison to the control experiment

(FIGURE 17 and TABLE 5). The latter group contained our positive controls FOS, JUN, JUNB and EP300 (all with enrichment factors between 12 and 20), as well as further proteins that were described to interact with NFATc2: 14-3-3ζ (4.9, 16.0), casein kinase-1 (12.2, 33.7), EGR1 (6.8, 25.5), IRF2BP2 (7.7, 20.4), GSK3β (9.8, 10.6))[153,157,181,183,234] or other NFAT isoforms (CREB1 (16.0, 66.2), PARP1 (7.1, 21.1))[164,233]. The enrichment of these known NFAT interactors supported the validity of the MS data (TABLE 6).

Interestingly, 45 of the proteins that were enriched with NFATc1L were also found to be enriched together with NFATc2 (FIGURE 17C and TABLE 6), which is 71 % of the first group. This indicates that there is a substantial overlap of interaction partners of NFATc1L and NFATc2. This finding is not surprising, due to the high degree of conservation between both isoforms and the functional overlap that is described for different NFAT family members (see SECTION 1.3.5).

As before, the list of enriched proteins was analyzed for functional annotation clusters using the DAVID 6.7 software package. Again, a large proportion of the enriched proteins is involved in the regulation of transcription (82 out of 160, or 51 %), including 42 designated transcription factors. Another major group of 28 proteins is assigned to be part of the DNA damage response. As seen for NFATc1L, several members of the SWI/SNF chromatin-remodeling complex were enriched together with NFATc2. Furthermore, seven members of another chromatin-remodeling complex, the NuRD complex (GATAD2A, CHD4, HDAC1, RBBP4, MTA1, MTA2, and MBD3) were enriched in CoIPs with NFATc2, but not with NFATc1.

We carried out additional experiments to prove some of the protein interactions with NFATc2, which were suggested by the MS data. We performed CoIPs from cells over-expressing either NFATc2-AVI and BirA, or wild-type NFATc2 and BirA just as before and analyzed the eluates by western blot (FIGURE 19). By this, we confirmed the interaction between NFATc2 and RPTOR (enrichment values of 17.1 and 20.8), WDR48 (5.9, 12.8), CHEK1 (13.4, 4.7), SATB1 (6.2, 10.4), Ikaros (16.7, 41.0), Helios (10.4, 62.3), SCAI (12.7, 45.8), runt-related transcription factor 1 (RUNX1, 7.0, 14.4) and CREB1 (16.0, 66.2), which were all suggested by the CoIP-MS data for the first time.

To summarize, by performing CoIP MS experiments, we could identify a large list of so far unknown, potential interaction partners of NFATc1 and NFATc2. Interestingly, our data suggest that many of these proteins can interact with both NFATc1 and NFATc2. As assumed, a large proportion of the proteins is involved in the regulation of transcription. The quality of

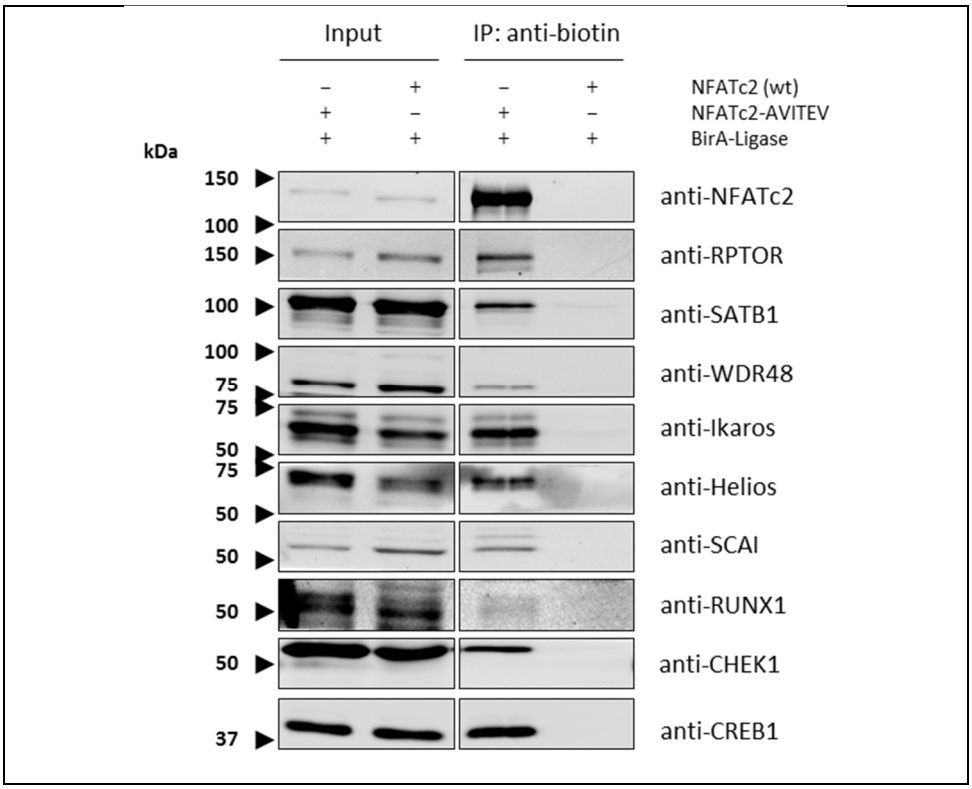

FIGURE 19. Co-immunopurification of NFATc2 complexes. Jurkat cells expressing the indicated transgenes were stimulated with PMA/ionomycin for 2 h. NFATc2-AVITEV containing complexes were isolated from nuclear extracts with streptavidin-coupled agarose beads and eluted by TEV protease cleavage and the eluates were analyzed by immunoblotting. Cells over-expressing NFATc2 wild-type (without tag) and BirA-ligase were used as control cells. Images are representative for two independent experiments.

this list of potential NFAT interactors is underscored by the presence of several known NFAT interacting proteins. Furthermore, we were able to confirm a handpicked subset of newly identified interactions by CoIP-western blot (e.g. RUNX1, Ikaros, Helios and RPTOR). Thus, it is very likely that further proteins from the list are indeed interaction partners of NFAT proteins.

3.2.6. NFATc2 and Ikaros Interact in Primary Human T Helper Cells after TCR Stimulation

During the present study, we have isolated NFAT containing protein complexes from Jurkat cells that overexpress epitope-tagged variants of NFATc1 or NFATc2. By performing MS analysis of these protein complexes, we identified numerous potential interaction partners of human NFAT proteins. A subset of these suggested interactions could be confirmed by western blot analysis of analogously yielded, NFAT-containing protein complexes.

CoIP-western blot with overexpressed, epitope-tagged proteins is widely used to confirm suggested protein-protein interactions. However, such studies suffer the caveat of non-

physiologic conditions. The presence of the tag and aberrant high expression levels of one or both proteins might lead to protein-protein interactions that would not occur *in-vivo*. Therefore, we aimed to prove the observed NFAT interactions under more physiological conditions. At first, we tried to establish NFAT CoIPs from wild-type Jurkat cells using several antibodies specific for NFATc1 and NFATc2. This approach avoids the use of overexpression and the presence of a protein tag for isolation. Unfortunately, this was not successful in our hands, as we did not observe the co-purification of any protein, not even of the positive controls JUN, FOS and EP300 (data not shown), together with NFATc1 or NFATc2.

As an alternative method to confirm protein-protein interactions under more physiological conditions, we employed the *proximity ligation assay* (PLA)[235]. In this assay, the recognition of two proximate proteins by differently labeled antibodies results in signals that can be detected by fluorescence microscopy (for further explanations, please refer to CHAPTER 2.2.1.8). By this method, protein-protein interactions can be studied within primary wild-type cells and on a single cell-level.

Exemplarily, we aimed to confirm the interaction between NFATc2 and Ikaros in primary human T cells by using the PLA. Ikaros is a transcription factor that is exclusively expressed in hematopoietic cells and is an important regulator of lymphocyte differentiation and function[117,236,237]. Thus, both Ikaros and NFAT are involved in the regulation of T cell activation and differentiation. While an interaction of both transcription factors had not been shown yet, our previous CoIP data suggested such an interaction.

To test whether NFAT and Ikaros interact in primary human T helper cells, we isolated CD4 positive T cells from the blood of healthy donors. The cells were stimulated with PMA and ionomycin or with anti-CD3/CD28-coupled beads for 1 h and the PLA was performed using a monoclonal mouse-anti-NFATc2 antibody and a polyclonal rabbit-anti-Ikaros antibody. As PLA probes, secondary antibody conjugates against rabbit- and mouse-Ig were used. An automated software was employed to determine the number of signals per cell from at least 170 individual cells.

Untreated T helper cells showed only few PLA signals per cell (median = 1, FIGURE 20A). Strikingly, the median amount of signals per cell increased to 16 when cells were stimulated with PMA and ionomycin, while the addition of CsA reduced the amount of signals per cell to the level of unstimulated cells. Cells stimulated with anti-CD3/CD28 beads also showed an augmented signals-per-cell ratio (median = 9). While there was a lower frequency of cells with five and more signals per cells compared to PMA/ionomycin stimulated cells

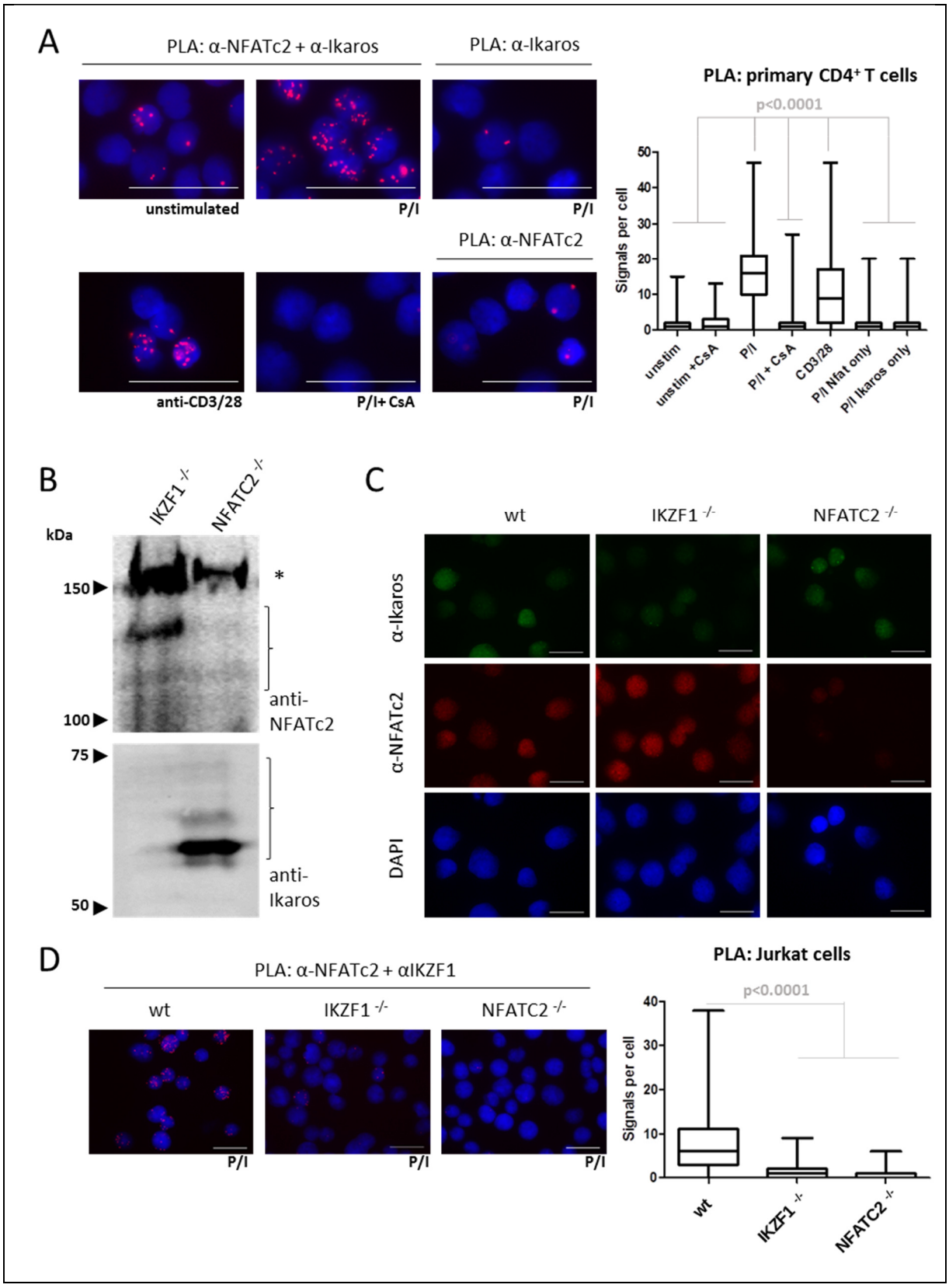

FIGURE 20. Confirmation of NFATc2-Ikaros interaction by proximity ligation assay (PLA). A: PLA using primary CD4+ T cells. Nuclear staining (DAPI) is depicted in blue and PLA signals are depicted in red. For control experiments, one of the primary antibodies was exchanged for an isotype-matched control antibody. B and C: Analysis of CRISPR/Cas9 induced knock-out of IKZF1 and NFATc2 in Jurkat cells. Jurkat IKZF1$^{-/-}$ and NFATC2$^{-/-}$ cells show no signal for the respective protein in immunoblot staining (B) and reduced signal in immuno-histochemistry staining (C). D: PLA using Jurkat wt, IKZF1$^{-/-}$ or NFAT$^{-/-}$ cells. All images are representative for two independent experiments. P/I: PMA/ionomycin, CsA: Cyclosporine A. * marks an unspecific band of the used NFATc2 antibody. P-values by Kruskal-Wallis test. Size bars shown are 30 µm.

(62 % versus 92 %), the median signal count of these subsets did not differ significantly (data not shown). Altogether, this indicates that NFATc2 and Ikaros interact in stimulated, but not in unstimulated human T helper cells.

We performed further control experiments to test the specificity of the signals. When one of the antibodies was exchanged for an isotype matched control antibody, again only few signals per cell (median = 1) were detectable in PMA/ionomycin treated cells (FIGURE 20A). A second independent experiment confirmed all findings from the former one (data not shown). Median signals per cell were augmented in PMA/ionomycin (median = 10) and anti-CD3/CD28-beads stimulated cells (median = 4) compared to unstimulated or CsA treated cells (both: median = 0). The differences between stimulated and unstimulated, CsA treated and control cells were highly significant ($p<0.0001$) in both experiments, as confirmed by Kruskal-Wallis test.

As with all antibody dependent assays, the PLA requires high quality antibodies to produce reliable results. Importantly, even minor cross reactivity of one antibody could lead to false-positive signals that dominate the PLA. Hence, isotype controls are only weak controls, as they cannot resemble cross-reactivity of the used antibodies. Therefore, we generated knock-out Jurkat cell lines for NFATc2 and Ikaros using the CRISPR/Cas9 system to control whether the PLA signals in our system originate from specific binding of the antibodies to NFATc2 and Ikaros. The nuclease Cas9 is guided by an RNA to a specific genetic locus to introduce double strand breaks[238–240]. These are repaired by the error-prone non-homologous end-joining pathway, causing a phenotypic knock-out by nonsense or frame-shift mutation. Transfected Jurkat cells were expanded clonally and phenotypic knock-out was detected and confirmed by western blot (FIGURE 20B). Immuno-histochemistry staining with primary and secondary antibodies showed that the NFATc2 signal was strongly reduced in the NFATc2 knock-out cells compared to wild-type cells (FIGURE 20C). In Ikaros knock-out cells, signals originating from Ikaros antibody were also reduced, albeit to a lesser extent.

We used these knock-out cell lines along with wild-type Jurkat cells to perform a PLA experiment under identical conditions, i.e. using the same antibodies against Ikaros and NFATc2. In wild-type cells, up to 40 signals per cell (median = 6) were detected (FIGURE 20D). In contrast, less than 10 signals per cells were detected from Ikaros knock-out and NFATc2 knock-out cells (median = 1 and 0, respectively). In a second experiment, median signals per cell count was 2 for the wild-type cells and for the knock-out cells 1 and 0, respectively (data not shown). In both cases, the differences between wild-type and the knock-outs were highly significant ($p<0.0001$) as confirmed by Kruskal-Wallis test. This confirmed that the signals in

the PLA are strongly dependent on the presence of both NFATc2 and Ikaros, whereas unspecific binding events do not account for the highly augmented signals in stimulated cells.

To summarize, these experiments provide strong evidence that Ikaros and NFATc2 interact in primary human T helper cells after stimulation with PMA and ionomycin or after TCR/co-receptor engagement (FIGURE 20). The degree of interaction per cell seemed to be independent of the mode of stimulation, while interaction of both proteins was detected in a higher number of cells after PMA/ionomycin stimulation (see above). Thus, we could confirm the interaction between these two transcription factors, which was for the first time suggested by the CoIP-MS experiment, via an unrelated, orthogonal method. This again strengthens the validity of our experimental approach to search for NFAT interactors by CoIP-MS.

3.2.7. NFATc2 Interactions Divide into DNA-Dependent and DNA-Independent

The interaction of nuclear proteins can be mediated or stabilized via binding to DNA molecules. To prove whether the interaction between NFATc2 and its interactors are dependent on DNA binding, we performed co-purification experiments in the presence or absence of the DNA intercalating agent GelRed. GelRed stretches the DNA, thus disturbing interaction of DNA binding proteins to the DNA. As a result, interactions that are solely mediated or strengthened by DNA binding should be reduced in the presence of GelRed.

As shown in FIGURE 21, comparable amounts of NFATc2 and GFP were obtained from CoIP experiments in the presence or absence of the agent (upper panel). Interestingly, the addition of GelRed reduced the amount of co-purified protein for a subgroup of the regarded proteins, albeit not for all. Strikingly, the group of affected proteins consisted of transcription factors only (RUNX1, Helios, Ikaros, JUN, FOS, SATB1, FIGURE 21, lower panel). This indicates that the interaction of NFATc2 with other transcription factors is often mediated or strengthened by DNA binding.

It is noteworthy that the addition of GelRed did not completely abrogate any of the observed NFAT protein interactions, which can be explained by two competing possibilities: First, the observed protein-protein interaction might be present, albeit weak in solution, but are strengthened by binding to the same DNA molecule or region. In the presence of GelRed, the latter enhancement is lost and the reduced signal corresponds to the remaining, weaker interaction that occurs in solution. Second, the observed protein-protein interactions might occur exclusively in the presence of DNA. However, the effect of GelRed disturbs only a portion of the formed DNA-transcription factor-complexes, while stronger, perhaps higher-

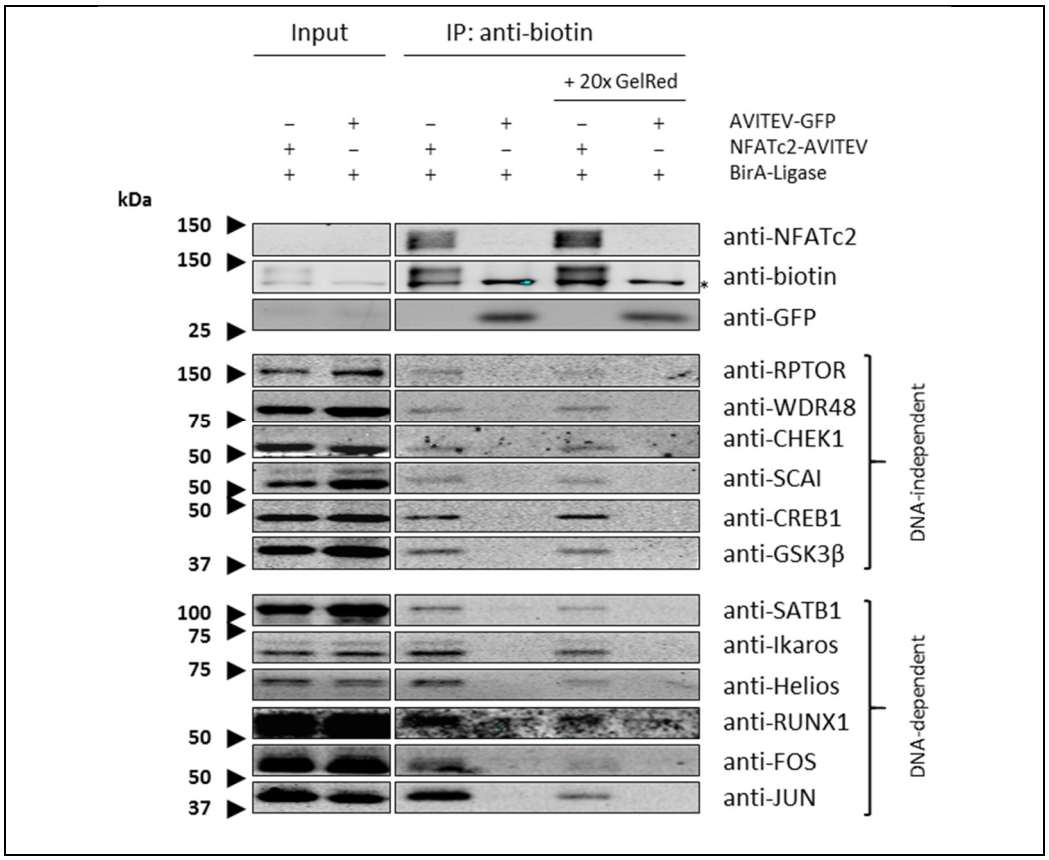

FIGURE 21. Dependency of NFATc2 interactions on DNA binding. Jurkat cells expressing the indicated transgenes were stimulated with PMA/ionomycin for 2 h. NFATc2-AVITEV or AVITEV-GFP containing complexes were isolated from nuclear extracts with streptavidin-coupled agarose beads in the presence or absence of the DNA intercalating agent GelRed. Proteins were eluted by boiling in 2x Laemmli buffer and eluates were analyzed by immunoblotting. Images are representative for three independent experiments.

order complexes are more stable and remain unaffected by the agent. It remains elusive which of both effects is relevant for each of the affected interactions, or whether even both effects contribute to the observed picture. In any case, the observed reductions in signal intensity demonstrated that the interaction of NFAT with the mentioned transcription factors is – at least in part – dependent on DNA binding.

In contrast, the interaction between NFATc2 and the transcription factor CREB1 was not affected by the presence of the intercalating agent. The same was the case for the interactions with RPTOR, WDR48, SCAI, GSK3β and CHEK1, which all are not known to bind directly to DNA (FIGURE 21, middle panel). Thus, the interaction of NFATc2 with these proteins appears to occur independent of DNA binding.

As a negative control for this experiment, we used nuclear extracts from cells that overexpressed a GFP fused to the AVITEV-tag. All tested proteins co-purified with the NFATc2-AVITEV fusion protein, but not with the AVITEV-GFP fusion protein. By this, we

proved that the enrichment of these proteins is dependent on the NFAT moiety of the fusion protein and is not mediated by the AVITEV tag.

To summarize, we showed that the interaction of NFAT with most of the tested transcription factors is reduced in the presence of GelRed, which indicates that these interactions are at least in part mediated by DNA binding. In contrast, NFAT and CREB1 seem to interact independently of DNA binding. The same is true for the interaction of NFAT and further proteins that are no designated transcription factors.

3.2.8. Co-Occurrence of NFAT DNA Binding Motifs with those of other Transcription Factors

Transcription factors constituted a large subset of the (potential) NFAT interactors that we had identified by CoIP-MS experiments (TABLE 6). The CoIPs in the presence of an intercalating agent had revealed that interaction of NFATc2 with several other transcription factors is at least in part mediated by DNA binding (FIGURE 21). Thus, we speculated that several of these enriched transcription factors cooperate with NFAT at the level of DNA binding, forming tripartite or higher-order complexes. In this way, sequence specific binding to vicinal DNA sequences might enhance protein-protein interactions, and the protein-protein interactions can enhance binding of both factors to a cognate DNA sequence. This mechanism could explain the reduced protein-protein interaction of NFAT with other transcription factors in the presence of GelRed. We hypothesized that if cooperative DNA binding is responsible for the observed interaction of NFAT with other transcription factors, then binding motifs for these transcription factors should be found enriched near those for NFAT.

3.2.8.1. Binding Motifs for AP-1 proteins, RUNX and Ets-Factors Are Enriched in Regions of NFAT Binding

To investigate this hypothesis, we took advantage of a recently published ChIP-Seq dataset that identified over 24.000 NFATc2 binding sites in primary murine $CD8^+$ T-lymphocytes one hour after stimulation[213]. We remapped the reads to the current mouse genome MM10 and extracted the peak regions (refer to chapter 2.2.3.1. for methodic details). The identified peak regions had a length range of 142 to 5816 base pairs, whereas 95 % of the peaks were within a range of 142 to 545 base pairs. The median length of all peaks was 234 base pairs.

Using the oPOSSUM software platform, known transcription factor binding motifs were mapped within these regions[241]. First, we examined which transcription factor binding motifs are enriched in this collection of regions of confirmed NFATc2 binding. As expected, NFAT binding motifs were highly enriched in the dataset (FIGURE 22, x-axis). Additionally, we found

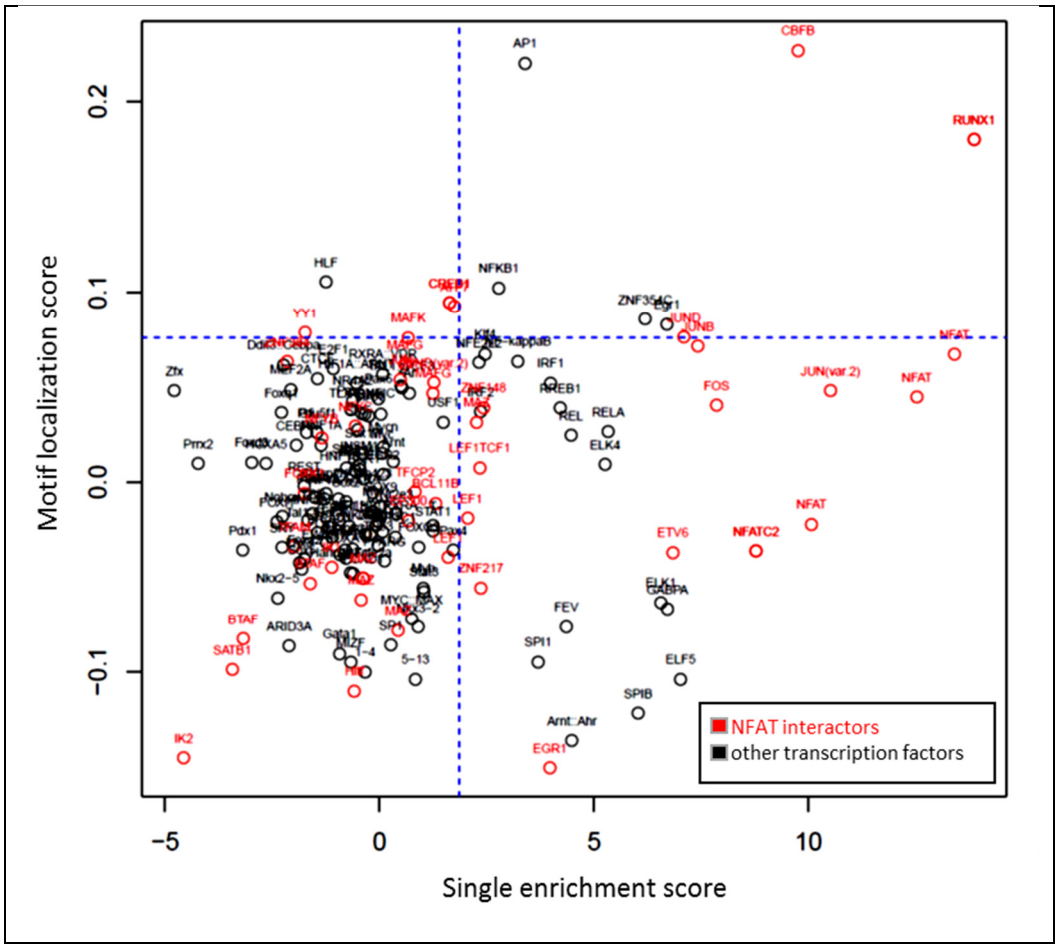

FIGURE 22. Occurrence and localization of transcription factor binding motifs in regions of NFATc2 binding. oPOSSUM was used to identify over-represented binding motifs for transcription factors in a dataset of NFATc2 ChIP-Seq peaks from activated murine $CD8^+$ T cells (x-axis). Furthermore, the localization of these motifs relative to present NFAT binding motifs was determined (y-axis). High values indicate that the motif is preferentially found in proximity to NFAT binding motifs. Transcription factors that were found enriched in the CoIP-MS experiments with NFAT proteins are depicted in red. The blue dashed line marks the level of significant enrichment compared to a matched background dataset.

a strong enrichment of motifs for AP1 like sites (JUN, JUND, JUNB and FOS), as well as RUNX binding motifs. To a lesser extent, also motifs for Ets-like transcription factors (ETV6, ELK1, ELK4 and ELK5) and κB sites were over-represented.

Thus, this analysis revealed the enrichment of several transcription factor-binding sites in the regions of NFAT binding, which indicates that these transcription factors are involved in the regulation of a significant subset of NFAT target genes in cytotoxic T cells. In other words, NFAT and AP1-, RUNX- or Ets-like factors might regulate an overlapping set of genes in those cells. However, the analysis did not provide information on whether these motifs occur in close vicinity to each other, which would allow cooperative binding.

To investigate the occurrence of binding sites in spatial relation to NFAT binding sites, we performed an anchored combination site analysis. Using this algorithm of oPOSSUM, we analyzed which transcription factor motifs are found more likely in the vicinity of the NFAT

motifs. Here, we found that especially AP1 and RUNX/CBFB binding motifs are found near the NFAT motifs (FIGURE 22, y-axis), which is in line with the results obtained from the original report of this dataset[213]. A weaker, but still significant enrichment in the vicinity of NFAT motifs was found for CRE (CREB1, ATF7), helix-like *transcription factor* (HLF) and NFκB (NFKB1) motifs.

3.2.8.2. Pairs of Binding Motifs for NFAT and AP1, CRE and RUNX Are Found Preferentially in a Distinct Distance and Orientation

During this study, we had identified more than 40 transcription factors as potential NFAT interacting proteins. Our previous analyses showed that the binding motifs of some of these transcription factors (e.g. those motifs for AP1- and RUNX- and CRE-binding-proteins) are preferentially found near NFAT DNA-binding motifs. Together, this hints towards the possibility that NFAT and the mentioned transcription factors cooperatively bind to composite DNA sequences.

In the case that two (or more) transcription factors cooperate in DNA binding, it is likely that they form a well-defined complex that relies on protein-protein interactions as well as protein-DNA interactions. The architecture of such a complex would more or less dictate the orientation and distance of the individual DNA binding domains. Thus, to allow for cooperative binding, the individual recognition sequences should occur in a certain orientation to each other and in a defined distance.

To determine whether any of the binding motifs of the discovered transcription factors preferentially occurs in a defined distance to NFAT binding motifs, we used the analytic tool *cobindR*[214]. This program recognizes pairs of transcription factor binding motifs in a given dataset and annotates the distance between both motifs. Subsequently the distribution of the distances is analyzed for over-represented distances.

FIGURE 23 shows the results for the association of NFAT motifs with these for AP1, which was by far the most significant association. The upper chart depicts the incidence of the observed distances of AP1 motifs relative to a recognized NFAT motif. Negative distance means the AP1 motif is found upstream of the (forwardly orientated) NFAT motif, while positive distances mean that the AP1 motif is found downstream. In the lower chart, a normalized background is added in red and a significance border in a red dashed line. There is a large amount of NFAT:AP1 motif pairs that occur in a distance of +1, which results in a very prominent peak at this site. After background subtraction, this combined binding motif appeared approximately 700 times in our dataset. Since the association between NFAT and AP1

is well described[150,213], this observation proved our concept and encouraged us to take a closer look at further pairs.

The *cobindR* data also revealed a highly significant enrichment of RUNX binding sites in direct vicinity to NFAT binding motifs (FIGURE 24A). The most common position of the RUNX motif in our dataset is -1 relative to a NFAT motif. This means, while the AP1 motif is preferentially located downstream of the NFAT motif, the RUNX motif is rather found one base pair upstream of it.

In contrast to the AP1 motif, the RUNX consensus motif (as the NFAT motif) is not palindromic. Therefore, we included the different possible orientations of both motifs into the *cobindR* analysis (FIGURE 24 B). Interestingly, only the forwardly orientated RUNX motif is found enriched at position -1 in relation to the forwardly orientated NFAT binding motifs (FIGURE 24B, upper panel), while for the reverse orientation, no distance to NFAT is enriched over background (FIGURE 24B, lower panel). When all four possible orientations of the motifs are regarded, only the combination of the forward RUNX motif upstream to the forward NFAT motif was enriched. We used the motifs of the preferred orientation and generated a corporate consensus binding sequence of the postulated NFAT-RUNX pair, which is depicted in FIGURE 24. The RUNX-NFAT motif was found approximately 200 times in the dataset.

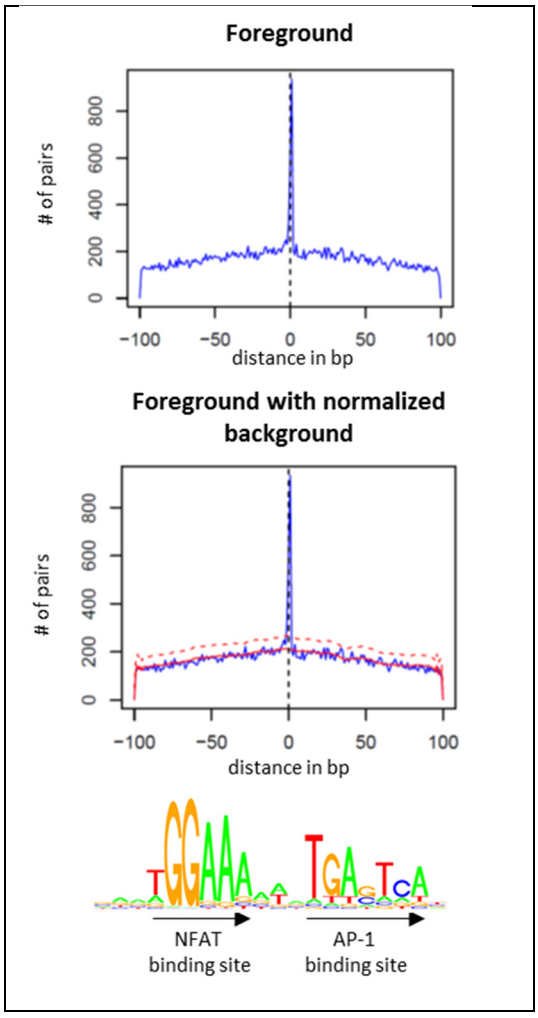

FIGURE 23. AP1 and NFAT binding motifs are notably found in particular distance to each other. Pairs of NFAT and AP1 recognition motifs were mapped in regions of NFATc2 binding in activated murine CD8$^+$ T cells, as determined by NFATc2 ChIP-Seq. The distribution of occurring distances of the AP1 motif relative to the forwardly orientated NFAT motif is blotted. The red line shows normalized distribution of distances between NFAT and AP1 motif in a background dataset. The dashed red line marks the level of significance. A generated consensus sequence is depicted below.

An additional binding motif that was found preferentially in a defined distance to NFAT is the CRE motif. It constitutes the consensus-binding site of CREB1 and some transcription factors of the ATF family. The CRE consensus sequence (TGACGTCA) is similar to the AP1 consensus sequence (TGA[C or G]TCA) with the exception of an additional central nucleotide.

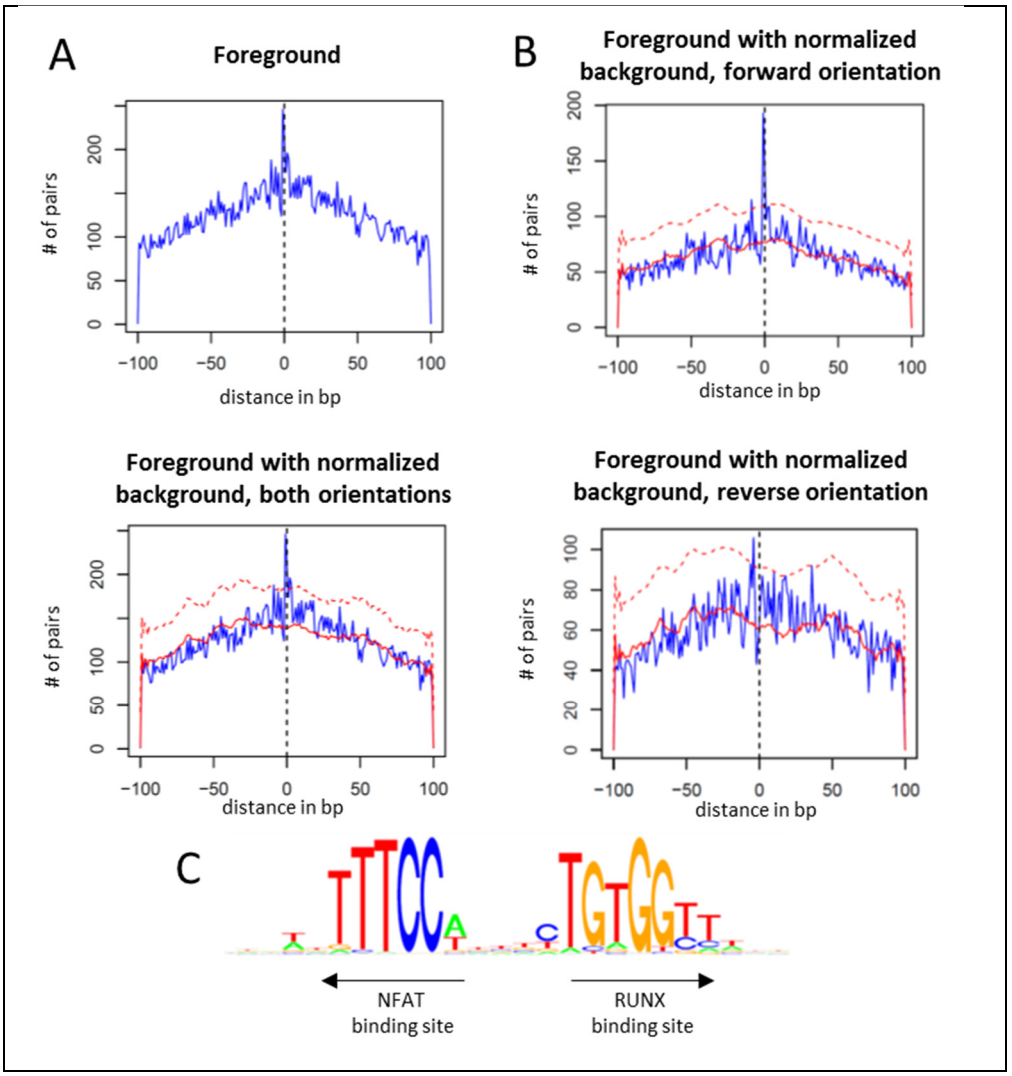

FIGURE 24. RUNX and NFAT binding motifs are notably found in particular distance and orientation to each other. Pairs of NFAT and RUNX recognition motifs were mapped in regions of NFATc2 binding in activated murine CD8⁺ T cells, as determined by NFATc2 ChIP-Seq. A: The distribution of occurring distances of the RUNX motif relative to the forwardly orientated NFAT motif is blotted. B: Occurring distances are subdivided into forward (upper chart) or reverse orientation (lower chart) of the RUNX motif. The red line shows normalized distribution of distances between NFAT and RUNX motifs in a background dataset. The dashed red line marks the level of significance. C: Consensus sequence generated from the sequences of B, upper chart.

Just as the AP1 motif, the CRE motif is found particularly one base pair downstream of the NFAT motif (FIGURE 25). Thus, the resulting NFAT-CRE motif is very similar to the previously identified NFAT-AP1 motif (FIGURE 23) with regard to sequence, distance and orientation

Overall, we found a significant enrichment of AP1, CRE and RUNX binding motifs in the vicinity of binding motifs for NFAT when we analyzed the distribution of transcription factor binding motifs in regions of confirmed NFAT binding. Strikingly, we observed that these motif pairs occur preferentially in a defined distance and orientation to each other, which suggests that their existence comprises a functional relevance.

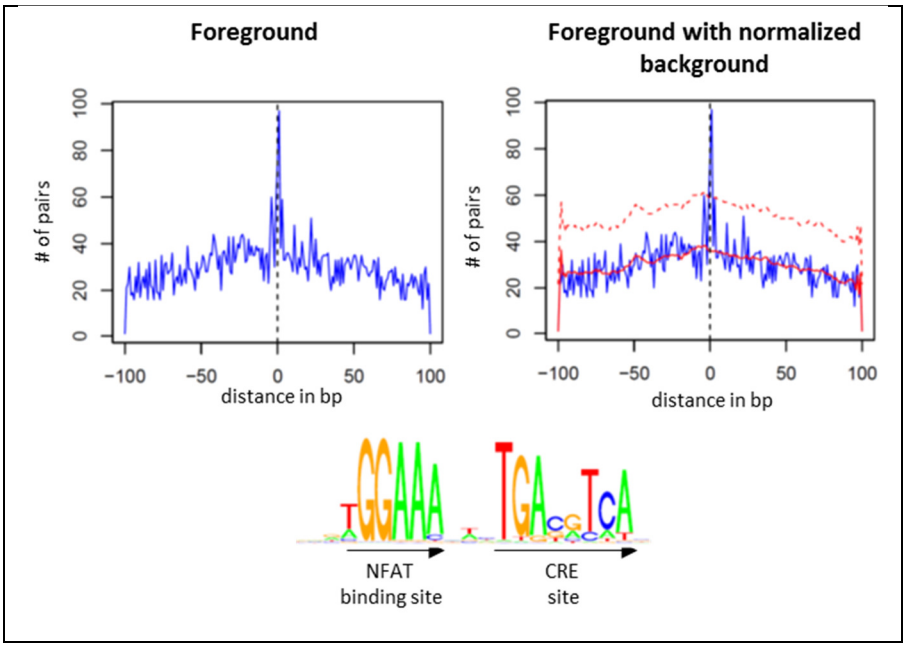

FIGURE 25. CRE and NFAT binding motifs are notably found in particular distance to each other. Pairs of NFAT recognition motif and CRE motif were mapped in regions of NFATc2 binding in activated murine $CD8^+$ T cells, as determined by NFATc2 ChIP-Seq. The distribution of occurring distances of the CRE motif relative to the forwardly orientated NFAT motif is blotted. The red line shows normalized distribution of distances between NFAT and CRE motif in a background dataset. The dashed red line marks the level of significance. A generated consensus binding sequence is depicted below.

4. Discussion

Without the protection from our immune system, we would succumb to omnipresent microbes within shortest time. Proper T cell function is crucial for the function of the immune system, and mutations that compromise T cell functions lead to fatal immunodeficiency[3]. Three main signaling pathways govern the activation of T cells upon stimulation: the Calcineurin/NFAT pathway, the MAP-kinase/AP1 pathway and the TCR induced NFκB pathway (FIGURE 1). Disruption of any of these pathways can impede T cell activation, leading to fatal immune failure[18,141].

During the present thesis, we aimed to enhance the current knowledge of important integrational processes within the T cell receptor induced signaling pathways. More precisely, we studied the composition and function of the cytoplasmic CBM-complex that induces the activation of NFκB transcription factors in response to TCR ligation. Furthermore, we investigated protein-protein interactions of NFAT family members with other proteins to advance the understanding of the regulation of NFAT's activity and function. The results of both parts will be discussed separately in the following chapter.

4.1. HOIP: A Novel Regulator of the CBM-Complex

The CBM-complex, which is constituted by the proteins BCL10, CARMA1 and MALT1, plays a crucial role in signal transduction and signal integration from the T cell receptor to the activation of the transcription factor NFκB. Multiple pathways impact on its dynamic regulation, such as calcium signaling via CaMKII and CaN, AKT signaling, Notch and caspase activation[39,59,71,82,84,87]. We aimed to identify further proteins that regulate NFκB activation at the level of the CBM-complex, thereby contributing to input signal integration. Using epitope-tagged BCL10 as a bait protein, we isolated the CBM-complex from Jurkat cells and analyzed its components by mass spectrometry (FIGURE 10, TABLE 3).

4.1.1. Isolation of the CBM-Complex: Known and Suspected Components

Many of the identified interacting proteins, such as CARMA1, cIAP1/2, A20 and TRAF2, were known interactors or regulators of the TCR induced NFκB signaling pathway, which validated our experimental setup[66,91,98]. The functions of **CARMA1** and **A20** within the CBM-complex are studied in great detail (see CHAPTER 1.3.4.1). In contrast, the roles of TRAF2 and CIAP proteins on TCR induced NFκB activation are less clear and will be discussed in the following.

Both **cIAP1 and cIAP2** can interact with BCL10 *in vitro*[95,218]. cIAP2 co-precipitates with BCL10 after T cell stimulation and has been assigned a negative role in TCR induced NFκB activation. cIAP2 can ubiquitinate BCL10, thus targeting it for degradation[91,94]. In line with this, cIAP2 over-expression reduced the levels of BCL10 and NFκB activation in response to TCR stimulation, while over-expression of an enzymatic dead form had the opposite effect[91]. Unfortunately, the role of cIAP1 was not even touched in that particular study; and, hence, remains elusive[94].

The role of **TRAF2** in TCR induced NFκB signaling is not well understood so far. Sun *et al*. showed, that knock-down of either TRAF2 or TRAF6 decreased IKK activity in an *in-vitro* assay after IP to 50 %, and simultaneous knock-down of both to 20 %, as did knock-down of TAK1 or MALT1[66]. In line with this, the knock-down of TRAF6 or TRAF2 reduced IL-2 production in Jurkat cells after CD3/CD28 activation to 80 %, the double knock-down to 20 % of control cells[66]. This points towards some redundancy in the role of TRAF2 and TRAF6. However, it is not clear whether TRAF2 can simply take over actions of TRAF6, or whether TRAF2 and TRAF6 are important for independent processes that can compensate for each other at a later point, if one component is missing.

It is noteworthy to mention here that some other known CBM-complex interacting proteins were absent from our dataset. In detail, we did not detect members of the downstream IKK complex in combination with IκBα nor TRAF6 and TAK1 that link CBM activity to IKK complex activation. Though, other studies had observed co-precipitation of IKK subunits with BCL10 and MALT[57,64,76]. This discrepancy might be due to different experimental settings, including the choice of bait, tag and the stringency of the washing procedure. Furthermore, work from Carvalho and co-workers indicated that the initial CBM-complex matures to a second cytoplasmic complex without CARMA1. Only this second complex includes IκBα, which is then phosphorylated in this microenvironment[68]. Thus, a selective isolation of a subset of the CBM-complex might also explain the discrepancies.

4.1.2. The LUBAC Constituents HOIP and HOIL1Associate with the CBM Complex

Aside of already known interactors, our MS data revealed HOIP and HOIL1 to associate with BCL10 after Jurkat cell stimulation with PMA and ionomycin (FIGURE 10). We could prove the association between HOIP and BCL10 in anti-CD3/CD28 stimulated Jurkat cells and in PMA/ionomycin stimulated primary human T helper cells by CoIP-western blot (FIGURE 11). However, we did not detect co-purification of HOIL1 by western blot. Since the protein was detected and enriched in both MS runs, it is very likely that the antibody we used against HOIL1

is not sensitive enough to detect the amount of protein that is present in the eluates. Dubois *et al*. found both HOIP and HOIL1 to interact with the CBM-complex in Jurkat cells after PMA/ionomycin or anti-CD3/CD28 stimulation (see below)[223]. This supports the view that additional to HOIP, HOIL1 is recruited to the active CBM-complex.

Initially, Kazuhiro Iwai and co-workers identified HOIP and HOIL1 as parts of a complex that can mediate the attachment of head-to-tail linked or linear ubiquitin chains[220]. This *linear ubiquitin assembly complex* (LUBAC) consists of the proteins HOIL1, HOIP and SHARPIN[220–222]. While K48 and K11 linked poly-ubiquitination is a signal for proteasomal degradation of the attached protein, linear and K63 linked ubiquitin chains are non-degradative and serve as modules for protein interaction and signal transduction[66,242].

Since it discovery, different reports have documented an important role for the LUBAC in signaling pathways that lead to the activation of NFκB in response to various triggers. The LUBAC plays a vital role in TNFα induced NFκB activation, which is markedly reduced by HOIP or HOIL-1 knock-out in murine embryonal fibroblasts[243,244]. The LUBAC is recruited to the activated TNFR1 complex in a TRAF2 and cIAP1/2 dependent, but r*eceptor interacting protein* (RIP) and NEMO independent way, although it can bind to NEMO[199,245]. The LUBAC can attach linear poly-ubiquitin chains to NEMO, which is thought to trigger NEMO oligomerization and subsequent IKKβ autophosphorylation[245]. In general, linear ubiquitin chains are indispensable for TNFα induced NFκB activation. However, in addition to the LUBAC, the ubiquitin ligases cIAP and TRAF2 can also attach linear ubiquitin chains to RIP in cooperation, at least *in vitro*[243,246].

B cells from transgenic mice that express only an ubiquitin ligase defective form of HOIP show reduced NFκB activation in response to TNFα receptor, CD40 and TACI stimulation, but no alterations in response to B cell receptor ligation[247]. Furthermore, the LUBAC is involved in NFκB activation as a response to toll-like receptor, nod-like receptor or inflammasome activation[248–250]. However, an involvement of the LUBAC in antigen receptor induced signaling to NFκB had not been described until recently. In contrast, our data showed that at least HOIP and HOIL1associate with the CBM-complex, suggesting a functional role in this specific signaling pathway.

While the present work was in progress, two other research groups published data that are completely in line with our findings. These reports showed that HOIP, HOIL-1 and SHARPIN interact with the CBM-complex after B- or T cell receptor stimulation[223,224]. The group of Nicolas Bidère published a report on the involvement of the LUBAC in TCR induced NFκB signaling[223]. Earlier, the group had identified *casein kinase-1α* (CK1α) to be associated

with the CBM-complex[81]. In this new study, they used CK1α as a bait protein to purify the CBM-complex from PMA/ionomycin stimulated Jurkat cells and analyzed the complex by mass spectrometry. By this, they also identified HOIP as an interactor of the CK1α-CBM-complex. HOIP co-precipitated with BCL10; and BCL10, MALT, HOIP, HOIL-1 and SHARPIN all co-precipitate with NEMO from Jurkat cells stimulated with either PMA/ionomycin or CD3/CD28-specific antibodies. Reversely, BCL10, MALT1 and CK1α co-precipitated with SHARPIN under the same conditions. Thus, this report by Nicolas Bidère's group backed up our findings that HOIP and HOIL-1 associate with the CBM-complex after TCR ligation.

4.1.3. Expression of HOIP Is Necessary for TCR Induced NFκB Activation and IL-2 Expression

We and others had observed that components of the LUBAC physically associate with the CBM-complex after TCR stimulation[223,224]. Since the CBM-complex governs the activation of NFκB transcription factors, this finding suggested that the LUBAC might contribute in one way or another to (complete) NFκB activation.

Indeed, Dubois and co-workers could prove that siRNA mediated knock-down of HOIP in Jurkat cells diminished MALT/BCL10 interaction with NEMO, NEMO ubiquitination, p65 nuclear translocation and NFκB activation in a luciferase reporter gene assay[223]. Furthermore, siRNA mediated knock-down of HOIP in primary human PBMCs reduced p65 translocation and almost completely abrogated IL-2 secretion after anti-CD3/CD28 stimulation of these cells. This indicates that HOIP not only interacts with the CBM-complex, but also positively regulates NFκB activity in response to TCR stimulation.

While HOIP and SHARPIN knock-down in Jurkat cells led to a reduced NFκB activation in the reporter gene assay, HOIL1knock-down had not such an effect[223]. Interestingly, reduced TCR induced NFκB activity after HOIP knock-down was completely restored to normal by transfection with both the wild-type HOIP and an E3-ligase deficient mutant of HOIP. In contrast, NFκB activation after TNFα stimulation was only rescued by ligase sufficient HOIP expression. In line with this, Dubois and coworkers also showed in the same report that a strong increase in linear ubiquitination in Jurkat cells is seen after TNFα stimulation, while this effect is very weak after PMA/ionomycin stimulation[223]. Taken together, this points towards a structural role of HOIP and SHARPIN, which is independent of linear ubiquitin ligase activity and differs from that one seen in TNFα signaling.

Work from Yibin Yang and co-workers showed that in ABC DLBCL tumor cells, in which the CBM-complex constantly activates NFκB signaling, LUBAC is important for

survival[224]. In these tumors, reduced NFκB activity and cell viability was caused by a peptide that disturbs the interaction between HOIP and HOIL1. These results underline parallels of the influence of LUBAC on antigen receptor signaling in B and T cells. However, the different implications on the role of HOIL1 pose questions. Since both reports did not address the effect of HOIL1knock-out on these cells, further work is needed to clarify whether there is indeed a differential importance of HOIL1in BCR and TCR signaling to NFκB, or whether the effect of the peptide has a different mode of action aside of simply holding HOIP and HOIL1 apart from each other. A straightforward experiment would be to test the effect of the described peptides on antigen receptor induced NFκB activation in T cells.

4.1.4. The LUBAC and the CBM: Open Questions

Two main questions remain regarding the role of HOIP and SHARPIN in the pathway from TCR to NFκB. The first affects the mechanism of how the LUBAC's proteins are recruited to the active CBM-complex. Since TRAF2 and cIAP are both necessary to recruit the LUBAC to the TNFR-complex, it is tempting to speculate whether both are also included in bridging the LUBAC to the CBM, as they are both present in the latter complex[199]. Via its zinc finger domain, HOIP can bind K63 linked poly-ubiquitin chains that can be generated by cIAP, but also other present E3 ligases, such as MIB2 or TRAF6[199]. To address this point, CoIP studies in combination with knock-out of the different ubiquitin ligases might clarify which proteins are crucial to link HOIP and SHARPIN to the CBM-complex. The other way around, it would be interesting to ascertain which domains of HOIP and/or SHARPIN are necessary for their recruitment. For example, one imposing question is whether an ubiquitin- or SHARPIN-binding deficit HOIP would still be recruited to the CBM-complex.

The second arising question is what function HOIP and SHARPIN proteins do have in this pathway, once they are recruited. Since the ubiquitin ligase activity of HOIP seems dispensable, the most likely explanation is that HOIP and SHARPIN physically link other involved proteins to the CBM-complex. Analogously to HOIP's and SHARPIN's role during the TNFα induced NFκB activation, one such a candidate is NEMO[245]. However, the interaction between the LUBAC and NEMO in TNFα stimulated cells is mainly dependent on linear poly-ubiquitin, which is bound by NEMO and HOIL1[199,251]. Since linear ubiquitin chains are dispensable for TCR induced NFκB activation, they are not likely to link both proteins in this pathway. Though, crystallization studies indicated that the HOIP-NEMO interaction is mediated by both ubiquitin-binding and direct interaction between HOIP's and NEMO's protein domains[252]. The latter ones may enhance NEMO recruitment even in the absence of linear ubiquitin chains, which is the case in the setting of TCR signaling to NFκB.

Interestingly, an interaction between HOIL1, TAB2 and TAB3 was described, too[253]. However, the report lacked evidences for a direct interaction. Since the interaction was dependent on the N-terminus of HOIL1, which also interacts with HOIP, it is possible that instead HOIP or SHARPIN interact with TAB2/3. Thus, the role of HOIP/SHARPIN could possibly be to bridge TAK1 via TAB2/3 to the CBM-complex. However, TAB2/3 strictly depend on ubiquitin binding to fulfill their role in TNFα induced NFκB activation. Since poly-ubiquitin chains are present on diverse CBM-complex proteins, it is doubtful that the TAB-TAK complex needs other proteins for recruitment[254].

Another possibility is that binding of HOIP to poly-ubiquitin-chains stabilizes the ubiquitin network via impeding destruction by the deubiquitinases CYLD and A20, thus enhancing IKK activation. Since HOIP knock-out already affects early phosphorylation of IκBα after antigen receptor stimulation, the inhibition of down-regulation cannot be the only mode of HOIP action, at least[223,224].

In summary, HOIP and SHARPIN bind to the CBM-complex after activation, a process which is possibly mediated by TRAF2 and cIAP. The presence of HOIP and SHARPIN, but not the enzymatic activity of HOIP, seem necessary for a robust recruitment of the IKK complex to the CBM, which is a prerequisite for the subsequent activation of NFκB transcription factors. A proposed model for the function of TRAF2, cIAP, HOIP and SHARPIN is depicted in FIGURE 26. However, both the mode of recruitment to and the precise function of HOIP and SHARPIN in the CBM-complex remain elusive.

To shed further light onto the contribution of HOIP and SHARPIN on TCR induced NFκB activation, reconstitution studies of knock-out or knock-down cells with mutated or truncated forms of the proteins might help to identify which modules of the proteins are needed here. Again, CoIPs of the CBM in the absence of HOIP or SHARPIN might be a thankful tool to identify proteins that are recruited only in the presence of these proteins. To this end, mass spectrometry investigations might also be enlightening to identify further HOIP and SHARPIN interactors.

Finally, HOIP and SHARPIN constitute new potential therapeutic targets to interfere with unwanted T cell activation. As Yang and coworkers showed, abrogation of HOIP interactions can inhibit the growth of tumor cells that rely on constitutive, CARMA1-dependent NFκB activation[224]. Similarly, HOIP, SHARPIN or TRAF2 might be targeted to down-modulate T cell activation in autoimmune diseases. Diminishing the recruitment of HOIP, SHARPIN and especially NEMO to the CBM-complex could reduce NFκB activation in activated T and B cells in a specific way. Since the CBM-complex is specific for antigen

receptor induced activation of this pathway, NFκB activation in other cells would be unaffected, which might reduce therapeutic side effects. As outlined, this requires further understanding of the role of HOIP and SHARPIN within the CBM-complex.

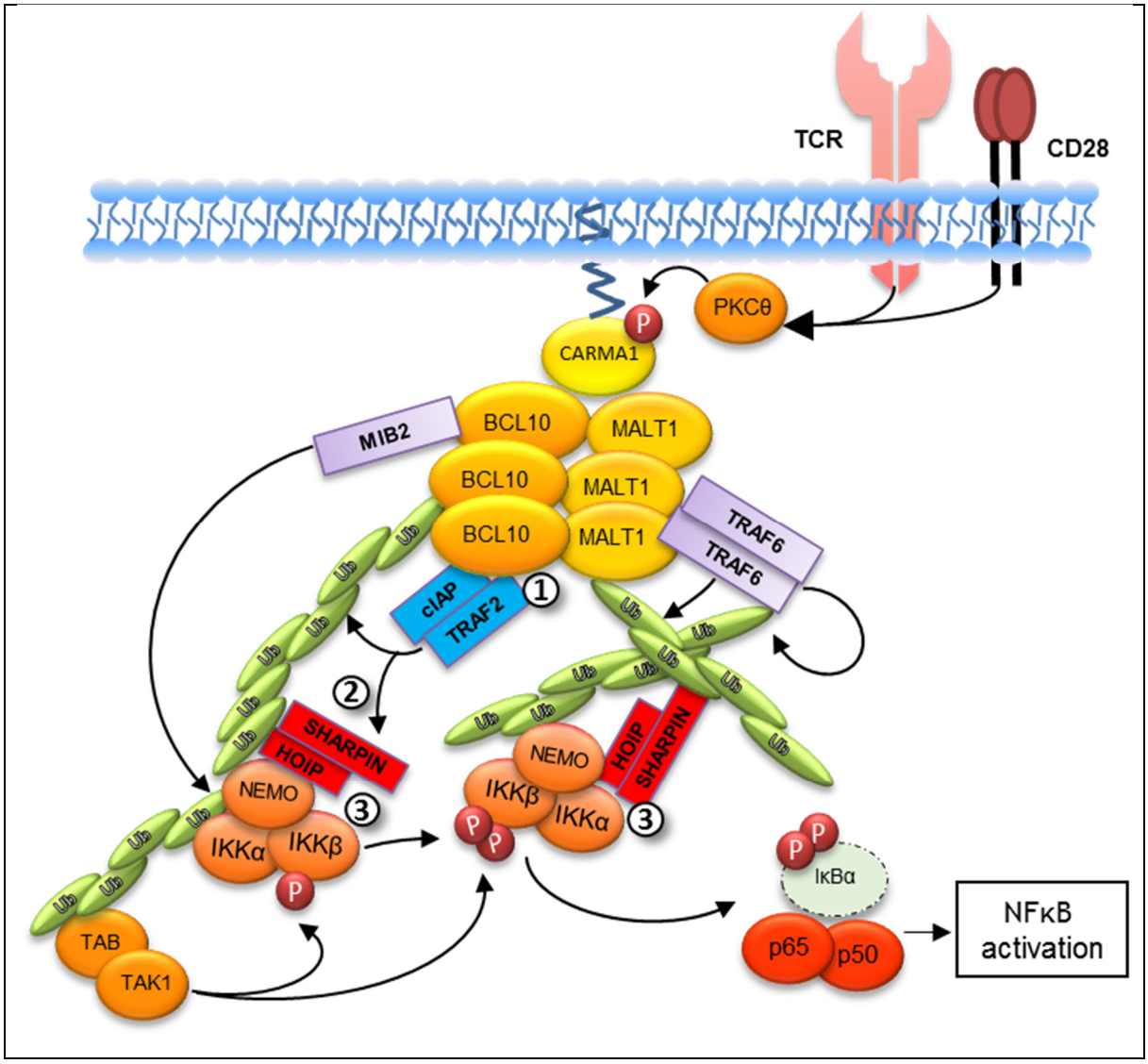

FIGURE 26. Model of the proposed function of TRAF2, cIAP, and LUBAC components during TCR induced NFκB activation. TRAF2 and cIAP bind to the activated CBM-complex via BCL10 (1). Both proteins are involved in the recruitment of HOIP and SHARPIN to BCL10, either via direct interaction and/or via extension of the ubiquitin network (2). HOIP and SHARPIN stabilize the binding of NEMO to the ubiquitin network at the CBM-complex, thereby supporting activation of the IKK complex and subsequent NFκB activation (3). For further details, please refer to the text. Ub: ubiquitin, P: phosphorylation.

4.2. Identification of NFAT Interaction Partners

4.2.1. General Remarks

The activation of NFAT family transcription factors is a hallmark of T cell activation. Murine T cells deficient for NFATc1 and NFATc2 completely fail to produce most T helper cell effector cytokines, and mutations in humans that prevent NFAT from translocating into the nucleus lead to severe combined immune defect[113,141]. Thus, NFAT proteins in general are indispensable for the function of T cells and the adaptive immune system as a whole.

The interaction of NFAT proteins with other transcription factors (e.g. FOXP3, AP1 or GATA3) strongly influences NFAT DNA binding sites and target gene activation[168,176,179]. To identify further proteins that shape the outcome of T cell receptor signaling via interaction with NFAT proteins, we performed CoIP-MS experiments. To this end, we overexpressed biotin-tagged forms of different NFAT proteins (short and long variant of NFATc1, NFATc2) in Jurkat cells, which were employed to isolate NFAT containing protein complexes.

4.2.1.1. Influence of Overexpression and the Biotin-Tag on NFAT Localization and Phosphorylation

To evaluate whether the epitope-tagged NFAT forms are a valid model to investigate NFAT interactions, we analyzed the translocation and phosphorylation patterns of the biotinylated NFAT forms in Jurkat cells. Normally, NFAT proteins are highly phosphorylated and located in the cytoplasm of unstimulated T cells. After stimulation, NFAT is dephosphorylated and translocated to the nucleus (FIGURE 4). By comparing NFAT phosphorylation and translocation patterns of tagged and untagged isoforms, we did not observe an influence of the tag on these processes (FIGURE 14). One exception was N-terminal tagged NFATc2, which was not translocated to the nucleus following stimulation, and was therefore excluded from further experiments.

However, contrary to our expectations, we observed a substantial amount of dephosphorylated NFAT proteins without stimulation, mainly in the nuclear fraction (FIGURE 14). Furthermore, a veritable amount of all over-expressed NFAT forms is found in the nucleus of unstimulated cells. The latter phenomenon was observed by others for NFATc1 in primary murine T helper cells after viral overexpression of either the long or short isoforms[146]. Thus, it seems that the overexpression of NFAT *per se* interferes with its phosphorylation status and sub-cellular location, which are tightly connected processes. Usually, NFAT kinases maintain NFAT in a phosphorylated state, which triggers its nuclear export. Both phosphorylation and export might be overstrained by the amount of overexpression. In addition, aberrations in the signaling of the used Jurkat cell line might contribute to the discrepancy from the expected

patterns[202]. Indeed, we observed that endogenously expressed (i.e. wild-type) NFATc1 and NFATc2 can be found in the nucleus of unstimulated Jurkat cells, albeit at lower levels than observed after over-expression (data not shown). The last observation suggests that both overexpression and the altered signaling in the cell line contribute to the aberrations from the expected patterns. These alterations should be considered when interpreting the results.

It is important to recall that the observed aberrations were the same for the employed tagged and the untagged, wild-type NFAT forms. This indicated that the AVITEV fusion proteins of NFAT are recognized and regulated by the cellular machinery just as the wild-type variants. In consequence, the tag should not disturb the majority of other protein-protein interactions that involve NFAT either. Thus, the employed NFAT-AVITEV fusion proteins constitute valid tools to study NFAT protein interactions.

4.2.1.2. JUN Is Likely to Be Cleaved by TEV Protease

The usefulness of the tagged NFAT proteins for the identification of interacting proteins was further demonstrated by the ability to co-purify known NFAT interactors (FIGURE 16). We could prove interactions between NFATc1L and NFATc2 with FOS, JUN, JUNB and EP300 by CoIP-western blot and CoIP-MS. Unexpectedly, we did not observe JUN co-purification in initial western blot experiments for which we employed TEV cleavage to release NFAT protein complexes from the streptavidin beads. One explanation is that the JUN protein has a likely TEV protease site (ERLIIQ-S), which is similar to the TEV consensus cleavage sequence (ExxYxQ-G/S). Elution of the proteins by TEV cleavage would also cut the JUN protein into two parts, which would then not show up at the expected height in western blot. Indeed, when elution was done by boiling in Laemmli buffer, JUN co-purification with NFATc1L and NFATc2 was detected by western blot (FIGURE 18, FIGURE 21). The cleavage did not interfere with detection of JUN in MS either, in which digested peptides and not complete proteins are detected (TABLE 6).

4.2.1.3. Discrepancy between the Amount of NFATc1S and NFATc1L Interactors

To identify so far unknown NFAT protein interactors, we isolated NFAT containing protein complexes from Jurkat cells that overexpress an epitope-tagged form of either NFATc1S, NFATc1L or NFATc2. Subsequently, these complexes were analyzed by mass spectrometry. As revealed by the MS analysis, a large amount of proteins was enriched in co-purification experiments with NFATc1L and NFATc2 proteins (TABLE 5 and FIGURE 17). In contrast, only a small number of proteins was enriched when NFATc1S was used as a bait. To a large part, this might be due to the weak overexpression of NFATc1S compared to NFATc2

or NFATc1L (FIGURE 13). Unfortunately, we were not yet successful to achieve equally high overexpression rates for both NFATc1 isoforms. Therefore, the absence of an identified NFATc1L interaction partner in NFATc1S experiments can have two reasons. First, the protein interacts with both isoforms, but the amounts of co-purified protein in the NFATc1S experiment are below the detection level of MS or western blot. Alternatively, second, the protein selectively interacts with NFATc1L. Since we cannot discriminate between those in our dataset, further experiments are necessary to investigate similarities and differences between the interactomes of the long and the short isoform. Reverse CoIP studies might be extremely enlightening towards the question, whether individual proteins preferentially interact with one NFATc1 isoform or the other. Nonetheless, the MS data indicate that CREB1, Ikaros, WDR48 and SCAI can interact with both NFATc1 isoforms and NFATc2. This also implies that the interaction takes place at the homologous NHR or RHR domains of NFAT, which are more conserved among the different isoforms[143].

4.2.1.4. Defining a Cut-Off for Potential and Confident Interactors

In contrast to the MS results from the BCL10 CoIPs, the distinction between background and potential interactors is much more difficult in the results of the NFAT experiments (compare FIGURE 10 and FIGURE 17). The enrichment factors of the quantified proteins were distributed continuously between 1 (not enriched) and more than 90 (highly enriched). Thus, any attempt to define a cut-off for (high) confident interaction will be subjective and arbitrary. Depending on the experiment, enrichment factor cut-offs of as low as 2 have been used to differentiate between background and potential interactors by other scientists[231,232]. In principle, higher enrichment values raise the confidence of a detected interaction. Irrespective of this value, suspected interactions should always be proven by further experiments, though, using another read-out than MS. When this is done, the importance of the cut-off is reduced from a determinant to a tool.

We chose to set the minimal cut-off to 3.0. This means, only proteins with an enrichment factor of at least 3.0 were regarded as potential interactors. We defined a further group of more confident interactors that were enriched more than 4.5 fold, which comprised roughly 60 % of the former group. Arguably, this group can be further shrunken by rising the requested enrichment value, thereby possibly further rising confidence. However, this might also prevent real interactions from being discovered. In line with this, we confirmed the interaction of NFATc2 with CHEK1 and WDR48 by CoIP-WB. The two proteins were enriched by a factor of only 4.5 and 5.9 in one of the two runs, respectively. Therefore, it seems reasonable to consider proteins with enrichment values above 4.5 as high confident interactors. The

mentioned group also contained our considered positive control protein (JUNB with ratios of 7.5-19.2, EP300 with ratios of 14.7-19.3) as well as further proteins that interact physically with NFAT, according to reports from other groups (e.g. EGR1, IRF2BP1, PARP1, ratios between 6.8 and 25.5)[164,181,183]. Thus, we could confirm these interactions by our approach. The presence of these proteins in our dataset in reverse validated our experimental settings.

4.2.1.5. Absence of Proof Is not a Proof of Absence

Before we discuss the implications of the presence of enriched proteins within our dataset, we want to draw the attention towards those proteins that were not enriched during our experiments. Albeit we confirmed a subset of known NFAT interactions, other known NFAT interacting proteins (e.g. GATA3, FOXP3, IRF4) are absent from our datasets. This can have several reasons. First, obviously, proteins that are not expressed in the employed Jurkat cells, or that are not expressed under the experimental conditions, cannot be co-purified at all. For example, this applies to FOXP3, which is mainly expressed in regulatory T cells, but not in Jurkat cells (own data, not shown). Second, due to different detection limits, not every enriched protein will be identified during the MS runs. For example, we observed co-purification of JUN together with NFATc1L by western blot (FIGURE 18). In contrast, JUN was not detected during the CoIP-MS experiments when NFATc1L was used as a bait. Therefore, the MS data did not suggest the interaction of NFATc1L with JUN (TABLE 6). Third, due to our experimental settings, we were only able to detect interactions that take place after 2 hours of PMA/ionomycin stimulation in Jurkat cells. Accordingly, interactions that occur at other stimulation time points or those that require other stimuli (e.g. cytokine receptor signaling) were not accessible to our investigations. Fourth, the employed protocol for complex isolation probably maintains the stability of certain protein complexes while destabilizing others. Thus, the usage of buffers, ultrasound or digesting enzymes ought to be adjusted to detect a particular protein-protein interaction. For all these reasons, the absence of proof for a certain interaction in this dataset should neither be interpreted as a proof of absence, nor as a general weakness of the employed methods.

4.2.1.6. Towards the Confidence and Nature of Suggested Interactions

Unless there is any further evidence, we designated enriched proteins as potential interactors of NFAT proteins, whose interaction has yet to be confirmed in further experiments. For a number of proteins (Ikaros, Helios, CREB1, RUNX1, SATB1, CHEK1, WDR48, SCAI, RPTOR), we confirmed the interaction with NFAT proteins by CoIP-western blot during the present study (FIGURE 18, FIGURE 19). There are several reasons not to overrate the isolated data from the MS experiments. First, false designation of peptides to proteins might occur

during MS data analysis. False discovery rates are approximately 1 % with the chosen settings. To be more stringent, we demanded two unique peptides for every protein to be identified. Still, interactions should be proven by other methods to exclude the possibility of mistaken protein identification. Second, since no tagged protein was present in the control cells, we cannot exclude that enriched proteins bind to the tag rather than to NFAT. In one follow up experiment, we used cells overexpressing a GFP fusion protein with the same tag to control for this issue (FIGURE 21). By this, we could prove that none of the tested proteins interact with the AVITEV tag, but all interact with the NFAT proteins. However, this has yet to be proven for other proteins from the datasets.

It is important to notice that it is not possible to distinguish between direct and indirect interactors from our type of experiments. Possibly, interaction partners that appear with high enrichment ratios and high ratio counts in several MS experiments (SCAI, Ikaros, Helios, RPTOR, refer to TABLE A 1 –A3, page VII) are more likely to be direct binding partners of NFAT. To clarify the nature of individual interactions, further *in-vitro* studies are needed, such as *Förster resonance energy transfer* (FRET) based techniques or interaction studies using purified proteins.

A further caveat of our approach is posed by the presence of DNA (and RNA) in our experiments. Since NFAT binds to DNA, we also co-purified these DNA strands along with the NFAT proteins. Proteins that bind to DNA, either (sequence-) specifically or non-specifically might thus also be enriched in our datasets. This might be the case for the group of enriched proteins that are involved in the response to DNA damage (TABLE 6). As we isolated sonicated DNA along with NFAT proteins, this also means an enrichment of proteins that associate with double strand breaks. This especially accounts for the proteins XRCC5, XRCC6 and PRKDC, which are known to form a complex that allocates to sites of DNA strand breaks[255].

A similar question arises for the postulated interactions between NFAT and other transcription factors. Those factors that do not interact with NFAT (-complexes), but often bind DNA sites close to NFAT, could also be enriched in our experiments. It is noteworthy, though, that several transcription factor families, such as IRFs, NFκB factors or STAT proteins, are not enriched in our datasets. These factors are known to co-regulate a set of genes together with NFAT and are enriched in DNA-regions of NFAT binding (reviewed by Kleiter *et al.*[112], FIGURE 22). Thus, their absence slightly suggests that the co-purified transcription factors are enriched rather specifically via protein-protein interaction and not via independent binding to the same DNA molecule. However, further experiments are needed to determine the nature of

the interactions between NFAT and other transcription factors. For example, the presence of DNase and RNase in CoIPs should abrogate those 'artificial' interactions that are mediated by DNA only, while other interactions should remain unaffected.

Although co-immunopurification studies with western blot as a readout have been the most widely used method for the confirmation of suspected protein interaction, this technique possesses certain drawbacks and limitations. Especially when the bait protein is overexpressed, its artificially high abundance might lead to interactions that do not occur under physiological expression levels. As seen with the NFAT overexpressing cell lines, overexpression might also interfere with the protein's function and localization (see above). To exclude this, the interacting proteins can be co-purified from endogenous expression levels using appropriate antibodies. At best, this is done with primary cells. However, there are certain circumstances where this approach is limited. For example, this can be the case when the proteins are expressed at low levels, available antibodies are poor or when studying low-affinity interactions.

Indeed, we were not yet successful in the establishment of NFAT co-immunoprecipitations with two different NFAT specific antibodies, not even with cells that overexpressed wild-type NFATc2 (data not shown). This is in line with the fact that most of the known NFAT interactions were proved by IPs after overexpression of NFAT and its interaction partner in non-lymphoid cell lines, or by *in-vitro* interaction studies with recombinantly expressed proteins[162,164,169,183,229,233,256,257]. When CoIPs at endogenous levels are not successful, other techniques should be used to confirm suspected protein-protein interactions.

Several other methods exist that allow studying protein-protein interactions. Optical techniques like *bioluminescence resonance energy transfer* (BRET) or *bimolecular fluorescence complementation* (BiFC) can be used to prove a suspected interaction between two proteins. However, both techniques require both interacting proteins to be overexpressed as large fusion proteins. Thus, they are rather laborious and artificial. However, recent advances in genome editing would allow the expression of the respective fusion proteins from the endogenous loci[258].

The *proximity ligation assay* (PLA) can be used to confirm protein-protein interactions. The advantage of this technique is that it does not rely on fusion proteins and, thus, works with wild-type cells. Indeed, we could confirm the interaction between NFATc2 and Ikaros in primary human T helper cells using the PLA (FIGURE 20). By the use of CRISPR/Cas9-induced knock-out clones for both proteins, we confirmed the specificity of the employed assay.

However, the need for highly specific antibodies that work in this method and the requirement of knock-out controls limit this technique to low throughput.

4.2.1.7. Bioinformatics Suggest Cooperative DNA Binding of NFAT with RUNX- and CRE-binding Proteins

In silico analysis can also contribute to the confirmation of functional protein interaction. Through the analysis of public datasets, we showed that RUNX, CREB1 and AP1 consensus DNA binding motifs are found enriched in direct vicinity to NFAT binding motifs (FIGURE 23 - FIGURE 25). These pairs preferentially exist in a distinct distance and orientation. This finding strongly suggests cooperative DNA binding of these factors with NFAT and functional protein-protein interactions.

Cooperative DNA binding of NFAT and AP1 is already well described. Interestingly, DNA binding of NFAT-AP1-complexes is not restricted to combined consensus sequences. They also associate with degenerated composite motifs, to which isolated NFAT or AP1 bind only with low affinity[168]. For NFAT-RUNX and NFAT-CREB1, cooperative DNA binding has yet to be proven. To this end, DNA pull down experiments could be performed to determine whether binding of one factor augments binding of the other one to a composite DNA sequence. If this is the case, it will be interesting to investigate cooperative binding to degenerated composite binding motifs, which would dramatically increase the number of suspected target genes. Furthermore, it will be enlightening to determine the influence of the protein-protein interaction on those genes. As for NFAT-AP1, crystal structures of (DNA-bound) NFAT-complexes could shed light on the interaction interfaces and enable the development of peptide inhibitors that target particular NFAT interactions selectively. This would facilitate the study of these complexes with regard to their importance in T cell activation and development.

To summarize, this thesis provides a list of potential NFAT interactors (TABLE 6). The confidence of this list of interactions is strengthened by the fact that it contains proteins, whose interaction with NFAT had been already described (e.g. JUN, FOS, EP300, GSK3β). Additionally, further proteins were co-purified with NFAT that had not been known yet to interact physically with NFAT proteins, such as Ikaros, CHEK1 or RPTOR (Table 7). The potential role of these and some further interactions will be highlighted in the following chapter.

TABLE 7. List of known, confirmed and selected potential NFAT interaction partners that were enriched by CoIP-MS during the present thesis.

Gene ID	Enriched in CoIP-MS experiment with			Confirmed by western blot
	NFATc1S	NFATc1L	NFATc2	
		Known interaction partners		
JUN			++	+
FOS			++	+
JUNB	++		++	+
IRF2BP2			++	
PARP1			++	
CREB	++	+	++	+
YWHAQ			++	
YWHAZ			++	
CSNK1D	++	++	++	
GSK3B	++	++	++	+
RUNX1				+
EP300	++		++	+
EGR1			++	
CREBBP	++			
		Interaction confirmed by WB in this study		
SATB1	+		++	+
RPTOR	++		++	+
CHEK1	++		++	+
IKZF1	++	+	++	+
IKZF2	++		++	+
SCAI	++	++	++	+
WDR48	++	++	++	+
		Interaction not yet confirmed		
CABIN1			++	
YWHAB			++	
YWHAE			++	
YWHAG			++	
RANBP1	++		++	
NEK6/7	++			
PLK1			++	

4.2.2. Implications of Selected Interactions

4.2.2.1. CREB1 and NFAT-CRE Binding Motifs

One of the most enriched proteins in all MS runs was the transcription factor CREB1 (TABLE A 1 – A 3). CREB1 is able to bind to *cAMP response element* (CRE) sites with the consensus sequence TGACGTCA, or CRE half sites (CGTCA). Activation of CREB1 is triggered by a variety of stimuli, including G-protein coupled receptors and stress kinases. After TCR ligation, CREB1 is activated by *mitogen- and stress-activated protein kinase-1/2* (MSK1/2) mediated phosphorylation[259–261]. This process is dependent on PKA, ERK1/2, p38 and (partially) PKC.

CREB1 is an important regulator of T cell proliferation, and expression of IL-4, IL-10, IFNγ and probably IL-2[262–265]. Furthermore, CREB1 plays a role in the maintenance of FOXP3 expression in regulatory T cells, contributing to their stability[266]. Since many of these genes are also regulated by NFAT, it is possible that NFAT and CREB1 cooperate to regulate the expression of the corresponding proteins.

In a recent report, Park *et al*. showed that both CREB1 and NFATc1 bind to the *receptor activator of nuclear factor kappa-B ligand* (RANKL) promoter in murine osteoclasts, resulting in transcriptional activation. As detected by ChIP, overexpression of one factor enhanced binding of the other to the promoter, indicating that NFAT and CREB1 can cooperatively bind to DNA. The claimed binding sites of NFAT and CREB1 in the RANKL promoter have a distance of roughly 100 base pairs, which suggest either binding in *trans* rather than in *cis*, or integration of both proteins into larger complexes.

Remarkably, in contrast to all other regarded transcription factors, CREB1-NFATc2 interaction was not reduced in the presence of the DNA intercalator GelRed (FIGURE 21). This indicates that NFATc2 and CREB1 interaction occurs independent of DNA binding. Nonetheless, the affinity of NFAT and CREB1 binding in complex to a composite DNA site might be significantly higher than binding of each factor alone. Interestingly, we found an enrichment of composite NFAT-CRE sites in regions of NFAT binding, which might be bound by NFAT-CREB1 complexes (FIGURE 25).

However, CREB1 is not the only factor that binds to CRE sites. Closely related factors, such as CREM and members of the ATF family, have similar binding preferences. Moreover, transcription factors of the AP1 family can also bind to the CRE, whereas binding of CREB1 to the consensus AP1 sequence (TGA[G/C]TCA) seems not possible[267]. It is noteworthy that the identified NFAT-CRE sites are congruent with the NFAT-AP1 sites with regard to distance and orientation (compare FIGURE 23 and FIGURE 25). Thus, it is likely that NFAT-AP1 complexes can bind to the identified NFAT-CRE sites. If NFAT-CREB1 complexes could bind these sites, too, competitive binding of both complexes could shape the expression profile of the target genes. However, further studies are needed that characterize the sites, modus and orientation of NFAT-CREB1 interaction in the presence or absence of DNA binding.

To add a further level of complexity to this point, several members of the ATF family can form heterodimers with JUN and FOS proteins that can bind to CRE sequences[42]. CREB1 cannot form heterodimers with JUN, but with ATF2[268]. Thus, so far, one can only speculate whether the identified NFAT-CRE sites are preferentially bound by NFAT and individual CRE binding proteins.

4.2.2.2. RUNX and NFAT: Cooperative DNA Binding?

The family of RUNX transcription factors comprises RUNX1-3, out of which RUNX1 and RUNX3 are expressed in T cells. RUNX proteins play a crucial role in T cell development and differentiation[269]. They associate with *core binding factor beta* (CBFB), which was also co-purified with NFAT in our experiments. Functional cooperation of NFAT and RUNX proteins has been described in a number of settings. For instance, RUNX1 and NFAT do co-operate in driving transcription from different cytokine loci, such as IL-2, IFNγ and IL-17[185,270,271]. RUNX1, FOXP3 and NFAT contribute to the expression of GITR, CTLA4 and CD25 in T_{regs}, all hallmark proteins of this lineage[272]. In contrast, NFAT-RUNX3 cooperation suppresses the expression of IL-4 in TH1 cells[257]. In their report, Sung Ho Lee *et al*. also claimed a physical interaction between RUNX3 and NFATc1[257]. Unfortunately, the shown evidence was rather weak, as the authors did not provide crucial experimental controls to their CoIP experiments.

In the present thesis, we provide evidence that RUNX and NFAT might bind to DNA as a complex. First, we could prove interaction between RUNX1 and NFAT proteins in Jurkat cells (FIGURE 19). This interaction was (at least in part) mediated by DNA (FIGURE 21). Second, our work revealed that in regions of NFAT binding, potential NFAT and RUNX binding sites are found in close proximity. These sites preferentially occur in direct vicinity with a particular distance and orientation to each other (FIGURE 24). Out of four possible orientations that the two motifs could adopt, only one is enriched. Especially the last observation indicates that RUNX and NFAT proteins form a tripartite complex with DNA that involves protein-protein interactions. In contrast, competitive binding would probably not prefer a certain orientation. Similar results were already mentioned by Yue-Hien Lee *et al*., who found that the combination of NFAT and RUNX binding motifs was overrepresented in the promoter regions of T_{reg} associated genes[273]. Strikingly, the distance of both binding sites in the found pairs mainly was less than 20 base pairs, which is consistent with our findings. Analogue to the NFAT-AP1 complex, NFAT-RUNX complexes might bind to and enhance the expression of common target genes only when both proteins are present in an active state. Thereby, the NFAT-RUNX interaction might integrate antigen receptor signaling (NFAT) and the individual differentiation status or phenotype of a cell (RUNX).

4.2.2.3. Ikaros: Repressor of NFAT Transactivation?

The transcriptional repressor Ikaros is an important regulator of lymphocyte differentiation and function as well as a potent tumor suppressor. Ikaros associates with the NuRD chromosome remodeling complex and recruits it to lymphoid lineage genes[274]. By

limiting the expression of the master transcription factor TBET, Ikaros promotes the differentiation of T cells towards the T_{H2} phenotype[275]. Interestingly, T cells that are stimulated in the presence of regulatory T cells express high levels of Ikaros. The upregulation of Ikaros expression is NFATc2 dependent and Ikaros is necessary for the T_{reg} mediated inhibition of these cells[117]. In a similar fashion, Ikaros suppresses IL-2 production in anergic T cells[276]. Reversely, T cells do not require co-stimulatory signals to induce IL-2 induction in the absence of Ikaros.

During this study, we provide evidence that Ikaros (IKZF1) interacts with NFATc2. Ikaros very robustly co-purified with NFATc1 and NFATc2 (FIGURE 18, FIGURE 19). Furthermore, we could confirm the interaction of NFATc2 and Ikaros in primary human T cells by PLA (FIGURE 20). The amount of co-purified Ikaros was reduced in the presence of GelRed, indicating that NFAT-Ikaros interaction is (at least in part) mediated by DNA binding (FIGURE 21). However, we did not find Ikaros binding motifs enriched in regions of NFAT binding from CD8 T cells (FIGURE 22). This does not exclude NFAT and Ikaros interaction bound to different DNA strands, i.e. *in trans*, though.

Thus, it remains to be established whether Ikaros and NFAT can bind to vicinal DNA sequences. It is tempting to speculate that under anergic conditions, Ikaros suppresses the expression of activation related NFAT target genes, while not affecting genes necessary for anergy induction. This would require sequence specific binding of both Ikaros and NFAT to certain genomic targets. Another possibility is that Ikaros interacts with NFAT in a more general way, thereby repressing NFAT target gene expression until other processes (e.g. binding of other transcription factors to the same locus, or inactivation of Ikaros) counteract this repression. NFAT reporter gene assays combined with knock-down or overexpression of Ikaros could provide first hints toward this aspect. In either way, additional experiments are needed to further characterize the Ikaros-NFAT interaction and its significance for T cell signaling.

4.2.2.4. IRF2BP1 and IRF2BP2: Two Further Suppressors of NFATc2 Transactivation?

Recently, the interaction between NFATc2 and IRF2BP2 was identified during a yeast-two-hybrid screen[183]. IRF2BP2 was shown to reduce NFATc2 transcriptional activity[183]. Additional to IRF2BP2, its paralogue IRF2BP1 was also enriched in CoIPs with NFATc2 (TABLE 6). Since the interacting RING finger domain is highly conserved between both proteins, it is likely that they can bind to NFAT analogously and competitively. In contrast to IRF2BP2, IRF2BP1 possesses E3 ubiquitin ligase activity and might thereby modulate

NFATc2 protein stability and transactivation potential[277]. Consistent with the mentioned report, we observed no enrichment of any of the two proteins in experiments with NFATc1[183].

4.2.2.5. SATB1: Chromatin Opening at Sites of NFAT Binding?

In this report, we observed co-purification of the transcription factor SATB1 along with NFATc1 and NFATc2 (FIGURE 18, FIGURE 19). SATB1 was shown by others to be essential for the production of the cytokines IL-4, IL-5 and IL-13 after stimulation of T_{H2} cells[278]. Stimulation of these cells induces SATB1 expression, and SATB1 induces an open chromatin structure to the combined cytokine locus. Consistently, knock-down of SATB1 impedes expression of these T_{H2} related cytokines[278]. Since their expression is dependent on NFAT binding to the promoters, it is possible that NFAT is involved in recruiting SATB1 to its target genes. As a result, SATB1 induced chromatin structure remodeling might contribute to poise the gene locus for (enhanced) target gene expression.

4.2.2.6. SCAI, WDR48 and RPTOR: DNA Independent NFAT-Interactors

Aside of transcription factors, three other proteins – RPTOR, SCAI and WDR48 – were enriched with all NFAT variants in every mass spectrometry run and were confirmed by western blot (TABLE 6, FIGURE 18, FIGURE 19). The association of these proteins with NFAT was not affected by GelRed, which points towards a DNA independent mode of interaction (FIGURE 21). WDR48 acts as a co-activator of different de-ubiquitinases[279]. As such, it could possibly modulate de-ubiquitination of NFAT proteins or other NFAT interactors, thereby affecting their stability and function. The protein SCAI interacts with the SWI/SNF chromosome-remodeling complex, of which many compounds were also enriched in our MS dataset. By recruiting this complex to the DNA, SCAI can regulate gene expression[280]. However, in contrast to Jurkat cells, we did not detect SCAI expression in human CD4 T cells (data not shown), which is coherent with data from another group that did not see any SCAI expression in murine spleen[280]. Thus, it is doubtful that SCAI is an interaction partner of NFAT in primary lymphocytes. Since NFAT is expressed in many other tissues, interaction between NFAT and SCAI proteins might play a role in other cells and organs.

RPTOR is a scaffold protein of the *mammalian target of rapamycin* (mTOR) complex-1. The activity of this kinase complex is mainly driven by the nutrition status of a cell, thus integrating metabolic information into cell signaling. However, other signals, such as growth factors, PI3K signaling and TCR ligation, also trigger activation of mTOR[281]. mTOR activity is necessary for proper immune cell activation, as inhibition by rapamycin blocks IL-2 production in T cells. Furthermore, mTOR restricts FOXP3 production and thus T_{reg} induction by a poorly defined mechanism[282]. RPTOR could possibly link the kinase mTOR to NFAT.

Interestingly, mTOR has been shown to phosphorylate NFATc4, thereby retaining NFATc4 in an inactive state[283]. However, this is not in line with the activating role that mTOR has on IL-2 production. Future studies might reveal whether the mTOR complex indeed regulates the activity of other NFAT isoforms. If this were the case, this crosstalk would constitute an interesting link between the targets of two widely used immunosuppressive drugs, CsA and rapamycin.

4.2.2.7. CHEK1, NEK6, NEK7 and PLK: Potential NFAT Kinases?

Additionally, we also identified a group of NFAT interacting proteins that might regulate NFAT activity and stability via phosphorylation. The enriched kinases GSK3β and casein kinase are known NFAT kinases that trigger its re-phosphorylation and thereby nuclear export[152,153]. In the present thesis, we revealed that also the serine/threonine kinase CHEK1 interacts with NFATc2 (FIGURE 19) and potentially with NFATc1 (TABLE 6). This interaction is independent of DNA binding, as it is not decreased in the presence of an intercalating agent (FIGURE 21). CHEK1 is known to phosphorylate the transcription factor RelA, thereby repressing its potential for transactivation[284]. Because NFAT proteins are also highly regulated by phosphorylation and dephosphorylation, a regulatory role for CHEK1 on NFAT activity seems possible. The same possibility exists for the kinases *polo-like kinase-1* (PLK1) and *never in mitosis-related kinase-6/7* (NEK6/7) that were found enriched in the MS experiments (TABLE 6). Interestingly, all three kinases are related to the regulation of mitosis and are activated during DNA damage response[285–288]. This suggests that there might be cell cycle dependent regulation of NFAT activity. In the light of NFAT playing a well-known role as a oncogene in several tumors, the interdependence between cell cycle kinases and NFAT appears interesting[118,289]. Without further evidence that these kinases are indeed able to phosphorylate NFAT, this remains speculative, though. NFAT reporter gene assays or NFAT translocation assays may be used to determine NFAT activity under conditions where these kinases are either activated or inhibited.

4.2.2.8. 14-3-3 Proteins, RANBP9 and CABIN-1: Regulators of NFAT Phosphorylation and Activation

14-3-3 proteins bind to phosphorylated NFAT, which interferes with NFAT transcriptional activity[157]. Beside the known NFAT interactors 14-3-3θ and 14-3-3ζ, we present allusions that also the isoforms 14-3-3β, 14-3-3γ and 14-3-3ε can bind to NFAT (TABLE 6). This points towards a redundancy in this function of 14-3-3 proteins. *Calcineurin binding protein-1* (CABIN1) is another negative regulator of NFAT activity that was co-purified with NFAT proteins. CABIN1 can bind to CaN, thereby preventing dephosphorylation of NFAT by

this phosphatase[290]. Our results imply that additional binding of CABIN1 to NFAT proteins might also contribute to this regulatory process (TABLE 6). The protein *ran binding protein-9* (RANPB9), which is a known inhibitor of the DYRK1 kinase[291], was revealed as another potential interactor of NFATc1 and NFATc2 by the CoIP-MS experiments (TABLE 6). Given the important role of DYRK kinases in regulating NFAT activity by phosphorylation, it would be interesting to investigate whether NFAT-RANPB9 binding might affect NFAT activity[156].

4.2.3. Concluding Remarks

In the present thesis, we provided a list of potential, so far unknown NFAT interaction partners. Out of these, the interactions of NFAT with Ikaros, Helios, CREB1, RUNX1, SATB1, CHEK1, WDR48, SCAI, and RPTOR have been confirmed by CoIP-WB. In general, there is a strong need for further experiments that concentrate on individual interaction partners. For instance, it will be important to prove their interaction with NFAT under physiological conditions, to distinguish between direct and indirect interactions and to define interacting domains. Furthermore, functional studies will provide information on how and to which extend individual interaction partners influence the stability, activity, localization or target specificity of NFAT proteins. To this end, it will be enlightening to investigate the impact of genetic ablation of an individual factor on NFAT localization, promoter binding or transactivation capacity. Finally, this will improve our understanding of how NFAT – in concert with a plethora of other proteins – controls the activation of lymphocytes in health and disease.

4.2.4. Outlook

Evolution usually preserved only those features and mechanisms that are useful. Therefore, I hypothesize that each occurring protein-protein interaction has a functional relevance. This also applies to the more than 100 potential interaction partners of NFAT proteins that we identified during the present thesis.

In the course of this chapter, we have discussed the caveats of our study; and we suggested future experiments that can circumvent them, thus strengthening the confidence in individual interactions. In general, each newly identified interaction can be the starting point for a complete project that might focus on the molecular interaction or its functional significance. Future studies will attend to these questions.

During the preceding section, we highlighted the functional implication of selected interactions of NFAT with other proteins. Moreover, we draw perspectives for future experiments to study these particular interactions in more detail. In this final chapter, we would

like to discuss more general concepts and strategies that can be applied to study the nature and significance of individual interaction pairs.

When transcription factors interact, it is likely that they can bind to overlapping DNA sequences, thereby cooperating in the regulation of common target genes. Thus, it would be enlightening to obtain ChIP-Seq data from NFAT and interacting transcription factors (e.g. CREB1, RUNX1, Ikaros, SATB1) and search these datasets for common or overlapping binding sites. Importantly, this will only be productive if the datasets are comparable. At best, they are acquired from the same cell type under identical culture and stimulation conditions, in the same lab, using an identical protocol. The major challenge for this approach is the availability of antibodies that work in ChIP-Seq. For NFAT, all reported ChIP-Seq data were acquired with antibodies that are not commercially available[213,292].

The identification of overlapping binding sites would imply cooperative binding of the interacting transcription factors, as our bioinformatic analyses suggest for NFAT-CREB1 and NFAT-RUNX. Further experiments to prove this hypothesis might involve ChIP with knock-down or overexpression of one transcription factor; or pull-down experiments with DNA-oligonucleotides that span the suspected composite DNA binding site[233,293]. A recent report very elegantly employed *systematic evolution of ligands by exponential enrichment* (SELEX) to identify heterodimeric binding sites for transcription factor pairs, thereby proving cooperative DNA binding at least *in vitro*[294]. Similar experiments for NFAT and its interaction partners would be enlightening as well.

Importantly, data on overlapping and non-overlapping binding sites would allow drawing conclusions on the functional significance of individual NFAT interactions with other transcription factors. For example, it is tempting to speculate that the lymphocyte specific transcription factor Ikaros suppresses the expression of non-lymphoid NFAT target genes via interaction with NFAT. Thereby Ikaros would reduce the entity of NFAT target genes to a lymphocyte specific subset. If this is the case, overlapping NFAT-Ikaros binding should be found preferentially at genes that are repressed in lymphocytes. For Notch, such a T cell specific shaping of target genes via selective suppression by Ikaros was recently described[295]. However, whether a similar mechanism exists for NFAT and Ikaros remains speculative, yet.

Nonetheless, related mechanisms are also conceivable for the interaction of NFAT with further transcription factors. It appears possible, that under different cellular conditions (stimulation conditions, differentiation status), individual NFAT interaction partners might influence the binding and the activation potential of NFAT. In this way, RUNX1, CREB1 or others might act in concert with NFAT to bind and activate individual common target genes,

which are only expressed when both transcription factors are present and active. This would help to explain how NFAT activation could have different outcomes, depending on the cellular activation and differentiation status[112]. NFAT ChIP-Seq in the presence and absence of one (active) interacting transcription factor might give hints whether a particular interaction influences the binding spectrum of NFAT.

Another interesting point is that NFAT has been shown to be involved in *de novo* opening of genomic region upon T cell receptor activation[296]. Thus, an imposing question is to which extent the interaction of NFAT with other proteins influences epigenetic remodeling at DNA sites of NFAT binding. Beside the well-known recruitment of histone-deacetylases by NFAT, the cooperation with transcription factors such as SATB1 might further enhance chromatin remodeling[182,230,278]. To address this question, it might be enlightening to examine histone modifications (acetylation, methylation) at DNA sites where NFAT binds in cooperation with interacting transcription factors. Again, determination of those sites by ChIP-Seq would be a pre-requirement.

Finally, it is inevitable to study the molecular mechanisms of the individual interactions in order to shed light on the importance of a certain protein-protein interaction. This involves defining the interaction interface of the two interacting proteins on a molecular level, either by obtaining x-ray crystallographic data or by mutational analysis, such as alanine scans. The knowledge of the interacting domains and involved amino acid residues would allow disturbing the interaction via genome editing, knock-out/reconstitution or interface spanning peptides in a specific way. By this, it is possible to investigate the significance of a given interaction on a cellular level. Strikingly, such studies are much more specific and enlightening than depletion of one interaction partner, since the latter approach might have massive additional effects that would prevent any conclusion.

Furthermore, being able to disturb an important protein-protein interaction clears the way for therapeutic interference. To this end, peptides that enhance anti-tumor immunity by blocking the NFAT-FOXP3 interaction, or immunosuppressive peptides that block the interaction of CaN and NFAT constitute promising agents to treat cancer or autoimmune diseases with reduced side effects[297–299]. Blocking the interaction between NFAT and other proteins may influence T cell activation under specific pathophysiological conditions or drive T helper cell differentiation into a beneficial direction. Ultimately, in-depth studies of NFAT interactions may once lead to the development of more specific, potent immune-modulating therapies.

5. Summary (English)

A T cell is activated by the binding of a specific antigen to its T cell receptor. Subsequently, signaling modules integrate information from the antigen receptor, environment and cellular background to produce an adequate outcome. Mechanistically, the activation of diverse transcription factors drives and shapes the cellular reaction in most cases. The transcription factors *nuclear factor of activated T cells* (NFAT) and *nuclear factor of κ light chain enhancer of activated B cells* (NFκB) play a pivotal role in T cell biology. Aberrations in their activation pathways can lead to immunodeficiency, autoimmune diseases and cancer development.

A complex that consists of CARMA1, BCL10 and MALT1 (CBM-complex) controls the activation of NFκB following TCR ligation by integrating input from different signaling pathways (PKCθ, calcineurin). Employing a combination of co-immunopurification with mass spectrometry, we identified HOIP and HOIL1, two compounds of the linear ubiquitin assembly complex LUBAC, as so far unknown interactors of BCL10. We proved that HOIP interacts with BCL10 after TCR stimulation in Jurkat cells and after PMA/ionomycin stimulation in primary T helper cells. The presence of HOIP, but not its enzymatic activity, is necessary for complete NFκB activation after TCR/co-receptor engagement; a finding that was revealed in recent reports from other groups. Thus, HOIP constitutes a new potential target to modulate T cell activation. However, it remains unclear how LUBAC components are recruited to the CBM signaling complex and how they contribute to the activation of IKK and NFκB.

The activation of NFAT transcription factors is a hallmark of T cell activation and a pre-requisite for most T cell effector functions. NFAT readily interacts with other transcription factors. These interactions strongly influence the locus and the outcome of NFAT binding. Via binding to the IL-2 promoter, NFAT in a complex with AP1 promotes IL-2 expression, while a complex of NFAT and FOXP3 represses IL-2 expression. In the absence of interaction partners, NFAT binding to this locus is not detectable.

By combining co-immunopurification with mass spectrometry, we identified more than 100 potential previously unknown interaction partners of NFATc1 and NFATc2, including more than 40 transcription factors. We could confirm a range of these interactions in follow-up experiments, including those with Ikaros, CREB1 and RUNX1. Additionally, we identified potential common binding motifs of NFAT with these transcription factors by the use of bioinformatics. Thereby, we found that dimeric NFAT-RUNX and NFAT-CRE binding motifs are highly enriched within genomic regions of NFAT binding in activated cytotoxic T cells.

Further experiments, including ChIP-Seq and molecular interaction studies, will reveal how NFAT concerts T cell functions within different T cell subsets and how other proteins influence NFAT's activity to shape the outcome of T cell activation. This may advance the development of more specific immune-modulatory treatments.

6. Zusammenfassung (Deutsch)

T-Zellen werden durch die Bindung eines spezifischen Antigens über ihren T-Zell-Rezeptor (TZR) aktiviert. Die vom Antigenrezeptor kommenden Signale werden in Signalkomplexen verarbeitet, mit zusätzlichen Informationen zu Umgebung und Zellstatus versehen und integriert, um eine adäquate Reaktion der Zelle auszulösen. Diese Reaktion wird in vielen Fällen durch die Aktivierung verschiedener Transkriptionsfaktoren ausgelöst und moduliert. Die Transkriptionsfaktoren *Kernfaktor in aktivierten T-Zellen* (NFAT) und *Kernfaktor des κ-Leichtkettenverstärkers in aktivierten B-Zellen* (NFκB) spielen eine entscheidende Rolle bei der T-Zellaktivierung. Anomalien in deren Regulierung führen zu Immundefekten, Autoimmunerkrankungen und Krebs.

Die NFκB-Aktivierung nach TZR-Stimulation wird vom CBM-Komplex (für CARMA1-BCL10-MALT1-Komplex) durch die Integration der Einträge verschiedener Signalwege kontrolliert. Durch Kombination von Co-Immunpräzipitation und Massenspektrometrie konnten wir die Proteine HOIP und HOIL1, die Teil des Ubiquitin-Ligase-Komplexes LUBAC sind, als Interaktionspartner von BCL10 identifizieren. Wir konnten zeigen, dass HOIP nach Stimulation sowohl in Jurkat-Zellen als auch in primären humanen T-Helferzellen mit BCL10 interagiert. Das Vorhandensein von HOIP – nicht aber dessen katalytische Aktivität – ist für eine komplette NFκB-Aktivierung nach T-Zellaktivierung essentiell, wie kürzlich erschienene Arbeiten anderer Gruppen offenbart haben. Somit ist HOIP ein neues potentielles Target zur Modulierung der T-Zellaktivierung. Unklar ist jedoch weiterhin, wie der LUBAC-Komplex zum CBM-Komplex rekrutiert wird und wie genau er zur Aktivierung von IKK und NFκB beiträgt.

Die Aktivierung von NFAT-Transkriptionsfaktoren ist Voraussetzung für die meisten T-Zell-Effektorfunktionen. NFAT interagiert mit anderen Transkriptionsfaktoren. Diese Interaktionen haben großen Einfluss darauf, an welchen DNA-Sequenzen NFAT bindet und welche Wirkung diese Bindung hervorruft. So hat NFAT beispielsweise im IL-2-Promoterbereich zusammen mit AP1 einen aktivierenden und mit FOXP3 einen inhibierenden Effekt auf die IL-2-Produktion. In Abwesenheit von Interaktionspartnern ist eine Bindung von NFAT im IL-2-Promoterbereich hingegen nicht nachweisbar.

Durch Kombination von Co-Immunpräzipitation und Massenspektrometrie konnten wir über 100 bislang unbekannte, potentielle Interaktionspartner von NFATc1 und NFATc2 identifizieren, darunter mehr als 40 Transkriptionsfaktoren. Einige dieser Interaktionen (darunter die mit CREB1, RUNX1 und Ikaros) konnten im Laufe dieser Arbeit verifiziert werden. Zusätzlich haben wir mithilfe bioinformatischer Methoden potentielle gemeinsame Bindungsstellen dieser Transkriptionsfaktoren mit NFAT identifiziert. Hierbei zeigte sich, dass in genomischen Regionen, die von NFAT in aktivierten zytotoxischen T Zellen gebunden werden, dimere NFAT-RUNX und NFAT-CRE Bindemotive stark gehäuft auftreten.

Weiterführende Experimente wie ChIP-Seq und molekulare Interaktionsstudien werden das Verständnis dafür schärfen, wie NFAT die T-Zell-Funktionen in verschiedenen T-Zelltypen moduliert, und wie andere Proteine die NFAT-Aktivität beeinflussen um die T-Zell-Aktivierung zu regulieren. Dies könnte die Entwicklung spezifischerer immun-modulierender Therapien vorantreiben.

7. References

1. Gould, S. J. *Full House*. (Harmony Books, 1996).
2. Wikipedia. Severe combined immunodeficiency. (2015). at <https://en.wikipedia.org/wiki/Severe_combined_immunodeficiency [2015-12-10]>
3. Sponzilli, I. & Notarangelo, L. D. Severe combined immunodeficiency (SCID): from molecular basis to clinical management. *Acta Biomed.* **82,** 5–13 (2011).
4. Hannibal, M. C. & Torgerson, T. *IPEX Syndrome*. *GeneReviews(®)* (1993). at <http://www.ncbi.nlm.nih.gov/pubmed/20301297 [15-12-11]>
5. Lisnevskaia, L., Murphy, G. & Isenberg, D. Systemic lupus erythematosus. *Lancet* **384,** 1878–1888 (2014).
6. Mak, T. W. The T cell antigen receptor: 'The Hunting of the Snark'. *Eur. J. Immunol.* **37 Suppl 1,** S83–93 (2007).
7. Murphy, K., Travers, P. & Walport, M. *Janeway's Immunobiology*. (Garland Science, 2007).
8. Klein, L., Kyewski, B., Allen, P. M. & Hogquist, K. A. Positive and negative selection of the T cell repertoire: what thymocytes see (and don't see). *Nat. Rev. Immunol.* **14,** 377–91 (2014).
9. Collado, J. A., Guitart, C., Ciudad, M. T., Alvarez, I. & Jaraquemada, D. The repertoires of peptides presented by MHC-II in the thymus and in peripheral tissue: A clue for autoimmunity? *Front. Immunol.* **4,** 442 (2013).
10. Sakaguchi, S., Miyara, M., Costantino, C. M. & Hafler, D. A. FOXP3+ regulatory T cells in the human immune system. *Nat. Rev. Immunol.* **10,** 490–500 (2010).
11. Osorio, F., Fuentes, C., López, M. N., Salazar-Onfray, F. & González, F. E. Role of dendritic ells in the induction of lympchocyte tolerance. *Front. Immunol.* **6,** 535 (2015).
12. Cantor, H. & Boyse, E. A. Functional subclasses of T-lymphocytes bearing different Ly antigens. I. The generation of functionally distinct T-cell subclasses is a differentiative process independent of antigen. *J. Exp. Med.* **141,** 1376–89 (1975).
13. Luckheeram, R. V., Zhou, R., Verma, A. D. & Xia, B. $CD4^+$T cells: differentiation and functions. *Clin. Dev. Immunol.* **2012,** 925135 (2012).
14. Appleman, L. J. & Boussiotis, V. A. T cell anergy and costimulation. *Immunol. Rev.* **192,** 161–80 (2003).
15. Brownlie, R. J. & Zamoyska, R. T cell receptor signalling networks: branched, diversified and bounded. *Nat. Rev. Immunol.* **13,** 257–69 (2013).
16. Eccleston, A. & Dhand, R. Signalling in cancer. *Nature* **441,** 423–423 (2006).
17. Grunebaum, E., Sharfe, N. & Roifman, C. M. Human T cell immunodeficiency: when signal transduction goes wrong. *Immunol. Res.* **35,** 117–26 (2006).
18. Al-Herz, W. *et al.* Primary immunodeficiency diseases: an update on the classification from the international union of immunological societies expert committee for primary immunodeficiency. *Front. Immunol.* **5,** 162 (2014).
19. Blumberg, P. M. Protein kinase C as the receptor for the phorbol ester tumor promoters: sixth Rhoads memorial award lecture. *Cancer Res.* **48,** 1–8 (1988).
20. Dolmetsch, R. E., Lewis, R. S., Goodnow, C. C. & Healy, J. I. Differential activation of transcription factors induced by Ca2+ response amplitude and duration. *Nature* **386,** 855–8 (1997).
21. Call, M. E., Pyrdol, J., Wiedmann, M. & Wucherpfennig, K. W. The organizing principle in the formation of the T cell receptor-CD3 complex. *Cell* **111,** 967–79 (2002).
22. Letourneur, F. & Klausner, R. D. Activation of T cells by a tyrosine kinase activation domain in the cytoplasmic tail of CD3 epsilon. *Science* **255,** 79–82 (1992).
23. Iwashima, M., Irving, B. A., van Oers, N. S., Chan, A. C. & Weiss, A. Sequential interactions of the TCR with two distinct cytoplasmic tyrosine kinases. *Science* **263,** 1136–1139 (1994).
24. Chan, A. C. *et al.* Activation of ZAP-70 kinase activity by phosphorylation of tyrosine 493 is required for lymphocyte antigen receptor function. *EMBO J.* **14,** 2499–2508 (1995).
25. Chan, A. C., Iwashima, M., Turck, C. W. & Weiss, A. ZAP-70: a 70 kd protein-tyrosine kinase that associates with the TCR zeta chain. *Cell* **71,** 649–662 (1992).
26. Zhang, W., Sloan-Lancaster, J., Kitchen, J., Trible, R. P. & Samelson, L. E. LAT: The ZAP-70 tyrosine kinase substrate that links T cell receptor to cellular activation. *Cell* **92,** 83–92 (1998).
27. Wardenburg, J. B. *et al.* Phosphorylation of SLP-76 by the ZAP-70 protein-tyrosine kinase is required for T-cell receptor function. *J. Biol. Chem.* **271,** 19641–19644 (1996).
28. Yablonski, D., Kuhne, M. R., Kadlecek, T. & Weiss, A. Uncoupling of nonreceptor tyrosine kinases from PLC-gamma1 in an SLP-76-deficient T cell. *Science* **281,** 413–416 (1998).
29. Zhang, W., Trible, R. P. & Samelson, L. E. LAT palmitoylation: its essential role in membrane microdomain targeting and tyrosine phosphorylation during T cell activation. *Immunity* **9,** 239–246 (1998).

30. Perez-Villar, J. J. & Kanner, S. B. Regulated association between the tyrosine kinase Emt/Itk/Tsk and phospholipase-C gamma 1 in human T lymphocytes. *J. Immunol.* **163,** 6435–6441 (1999).
31. Bogin, Y., Ainey, C., Beach, D. & Yablonski, D. SLP-76 mediates and maintains activation of the Tec family kinase ITK via the T cell antigen receptor-induced association between SLP-76 and ITK. *Proc. Natl. Acad. Sci. U. S. A.* **104,** 6638–6643 (2007).
32. Gupta, S. Mechanisms of transmembrane signalling in human T cell activation. *Mol. Cell. Biochem.* **91,** 45–50 (1989).
33. Nishizuka, Y. Protein kinase C and lipid signaling for sustained cellular responses. *FASEB J.* **9,** 484–496 (1995).
34. Garçon, F. *et al.* CD28 provides T-cell costimulation and enhances PI3K activity at the immune synapse independently of its capacity to interact with the p85/p110 heterodimer. *Blood* **111,** 1464–1471 (2008).
35. Chan, T. O., Rittenhouse, S. E. & Tsichlis, P. N. AKT/PKB and other D3 phosphoinositide-regulated kinases: kinase activation by phosphoinositide-dependent phosphorylation. *Annu. Rev. Biochem.* **68,** 965–1014 (1999).
36. Toker, A. Protein kinases as mediators of phosphoinositide 3-kinase signaling. *Mol. Pharmacol.* **57,** 652–658 (2000).
37. Le Good, J. A. *et al.* Protein kinase C isotypes controlled by phosphoinositide 3-kinase through the protein kinase PDK1. *Science* **281,** 2042–2045 (1998).
38. Wang, X., Chuang, H. C., Li, J. P. & Tan, T. H. Regulation of PKC-θ function by phosphorylation in T cell receptor signaling. *Front. Immunol.* **3,** (2012).
39. Zhao, Y. *et al.* TCR-induced, PKC-θ-mediated NF-κB activation is regulated by a caspase-8–caspase-9–caspase-3 cascade. *Biochem. Biophys. Res. Commun.* **450,** 526–531 (2014).
40. Rauscher, F. J. *et al.* Fos-associated protein p39 is the product of the jun proto-oncogene. *Science* **240,** 1010–6 (1988).
41. John, M., Leppik, R., Busch, S. J., Granger-Schnarr, M. & Schnarr, M. DNA binding of Jun and Fos bZip domains: homodimers and heterodimers induce a DNA conformational change in solution. *Nucleic Acids Res.* **24,** 4487–94 (1996).
42. Hai, T. & Curran, T. Cross-family dimerization of transcription factors Fos/Jun and ATF/CREB alters DNA binding specificity. *Proc. Natl. Acad. Sci. U. S. A.* **88,** 3720–3724 (1991).
43. Halazonetis, T. D., Georgopoulos, K., Greenberg, M. E. & Leder, P. c-Jun dimerizes with itself and with c-Fos, forming complexes of different DNA binding affinities. *Cell* **55,** 917–24 (1988).
44. Ebinu, J. O. *et al.* RasGRP links T-cell receptor signaling to Ras. *Blood* **95,** 3199–3203 (2000).
45. Roose, J. P., Mollenauer, M., Gupta, V. A., Stone, J. & Weiss, A. A diacylglycerol-protein kinase C-RasGRP1 pathway directs Ras activation upon antigen receptor stimulation of T cells. *Mol. Cell. Biol.* **25,** 4426–41 (2005).
46. Seternes, O. M. *et al.* Synergistic increase in c-fos expression by simultaneous activation of the ras/raf/map kinase- and protein kinase A signaling pathways is mediated by the c-fos AP-1 and SRE sites. *Biochim. Biophys. Acta* **1395,** 345–60 (1998).
47. Monje, P., Hernández-Losa, J., Lyons, R. J., Castellone, M. D. & Gutkind, J. S. Regulation of the transcriptional activity of c-Fos by ERK. A novel role for the prolyl isomerase PIN1. *J. Biol. Chem.* **280,** 35081–4 (2005).
48. Kaminuma, O., Deckert, M., Elly, C., Liu, Y. C. & Altman, A. Vav-Rac1-mediated activation of the c-Jun N-terminal kinase/c-Jun/AP-1 pathway plays a major role in stimulation of the distal NFAT site in the interleukin-2 gene promoter. *Mol. Cell. Biol.* **21,** 3126–36 (2001).
49. Hibi, M., Lin, A., Smeal, T., Minden, A. & Karin, M. Identification of an oncoprotein- and UV-responsive protein kinase that binds and potentiates the c-Jun activation domain. *Genes Dev.* **7,** 2135–48 (1993).
50. Hoesel, B. & Schmid, J. A. The complexity of NF-κB signaling in inflammation and cancer. *Mol. Cancer* **12,** 86 (2013).
51. Ruland, J. *et al.* Bcl10 is a positive regulator of antigen receptor-induced activation of NF-kappaB and neural tube closure. *Cell* **104,** 33–42 (2001).
52. Koseki, T. *et al.* CIPER, a novel NF kappaB-activating protein containing a caspase recruitment domain with homology to Herpesvirus-2 protein E10. *J. Biol. Chem.* **274,** 9955–9961 (1999).
53. Srinivasula, S. M. *et al.* CLAP, a novel caspase recruitment domain-containing protein in the tumor necrosis factor receptor pathway, regulates NF-kappaB activation and apoptosis. *J. Biol. Chem.* **274,** 17946–54 (1999).
54. Thome, M., Charton, J. E., Pelzer, C. & Hailfinger, S. Antigen receptor signaling to NF-kappaB via CARMA1, BCL10, and MALT1. *Cold Spring Harb. Perspect. Biol.* **2,** a003004 (2010).
55. Langel, F. D. *et al.* Multiple protein domains mediate interaction between Bcl10 and MALT1. *J. Biol. Chem.* **283,** 32419–32431 (2008).
56. Lucas, P. C. *et al.* Bcl10 and MALT1, independent targets of chromosomal translocation in malt lymphoma, cooperate in a novel NF-kappa B signaling pathway. *J. Biol. Chem.* **276,** 19012–19019 (2001).
57. Wegener, E. *et al.* Essential role for IkappaB kinase beta in remodeling Carma1-Bcl10-Malt1 complexes upon T cell activation. *Mol. Cell* **23,** 13–23 (2006).
58. Brenner, D. *et al.* Phosphorylation of CARMA1 by HPK1 is critical for NF-kappaB activation in T cells. *Proc. Natl.*

Acad. Sci. U. S. A. **106,** 14508–14513 (2009).

59. Cheng, J., Hamilton, K. S. & Kane, L. P. Phosphorylation of Carma1, but not Bcl10, by Akt regulates TCR/CD28-mediated NF-κB induction and cytokine production. *Mol. Immunol.* **59,** 110–6 (2014).
60. Sommer, K. *et al.* Phosphorylation of the CARMA1 linker controls NF-κB activation. *Immunity* **23,** 561–574 (2005).
61. Matsumoto, R. *et al.* Phosphorylation of CARMA1 plays a critical role in T Cell receptor-mediated NF-kappaB activation. *Immunity* **23,** 575–85 (2005).
62. Shinohara, H., Maeda, S., Watarai, H. & Kurosaki, T. IkappaB kinase beta-induced phosphorylation of CARMA1 contributes to CARMA1 Bcl10 MALT1 complex formation in B cells. *J. Exp. Med.* **204,** 3285–93 (2007).
63. Qiao, Q. *et al.* Structural architecture of the CARMA1/Bcl10/MALT1 signalosome: nucleation-induced filamentous assembly. *Mol. Cell* **51,** 766–79 (2013).
64. Zhou, H. *et al.* Bcl10 activates the NF-kappaB pathway through ubiquitination of NEMO. *Nature* **427,** 167–171 (2004).
65. Oeckinghaus, A. *et al.* Malt1 ubiquitination triggers NF-kappaB signaling upon T-cell activation. *EMBO J.* **26,** 4634–4645 (2007).
66. Sun, L., Deng, L., Ea, C. K., Xia, Z. P. & Chen, Z. J. The TRAF6 ubiquitin ligase and TAK1 kinase mediate IKK activation by BCL10 and MALT1 in T lymphocytes. *Mol. Cell* **14,** 289–301 (2004).
67. Noels, H. *et al.* A Novel TRAF6 binding site in MALT1 defines distinct mechanisms of NF-kappaB activation by API2middle dotMALT1 fusions. *J. Biol. Chem.* **282,** 10180–10189 (2007).
68. Carvalho, G. *et al.* Interplay between BCL10, MALT1 and IkappaBalpha during T-cell-receptor-mediated NFkappaB activation. *J. Cell Sci.* **123,** 2375–80 (2010).
69. Misra, R. S. *et al.* Caspase-8 and c-FLIPL associate in lipid rafts with NF-kappaB adaptors during T cell activation. *J. Biol. Chem.* **282,** 19365–74 (2007).
70. Bidère, N., Snow, A. L., Sakai, K., Zheng, L. & Lenardo, M. J. Caspase-8 regulation by direct interaction with TRAF6 in T cell receptor-induced NF-kappaB activation. *Curr. Biol.* **16,** 1666–71 (2006).
71. Su, H. *et al.* Requirement for caspase-8 in NF-kappaB activation by antigen receptor. *Science* **307,** 1465–1468 (2005).
72. Xu, G. *et al.* Crystal structure of inhibitor of kappaB kinase beta. *Nature* **472,** 325–330 (2011).
73. Polley, S. *et al.* A structural basis for IκB kinase 2 activation via oligomerization-dependent trans auto-phosphorylation. *PLoS Biol.* **11,** e1001581 (2013).
74. Wang, C. *et al.* TAK1 is a ubiquitin-dependent kinase of MKK and IKK. *Nature* **412,** 346–351 (2001).
75. Zhang, J. *et al.* An unexpected twist to the activation of IKKβ: TAK1 primes IKKβ for activation by autophosphorylation. *Biochem. J.* **1,** 531–537 (2014).
76. Wu, C.-J. & Ashwell, J. D. NEMO recognition of ubiquitinated Bcl10 is required for T cell receptor-mediated NF-kappaB activation. *Proc. Natl. Acad. Sci. U. S. A.* **105,** 3023–3028 (2008).
77. Stempin, C. C. *et al.* The E3 ubiquitin ligase mind bomb-2 (MIB2) protein controls B-cell CLL/lymphoma 10 (BCL10)-dependent NF-κB activation. *J. Biol. Chem.* **286,** 37147–57 (2011).
78. Li, Q. & Verma, I. M. NF-kappaB regulation in the immune system. *Nat. Rev. Immunol.* **2,** 725–734 (2002).
79. Bonizzi, G. & Karin, M. The two NF-κB activation pathways and their role in innate and adaptive immunity. *Trends Immunol.* **25,** 280–288 (2004).
80. Ferch, U. *et al.* MALT1 directs B cell receptor-induced canonical nuclear factor-kappaB signaling selectively to the c-Rel subunit. *Nat. Immunol.* **8,** 984–91 (2007).
81. Bidère, N. *et al.* Casein kinase 1alpha governs antigen-receptor-induced NF-kappaB activation and human lymphoma cell survival. *Nature* **458,** 92–96 (2009).
82. Shin, H. M. *et al.* NOTCH1 can initiate NF-κB activation via cytosolic interactions with components of the T cell signalosome. *Front. Immunol.* **5,** (2014).
83. Ruefli-Brasse, A. a, Lee, W. P., Hurst, S. & Dixit, V. M. Rip2 participates in Bcl10 signaling and T-cell receptor-mediated NF-kappaB activation. *J. Biol. Chem.* **279,** 1570–4 (2004).
84. Oruganti, S. R., Edin, S., Grundström, C. & Grundström, T. CaMKII targets Bcl10 in T-cell receptor induced activation of NF-κB. *Mol. Immunol.* **48,** 1448–1460 (2011).
85. Zeng, H. *et al.* Phosphorylation of Bcl10 negatively regulates T-cell receptor-mediated NF-kappaB activation. *Mol. Cell. Biol.* **27,** 5235–45 (2007).
86. Ishiguro, K. *et al.* Ca2+/calmodulin-dependent protein kinase II is a modulator of CARMA1-mediated NF-kappaB activation. *Mol. Cell. Biol.* **26,** 5497–508 (2006).
87. Frischbutter, S., Gabriel, C., Bendfeldt, H., Radbruch, A. & Baumgrass, R. Dephosphorylation of Bcl-10 by calcineurin is essential for canonical NF-κB activation in Th cells. *Eur. J. Immunol.* **41,** 2349–2357 (2011).
88. Palkowitsch, L. *et al.* The Ca2+-dependent phosphatase calcineurin controls the formation of the Carma1-Bcl10-

Malt1 complex during T cell receptor-induced NF-kappaB activation. *J. Biol. Chem.* **286,** 7522–34 (2011).

89. Scharschmidt, E., Wegener, E., Heissmeyer, V., Rao, A. & Krappmann, D. Degradation of Bcl10 induced by T-cell activation negatively regulates NF-kappa B signaling. *Mol. Cell. Biol.* **24,** 3860–73 (2004).
90. Lobry, C., Lopez, T., Israël, A. & Weil, R. Negative feedback loop in T cell activation through IkappaB kinase-induced phosphorylation and degradation of Bcl10. *Proc. Natl. Acad. Sci. U. S. A.* **104,** 908–913 (2007).
91. Hu, S. *et al.* cIAP2 is a ubiquitin protein ligase for BCL10 and is dysregulated in mucosa-associated lymphoid tissue lymphomas. *J. Clin. Invest.* **116,** 174–181 (2006).
92. Paul, S., Kashyap, A. K., Jia, W., He, Y.-W. W. & Schaefer, B. C. Selective autophagy of the adaptor protein Bcl10 modulates T cell receptor activation of NF-κB. *Immunity* **36,** 947–58 (2012).
93. Moreno-García, M. E. *et al.* Kinase-independent feedback of the TAK1/TAB1 complex on BCL10 turnover and NF-κB activation. *Mol. Cell. Biol.* **33,** 1149–63 (2013).
94. Hu, S., Alcivar, A., Qu, L., Tang, J. & Yang, X. CIAP2 inhibits anigen receptor signaling by targeting Bcl10 for degredation. *Cell Cycle* **5,** 1438–1442 (2006).
95. Yoneda, T. *et al.* Regulatory mechanisms of TRAF2-mediated signal transduction by Bcl10, a MALT lymphoma-associated protein. *J. Biol. Chem.* **275,** 11114–20 (2000).
96. Rebeaud, F. *et al.* The proteolytic activity of the paracaspase MALT1 is key in T cell activation. *Nat. Immunol.* **9,** 272–281 (2008).
97. Gewies, A. *et al.* Uncoupling Malt1 threshold function from paracaspase activity results in destructive autoimmune inflammation. *Cell Rep.* **9,** 1292–305 (2014).
98. Düwel, M. *et al.* A20 negatively regulates T cell receptor signaling to NF-kappaB by cleaving Malt1 ubiquitin chains. *J. Immunol.* **182,** 7718–28 (2009).
99. Hailfinger, S. *et al.* Malt1-dependent RelB cleavage promotes canonical NF-{kappa}B activation in lymphocytes and lymphoma cell lines. *Proc. Natl. Acad. Sci. U. S. A.* **108,** 14596–14601 (2011).
100. Jeltsch, K. M. *et al.* Cleavage of roquin and regnase-1 by the paracaspase MALT1 releases their cooperatively repressed targets to promote T(H)17 differentiation. *Nat. Immunol.* **15,** 1079–89 (2014).
101. Wiesmann, C. *et al.* Structural determinants of MALT1 protease activity. *J. Mol. Biol.* **419,** 4–21 (2012).
102. Pelzer, C. *et al.* The protease activity of the paracaspase MALT1 is controlled by monoubiquitination. *Nat. Immunol.* **14,** 337–45 (2013).
103. Turvey, S. E. *et al.* The CARD11-BCL10-MALT1 (CBM) signalosome complex: Stepping into the limelight of human primary immunodeficiency. *J. Allergy Clin. Immunol.* **134,** 276–84 (2014).
104. Willis, T. G. *et al.* Bcl10 is involved in t(1;14)(p22;q32) of MALT B cell lymphoma and mutated in multiple tumor types. *Cell* **96,** 35–45 (1999).
105. Lenz, G. *et al.* Oncogenic CARD11 mutations in human diffuse large B cell lymphoma. *Science* **319,** 1676–9 (2008).
106. Berridge, M. J. Inositol trisphosphate and calcium signalling. *Nature* **361,** 315–25 (1993).
107. Roos, J. *et al.* STIM1, an essential and conserved component of store-operated Ca 2+ channel function. *J. Cell Biol.* **169,** 435–445 (2005).
108. Wu, M. M., Buchanan, J., Luik, R. M. & Lewis, R. S. Ca2+ store depletion causes STIM1 to accumulate in ER regions closely associated with the plasma membrane. *J. Cell Biol.* **174,** 803–13 (2006).
109. Xu, P. *et al.* Aggregation of STIM1 underneath the plasma membrane induces clustering of Orai1. *Biochem. Biophys. Res. Commun.* **350,** 969–976 (2006).
110. Clipstone, N. A. & Crabtree, G. R. Identification of calcineurin as a key signalling enzyme in T-lymphocyte activation. *Nature* **357,** 695–697 (1992).
111. Klee, C. B., Crouch, T. H. & Krinks, M. H. Calcineurin: a calcium- and calmodulin-binding protein of the nervous system. *Proc. Natl. Acad. Sci. U. S. A.* **76,** 6270–6273 (1979).
112. Hermann-Kleiter, N. & Baier, G. NFAT pulls the strings during CD4+ T helper cell effector functions. *Blood* **115,** 2989–2997 (2010).
113. Peng, S. L., Gerth, A. J., Ranger, A. M. & Glimcher, L. H. NFATc1 and NFATc2 together control both T and B cell activation and differentiation. *Immunity* **14,** 13–20 (2001).
114. Aramburu, J. *et al.* Affinity-driven peptide selection of an NFAT inhibitor more selective than cyclosporin A. *Science* **285,** 2129–33 (1999).
115. Macián, F. *et al.* Transcriptional mechanisms underlying lymphocyte tolerance. *Cell* **109,** 719–731 (2002).
116. Vaeth, M. *et al.* Dependence on nuclear factor of activated T-cells (NFAT) levels discriminates conventional T cells from Foxp3+ regulatory T cells. *Proc. Natl. Acad. Sci. U. S. A.* **109,** 16258–63 (2012).
117. Shin, D. S. *et al.* Regulatory T cells suppress CD4+ T cells through NFAT-dependent transcriptional mechanisms. *EMBO Rep.* **15,** 991–999 (2014).
118. Müller, M. R. & Rao, A. NFAT, immunity and cancer: a transcription factor comes of age. *Nat. Rev. Immunol.* **10,**

645–656 (2010).

119. Baksh, S. *et al.* NFATc2-mediated repression of cyclin-dependent kinase 4 expression. *Mol. Cell* **10,** 1071–81 (2002).

120. Buchholz, M. *et al.* Overexpression of c-myc in pancreatic cancer caused by ectopic activation of NFATc1 and the Ca2+/calcineurin signaling pathway. *EMBO J.* **25,** 3714–3724 (2006).

121. Shaw, J. P. *et al.* Identification of a putative regulator of early T cell activation genes. *Science* **241,** 202–205 (1988).

122. Jain, J., McCaffrey, P. G., Valge-Archer, V. E. & Rao, A. Nuclear factor of activated T cells contains Fos and Jun. *Nature* **356,** 801–4 (1992).

123. Jain, J. *et al.* The T-cell transcription factor NFATp is a substrate for calcineurin and interacts with Fos and Jun. *Nature* **365,** 352–5 (1993).

124. McCaffrey, P. G. *et al.* Isolation of the cyclosporin-sensitive T cell transcription factor NFATp. *Science* **262,** 750–754 (1993).

125. Northrop, J. P. *et al.* NF-AT components define a family of transcription factors targeted in T-cell activation. *Nature* **369,** 497–502 (1994).

126. Miyakawa, H., Woo, S. K., Dahl, S. C., Handler, J. S. & Kwon, H. M. Tonicity-responsive enhancer binding protein, a rel-like protein that stimulates transcription in response to hypertonicity. *Proc. Natl. Acad. Sci. U. S. A.* **96,** 2538–2542 (1999).

127. Lopez-Rodríguez, C., Aramburu, J., Rakeman, A. S. & Rao, A. NFAT5, a constitutively nuclear NFAT protein that does not cooperate with Fos and Jun. *Proc. Natl. Acad. Sci. U. S. A.* **96,** 7214–7219 (1999).

128. Hoey, T., Sun, Y. L., Williamson, K. & Xu, X. Isolation of two new members of the NF-AT gene family and functional characterization of the NF-AT proteins. *Immunity* **2,** 461–472 (1995).

129. Prieschl, E. E., Gouilleux-Gruart, V., Walker, C., Harrer, N. E. & Baumruker, T. A nuclear factor of activated T cell-like transcription factor in mast cells is involved in IL-5 gene regulation after IgE plus antigen stimulation. *J. Immunol.* **154,** 6112–6119 (1995).

130. Yaseen, N. R., Maizel, A. L., Wang, F. & Sharma, S. Comparative analysis of NFAT (nuclear factor of activated T cells) complex in human T and B lymphocytes. *J. Biol. Chem.* **268,** 14285–14293 (1993).

131. Aramburu, J., Azzoni, L., Rao, A. & Perussia, B. Activation and expression of the nuclear factors of activated T cells, NFATp and NFATc, in human natural killer cells: regulation upon CD16 ligand binding. *J. Exp. Med.* **182,** 801–810 (1995).

132. Sitara, D. & Aliprantis, A. O. Transcriptional regulation of bone and joint remodeling by NFAT. *Immunol. Rev.* **233,** 286–300 (2010).

133. Xia, Y. *et al.* Electrical stimulation of neonatal cardiac myocytes activates the NFAT3 and GATA4 pathways and up-regulates the adenylosuccinate synthetase 1 gene. *J. Biol. Chem.* **275,** 1855–1863 (2000).

134. Lunde, I. G., Kvaloy, H., Austbo, B., Christensen, G. & Carlson, C. R. Angiotensin II and norepinephrine activate specific calcineurin-dependent NFAT transcription factor isoforms in cardiomyocytes. *J. Appl. Physiol.* **111,** 1278–1289 (2011).

135. Ho, A. M., Jain, J., Rao, A. & Hogan, P. G. Expression of the transcription factor NFATp in a neuronal cell line and in the murine nervous system. *J. Biol. Chem.* **269,** 28181–28186 (1994).

136. Schwartz, N., Schohl, A. & Ruthazer, E. S. Neural activity regulates synaptic properties and dendritic structure in vivo through calcineurin/NFAT signaling. *Neuron* **62,** 655–69 (2009).

137. Xanthoudakis, S. *et al.* An enhanced immune response in mice lacking the transcription factor NFAT1. *Science* **272,** 892–5 (1996).

138. Ranger, a M., Oukka, M., Rengarajan, J. & Glimcher, L. H. Inhibitory function of two NFAT family members in lymphoid homeostasis and Th2 development. *Immunity* **9,** 627–635 (1998).

139. Ranger, A. M. *et al.* The transcription factor NF-ATc is essential for cardiac valve formation. *Nature* **392,** 186–90 (1998).

140. Yoshida, H. *et al.* The transcription factor NF-ATc1 regulates lymphocyte proliferation and Th2 cytokine production. *Immunity* **8,** 115–124 (1998).

141. Feske, S., Draeger, R., Peter, H. H., Eichmann, K. & Rao, A. The duration of nuclear residence of NFAT determines the pattern of cytokine expression in human SCID T cells. *J. Immunol.* **165,** 297–305 (2000).

142. Serfling, E. *et al.* NFATc1/αA: The other face of NFAT factors in lymphocytes. *Cell Commun. Signal.* **10,** 16 (2012).

143. Macian, F. NFAT proteins: key regulators of T-cell development and function. *Nat. Rev. Immunol.* **5,** 472–484 (2005).

144. Chuvpilo, S. *et al.* Multiple NF-ATc isoforms with individual transcriptional properties are synthesized in T lymphocytes. *J. Immunol.* **162,** 7294–301 (1999).

145. Chuvpilo, S. *et al.* Alternative polyadenylation events contribute to the induction of NF-ATc in effector T cells. *Immunity* **10,** 261–269 (1999).

146. Chuvpilo, S. *et al.* Autoregulation of NFATc1/A expression facilitates effector T cells to escape from rapid apoptosis.

Immunity **16,** 881–95 (2002).

147. Muhammad, K. *et al.* NF-κB factors control the induction of NFATc1 in B lymphocytes. *Eur. J. Immunol.* **44,** 3392–402 (2014).
148. Hock, M. *et al.* NFATc1 induction in peripheral T and B lymphocytes. *J. Immunol.* **190,** 2345–53 (2013).
149. Nayak, A. *et al.* Sumoylation of the transcription factor NFATc1 leads to its subnuclear relocalization and interleukin-2 repression by histone deacetylase. *J. Biol. Chem.* **284,** 10935–46 (2009).
150. Chen, L., Glover, J. N., Hogan, P. G., Rao, A. & Harrison, S. C. Structure of the DNA-binding domains from NFAT, Fos and Jun bound specifically to DNA. *Nature* **392,** 42–48 (1998).
151. Okamura, H. *et al.* Concerted dephosphorylation of the transcription factor NFAT1 induces a conformational switch that regulates transcriptional activity. *Mol. Cell* **6,** 539–550 (2000).
152. Beals, C. R., Sheridan, C. M., Turck, C. W., Gardner, P. & Crabtree, G. R. Nuclear export of NF-ATc enhanced by glycogen synthase kinase-3. *Science* **275,** 1930–1934 (1997).
153. Okamura, H. *et al.* A conserved docking motif for CK1 binding controls the nuclear localization of NFAT1. *Mol. Cell. Biol.* **24,** 4184–4195 (2004).
154. Chow, C. W., Rincón, M., Cavanagh, J., Dickens, M. & Davis, R. J. Nuclear accumulation of NFAT4 opposed by the JNK signal transduction pathway. *Science* **278,** 1638–1641 (1997).
155. Gómez del Arco, P., Martínez-Martínez, S., Maldonado, J. L., Ortega-Pérez, I. & Redondo, J. M. A role for the p38 MAP kinase pathway in the nuclear shuttling of NFATp. *J. Biol. Chem.* **275,** 13872–13878 (2000).
156. Gwack, Y. *et al.* A genome-wide Drosophila RNAi screen identifies DYRK-family kinases as regulators of NFAT. *Nature* **441,** 646–50 (2006).
157. Chow, C. W. & Davis, R. J. Integration of calcium and cyclic AMP signaling pathways by 14-3-3. *Mol. Cell. Biol.* **20,** 702–12 (2000).
158. Rainio, E.-M. E.-M., Sandholm, J. & Koskinen, P. J. Cutting edge: Transcriptional activity of NFATc1 is enhanced by the Pim-1 kinase. *J. Immunol.* **168,** 1524–7 (2002).
159. Vázquez-Cedeira, M. & Lazo, P. A. Human VRK2 (vaccinia-related kinase 2) modulates tumor cell invasion by hyperactivation of NFAT1 and expression of cyclooxygenase-2. *J. Biol. Chem.* **287,** 42739–50 (2012).
160. Gómez-Casero, E., San-Antonio, B., Iñiguez, M. A. & Fresno, M. Cot/Tpl2 and PKCzeta cooperate in the regulation of the transcriptional activity of NFATc2 through the phosphorylation of its amino-terminal domain. *Cell. Signal.* **19,** 1652–61 (2007).
161. Willingham, a T. *et al.* A strategy for probing the function of noncoding RNAs finds a repressor of NFAT. *Science* **309,** 1570–1573 (2005).
162. Liu, Z. *et al.* The kinase LRRK2 is a regulator of the transcription factor NFAT that modulates the severity of inflammatory. *Nat. Immunol.* **12,** 1063–70 (2011).
163. Terui, Y., Saad, N., Jia, S., McKeon, F. & Yuan, J. Dual role of sumoylation in the nuclear localization and transcriptional activation of NFAT1. *J. Biol. Chem.* **279,** 28257–65 (2004).
164. Valdor, R. *et al.* Regulation of NFAT by poly(ADP-ribose) polymerase activity in T cells. *Mol. Immunol.* **45,** 1863–1871 (2008).
165. Chen, L. *et al.* Only one of the two DNA-bound orientations of AP-1 found in solution cooperates with NFATp. *Curr. Biol.* **5,** 882–9 (1995).
166. Stroud, J. C. & Chen, L. Structure of NFAT bound to DNA as a monomer. *J. Mol. Biol.* **334,** 1009–1022 (2003).
167. Falvo, J. V *et al.* A dimer-specific function of the transcription factor NFATp. *Proc. Natl. Acad. Sci. U. S. A.* **105,** 19637–19642 (2008).
168. Macián, F., López-Rodríguez, C. & Rao, a. Partners in transcription: NFAT and AP-1. *Oncogene* **20,** 2476–89 (2001).
169. Nguyen, T. N. *et al.* The C-terminal region of human NFATc2 binds cJun to synergistically activate interleukin-2 transcription. *Mol. Immunol.* **47,** 2314–2322 (2010).
170. Soto-Nieves, N. *et al.* Transcriptional complexes formed by NFAT dimers regulate the induction of T cell tolerance. *J. Exp. Med.* **206,** 867–76 (2009).
171. Jeon, M.-S. S. *et al.* Essential role of the E3 ubiquitin ligase Cbl-b in T cell anergy induction. *Immunity* **21,** 167–177 (2004).
172. Heissmeyer, V. *et al.* Calcineurin imposes T cell unresponsiveness through targeted proteolysis of signaling proteins. *Nat. Immunol.* **5,** 255–265 (2004).
173. Jenkins, M. K., Chen, C. A., Jung, G., Mueller, D. L. & Schwartz, R. H. Inhibition of antigen-specific proliferation of type 1 murine T cell clones after stimulation with immobilized anti-CD3 monoclonal antibody. *J. Immunol.* **144,** 16–22 (1990).
174. Safford, M. *et al.* Egr-2 and Egr-3 are negative regulators of T cell activation. *Nat. Immunol.* **6,** 472–480 (2005).
175. Bandukwala, H. S. *et al.* Structure of a domain-swapped FOXP3 dimer on DNA and its function in regulatory T cells. *Immunity* **34,** 479–91 (2011).

176. Wu, Y. *et al.* FOXP3 controls regulatory T cell function through cooperation with NFAT. *Cell* **126,** 375–87 (2006).

177. Bettelli, E., Dastrange, M. & Oukka, M. Foxp3 interacts with nuclear factor of activated T cells and NF-kappa B to repress cytokine gene expression and effector functions of T helper cells. *Proc. Natl. Acad. Sci. U. S. A.* **102,** 5138–5143 (2005).

178. Torgerson, T. R. *et al.* FOXP3 inhibits activation-induced NFAT2 expression in T cells thereby limiting effector cytokine expression. *J. Immunol.* **183,** 907–15 (2009).

179. Klein-Hessling, S. *et al.* Cyclic AMP-induced chromatin changes support the NFATc-mediated recruitment of GATA-3 to the interleukin 5 promoter. *J. Biol. Chem.* **283,** 31030–7 (2008).

180. Rengarajan, J. *et al.* Interferon regulatory factor 4 (IRF4) interacts with NFATc2 to modulate interleukin 4 gene expression. *J. Exp. Med.* **195,** 1003–12 (2002).

181. Decker, E. L. *et al.* Early growth responce proteins (EGR) and nuclear factors of activated T cells (NFAT) form heterodimers and regulate proinflammatory cytokine gene expression. *Nucleic Acids Res.* **31,** 911–921 (2003).

182. Youn, H. D., Chatila, T. a & Liu, J. O. Integration of calcineurin and MEF2 signals by the coactivator p300 during T-cell apoptosis. *EMBO J.* **19,** 4323–4331 (2000).

183. Carneiro, F. R. G., Ramalho-Oliveira, R., Mognol, G. P. & Viola, J. P. B. Interferon regulatory factor 2 binding protein 2 is a new NFAT1 partner and represses its transcriptional activity. *Mol. Cell. Biol.* **31,** 2889–901 (2011).

184. Afkarian, M. *et al.* T-bet is a STAT1-induced regulator of IL-12R expression in naïve CD4+ T cells. *Nat. Immunol.* **3,** 549–57 (2002).

185. Zhang, F., Meng, G. & Strober, W. Interactions among the transcription factors Runx1, RORgammat and Foxp3 regulate the differentiation of interleukin 17-producing T cells. *Nat. Immunol.* **9,** 1297–306 (2008).

186. Gomez-Rodriguez, J. *et al.* Differential expression of interleukin-17A and -17F is coupled to T cell receptor signaling via inducible T cell kinase. *Immunity* **31,** 587–97 (2009).

187. Liu, X. K., Lin, X. & Gaffen, S. L. Crucial role for nuclear factor of activated T cells in T cell receptor-mediated regulation of human interleukin-17. *J. Biol. Chem.* **279,** 52762–71 (2004).

188. Rudra, D. *et al.* Transcription factor Foxp3 and its protein partners form a complex regulatory network. *Nat. Immunol.* **13,** 1010–1019 (2012).

189. Banks, C. A. S. *et al.* Controlling for gene expression changes in transcription factor protein networks. *Mol. Cell. Proteomics* **13,** 1510–22 (2014).

190. Nobelprize.org. The Nobel Prize in Chemistry 2002: Information for the public. (2014). at <http://www.nobelprize.org/nobel_prizes/chemistry/laureates/2002/popular.html [2015-10-10]>

191. Beck, M. *et al.* The quantitative proteome of a human cell line. *Mol. Syst. Biol.* **7,** (2011).

192. Nagaraj, N. *et al.* Deep proteome and transcriptome mapping of a human cancer cell line. *Mol. Syst. Biol.* **7,** (2011).

193. Gygi, S. P. *et al.* Quantitative analysis of complex protein mixtures using isotope-coded affinity tags. *Nat. Biotechnol.* **17,** 994–9 (1999).

194. Ong, S.-E. *et al.* Stable isotope labeling by amino acids in cell culture, SILAC, as a simple and accurate approach to expression proteomics. *Mol. Cell. Proteomics* **1,** 376–386 (2002).

195. Zanivan, S., Krueger, M. & Mann, M. In vivo quantitative proteomics: The SILAC mouse. *Methods Mol. Biol.* **757,** 435–450 (2011).

196. Merl, J., Ueffing, M., Hauck, S. M. & von Toerne, C. Direct comparison of MS-based label-free and SILAC quantitative proteome profiling strategies in primary retinal Müller cells. *Proteomics* **12,** 1902–11 (2012).

197. Zhu, W., Smith, J. W. & Huang, C. M. Mass spectrometry-based label-free quantitative proteomics. *J. Biomed. Biotechnol.* **2010,** (2010).

198. Tate, S., Larsen, B., Bonner, R. & Gingras, A. C. Label-free quantitative proteomics trends for protein-protein interactions. *J. Proteomics* **81,** 91–101 (2013).

199. Haas, T. L. *et al.* Recruitment of the linear ubiquitin chain assembly complex stabilizes the TNF-R1 signaling complex and is required for TNF-mediated gene induction. *Mol. Cell* **36,** 831–44 (2009).

200. Oellerich, T. *et al.* SLP-65 phosphorylation dynamics reveals a functional basis for signal integration by receptor-proximal adaptor proteins. *Mol. Cell. Proteomics* **8,** 1738–1750 (2009).

201. Schneider, U., Schwenk, H. U. & Bornkamm, G. Characterization of EBV-genome negative 'null' and 'T' cell lines derived from children with acute lymphoblastic leukemia and leukemic transformed non-Hodgkin lymphoma. *Int. J. Cancer* **19,** 621–6 (1977).

202. Bartelt, R. R., Cruz-Orcutt, N., Collins, M. & Houtman, J. C. D. Comparison of T cell receptor-induced proximal signaling and downstream functions in immortalized and primary T cells. *PLoS One* **4,** (2009).

203. Marcilla, M., Alpizar, A., Paradela, A. & Albar, J. P. A systematic approach to assess amino acid conversions in SILAC experiments. *Talanta* **84,** 430–436 (2011).

204. Schäffer, U. *et al.* SnAvi - a new tandem tag for high-affinity protein-complex purification. *Nucleic Acids Res.* **38,** (2010).

205. Kim, J. H. *et al.* High cleavage efficiency of a 2A peptide derived from porcine teschovirus-1 in human cell lines, zebrafish and mice. *PLoS One* **6,** (2011).

206. Ran, F. A. *et al.* Genome engineering using the CRISPR-Cas9 system. *Nat. Protoc.* **8,** 2281–308 (2013).

207. Kim, D. *et al.* Digenome-seq: genome-wide profiling of CRISPR-Cas9 off-target effects in human cells. *Nat. Methods* **12,** 237–43, 1 p following 243 (2015).

208. Doench, J. G. *et al.* Rational design of highly active sgRNAs for CRISPR-Cas9-mediated gene inactivation. *Nat. Biotechnol.* **32,** 1262–7 (2014).

209. Söderberg, O. *et al.* Characterizing proteins and their interactions in cells and tissues using the in situ proximity ligation assay. *Methods* **45,** 227–232 (2008).

210. Leuchowius, K.-J., Weibrecht, I. & Söderberg, O. In situ proximity ligation assay for microscopy and flow cytometry. *Curr. Protoc. Cytom.* **Chapter 9,** Unit 9.36 (2011).

211. Allalou, A. & Wählby, C. BlobFinder, a tool for fluorescence microscopy image cytometry. *Comput. Methods Programs Biomed.* **94,** 58–65 (2009).

212. Stephanowitz, H., Lange, S., Lang, D., Freund, C. & Krause, E. Improved two-dimensional reversed phase-reversed phase LC-MS/MS approach for identification of peptide-protein interactions. *J. Proteome Res.* **11,** 1175–83 (2012).

213. Martinez, G. J. *et al.* The transcription factor NFAT promotes exhaustion of activated $CD8^+$ T cells. *Immunity* **42,** 265–78 (2015).

214. Benary, M., Kroeger, S., Lee, Y.-H. & Lehmann, R. cobindR: Finding co-occuring motifs of transcription factor binding sites, R package version 1.8.0. (2013). at <https://bioconductor.org/packages/release/bioc/html/cobindR.html [2016-01-02]>

215. Wang, D. *et al.* CD3/CD28 costimulation-induced NF-kappaB activation is mediated by recruitment of protein kinase C-theta, Bcl10, and IkappaB kinase beta to the immunological synapse through CARMA1. *Mol. Cell. Biol.* **24,** 164–71 (2004).

216. Egawa, T. *et al.* Requirement for CARMA1 in Antigen Receptor-Induced NF- B Activation and Lymphocyte Proliferation. **13,** 1252–1258 (2003).

217. Cox, J. & Mann, M. MaxQuant enables high peptide identification rates, individualized p.p.b.-range mass accuracies and proteome-wide protein quantification. *Nat. Biotechnol.* **26,** 1367–1372 (2008).

218. Yui, D. *et al.* Interchangeable binding of Bcl10 to TRAF2 and cIAPs regulates apoptosis signaling. *Oncogene* **20,** 4317–23 (2001).

219. So, T., Soroosh, P., Eun, S.-Y., Altman, A. & Croft, M. Antigen-independent signalosome of CARMA1, PKCθ, and TNF receptor-associated factor 2 (TRAF2) determines NF-κB signaling in T cells. *Proc. Natl. Acad. Sci. U. S. A.* **108,** 2903–8 (2011).

220. Kirisako, T. *et al.* A ubiquitin ligase complex assembles linear polyubiquitin chains. *EMBO J.* **25,** 4877–4887 (2006).

221. Tokunaga, F. *et al.* SHARPIN is a component of the NF-κB-activating linear ubiquitin chain assembly complex. *Nature* **471,** 633–636 (2011).

222. Ikeda, F. *et al.* SHARPIN forms a linear ubiquitin ligase complex regulating NF-κB activity and apoptosis. *Nature* **471,** 637–641 (2011).

223. Dubois, S. M. *et al.* A catalytic-independent role for the LUBAC in NF-κB activation upon antigen receptor engagement and in lymphoma cells. *Blood* **123,** 2199–203 (2014).

224. Yang, Y. *et al.* Essential role of the linear ubiquitin chain assembly complex in lymphoma revealed by rare germline polymorphisms. *Cancer Discov.* **4,** 480–493 (2014).

225. Macián, F., García-Rodríguez, C. & Rao, A. Gene expression elicited by NFAT in the presence or absence of cooperative recruitment of Fos and Jun. *EMBO J.* **19,** 4783–95 (2000).

226. Schatz, P. J. Use of peptide libraries to map the substrate specificity of a peptide-modifying enzyme: a 13 residue consensus peptide specifies biotinylation in Escherichia coli. *Biotechnology. (N. Y).* **11,** 1138–1143 (1993).

227. Beckett, D., Kovaleva, E. & Schatz, P. J. A minimal peptide substrate in biotin holoenzyme synthetase-catalyzed biotinylation. *Protein Sci.* **8,** 921–929 (1999).

228. Carrington, J. C. & Dougherty, W. G. A viral cleavage site cassette: identification of amino acid sequences required for tobacco etch virus polyprotein processing. *Proc. Natl. Acad. Sci. U. S. A.* **85,** 3391–3395 (1988).

229. Hwang, J. S. *et al.* NFAT1 and JunB cooperatively regulate IL-31 gene expression in CD4+ T cells in health and disease. *J. Immunol.* **194,** 1963–74 (2015).

230. García-Rodríguez, C. & Rao, A. Nuclear factor of activated T cells (NFAT)-dependent transactivation regulated by the coactivators p300/CREB-binding protein (CBP). *J. Exp. Med.* **187,** 2031–6 (1998).

231. Schwertman, P. *et al.* UV-sensitive syndrome protein UVSSA recruits USP7 to regulate transcription-coupled repair. *Nat. Genet.* **44,** 598–602 (2012).

232. Gunaratne, J. *et al.* Protein interactions of phosphatase and tensin homologue (PTEN) and its cancer-associated G20E mutant compared by using stable isotope labeling by amino acids in cell culture-based parallel affinity

purification. *J. Biol. Chem.* **286,** 18093–103 (2011).

233. Park, H.-J., Baek, K., Baek, J.-H. & Kim, H.-R. The cooperation of CREB and NFAT is required for PTHrP-induced RANKL expression in mouse osteoblastic cells. *J. Cell. Physiol.* **230,** 667–79 (2015).
234. Sharma, S. *et al.* Dephosphorylation of the nuclear factor of activated T cells (NFAT) transcription factor is regulated by an RNA-protein scaffold complex. *Proc. Natl. Acad. Sci. U. S. A.* **108,** 11381–11386 (2011).
235. Koos, B. *et al.* Analysis of protein interactions in situ by proximity ligation assays. *Curr. Top. Microbiol. Immunol.* **377,** 111–26 (2014).
236. Hahm, K. *et al.* Helios, a T cell-restricted Ikaros family member that quantitatively associates with Ikaros at centromeric heterochromatin. *Genes Dev.* **12,** 782–796 (1998).
237. Winandy, S., Wu, L., Wang, J. H. & Georgopoulos, K. Pre-T cell receptor (TCR) and TCR-controlled checkpoints in T cell differentiation are set by Ikaros. *J. Exp. Med.* **190,** 1039–48 (1999).
238. Jinek, M. *et al.* A programmable dual-RNA-guided DNA endonuclease in adaptive bacterial immunity. *Science* **337,** 816–21 (2012).
239. Cong, L. *et al.* Multiplex genome engineering using CRISPR/Cas systems. *Science* **339,** 819–23 (2013).
240. Mali, P. *et al.* RNA-guided human genome engineering via Cas9. *Science* **339,** 823–6 (2013).
241. Ho Sui, S. J. *et al.* oPOSSUM: Identification of over-represented transcription factor binding sites in co-expressed genes. *Nucleic Acids Res.* **33,** 3154–3164 (2005).
242. Chau, V. *et al.* A multiubiquitin chain is confined to specific lysine in a targeted short-lived protein. *Science* **243,** 1576–1583 (1989).
243. Blackwell, K. *et al.* Two coordinated mechanisms underlie tumor necrosis factor alpha-induced immediate and delayed IκB kinase activation. *Mol. Cell. Biol.* **33,** 1901–15 (2013).
244. Iwai, K. & Tokunaga, F. Linear polyubiquitination: a new regulator of NF-kappaB activation. *EMBO Rep.* **10,** 706–13 (2009).
245. Tokunaga, F. *et al.* Involvement of linear polyubiquitylation of NEMO in NF-kappaB activation. *Nat. Cell Biol.* **11,** 123–32 (2009).
246. Gerlach, B. *et al.* Linear ubiquitination prevents inflammation and regulates immune signalling. *Nature* **471,** 591–596 (2011).
247. Sasaki, Y. *et al.* Defective immune responses in mice lacking LUBAC-mediated linear ubiquitination in B cells. *EMBO J.* **32,** 2463–76 (2013).
248. Damgaard, R. B. *et al.* The ubiquitin ligase XIAP recruits LUBAC for NOD2 signaling in inflammation and innate immunity. *Mol. Cell* **46,** 746–58 (2012).
249. Rodgers, M. A. *et al.* The linear ubiquitin assembly complex (LUBAC) is essential for NLRP3 inflammasome activation. *J. Exp. Med.* **211,** 1333–47 (2014).
250. Emmerich, C. H. *et al.* Activation of the canonical IKK complex by K63/M1-linked hybrid ubiquitin chains. *Proc. Natl. Acad. Sci. U. S. A.* **110,** 15247–52 (2013).
251. Lo, Y.-C. *et al.* Structural basis for recognition of diubiquitins by NEMO. *Mol. Cell* **33,** 602–15 (2009).
252. Fujita, H. *et al.* Mechanism underlying IκB kinase activation mediated by the linear ubiquitin chain assembly complex. *Mol. Cell. Biol.* **34,** 1322–35 (2014).
253. Tian, Y. *et al.* RBCK1 negatively regulates tumor necrosis factor- and interleukin-1-triggered NF-kappaB activation by targeting TAB2/3 for degradation. *J. Biol. Chem.* **282,** 16776–82 (2007).
254. Kanayama, A. *et al.* TAB2 and TAB3 activate the NF-κB pathway through binding to polyubiquitin chains. *Mol. Cell* **15,** 535–548 (2004).
255. Pierce, A. J., Hu, P., Han, M., Ellis, N. & Jasin, M. Ku DNA end-binding protein modulates homologous repair of double-strand breaks in mammalian cells. *Genes Dev.* **15,** 3237–42 (2001).
256. Decker, E. L., Skerka, C. & Zipfel, P. F. The early growth response protein (EGR-1) regulates interleukin-2 transcription by synergistic interaction with the nuclear factor of activated T cells. *J. Biol. Chem.* **273,** 26923–30 (1998).
257. Lee, S. H. *et al.* Runx3 inhibits IL-4 production in T cells via physical interaction with NFAT. *Biochem. Biophys. Res. Commun.* **381,** 214–217 (2009).
258. Gaj, T., Gersbach, C. a & Barbas, C. F. ZFN, TALEN, and CRISPR/Cas-based methods for genome engineering. *Trends Biotechnol.* **31,** 397–405 (2013).
259. Kaiser, M., Wiggin, G. R., Lightfoot, K., Arthur, J. S. C. & Macdonald, A. MSK regulate TCR-induced CREB phosphorylation but not immediate early gene transcription. *Eur. J. Immunol.* **37,** 2583–95 (2007).
260. Muthusamy, N. & Leiden, J. M. A protein kinase C-, Ras-, and RSK2-dependent signal transduction pathway activates the cAMP-responsive element-binding protein transcription factor following T cell receptor engagement. *J. Biol. Chem.* **273,** 22841–7 (1998).
261. Hughes-Fulford, M. *et al.* Early immune response and regulation of IL-2 receptor subunits. *Cell. Signal.* **17,** 1111–24

(2005).

262. Pasquinelli, V. *et al.* IFN-gamma production during active tuberculosis is regulated by mechanisms that involve IL-17, SLAM, and CREB. *J. Infect. Dis.* **199,** 661–5 (2009).

263. Saraiva, M. & O'Garra, A. The regulation of IL-10 production by immune cells. *Nat. Rev. Immunol.* **10,** 170–81 (2010).

264. Zhang, F., Rincon, M., Flavell, R. A. & Aune, T. M. Defective Th function induced by a dominant-negative cAMP response element binding protein mutation is reversed by Bcl-2. *J. Immunol.* **165,** 1762–70 (2000).

265. Barton, K. *et al.* Defective thymocyte proliferation and IL-2 production in transgenic mice expressing a dominant-negative form of CREB. *Nature* **379,** 81–5 (1996).

266. Kim, H.-P. & Leonard, W. J. CREB/ATF-dependent T cell receptor-induced FoxP3 gene expression: a role for DNA methylation. *J. Exp. Med.* **204,** 1543–51 (2007).

267. Ryseck, R. P. & Bravo, R. c-JUN, JUN B, and JUN D differ in their binding affinities to AP-1 and CRE consensus sequences: effect of FOS proteins. *Oncogene* **6,** 533–542 (1991).

268. Dwarki, V. J., Montminy, M. & Verma, I. M. Both the basic region and the 'leucine zipper' domain of the cyclic AMP response element binding (CREB) protein are essential for transcriptional activation. *EMBO J.* **9,** 225–232 (1990).

269. Wong, W. F., Kohu, K., Chiba, T., Sato, T. & Satake, M. Interplay of transcription factors in T-cell differentiation and function: the role of Runx. *Immunology* **132,** 157–164 (2011).

270. Hu, H., Djuretic, I., Sundrud, M. S. & Rao, A. Transcriptional partners in regulatory T cells: Foxp3, Runx and NFAT. *Trends Immunol.* **28,** 329–32 (2007).

271. Komine, O. *et al.* The Runx1 transcription factor inhibits the differentiation of naive CD4+ T cells into the Th2 lineage by repressing GATA3 expression. *J. Exp. Med.* **198,** 51–61 (2003).

272. Ono, M. *et al.* Foxp3 controls regulatory T-cell function by interacting with AML1/Runx1. *Nature* **446,** 685–689 (2007).

273. Lee, Y.-H., Benary, M., Baumgrass, R. & Herzel, H. Prediction of regulatory transcription factors in T helper cell differentiation and maintenance. *Genome Inform.* **22,** 84–94 (2010).

274. Yoshida, T. & Georgopoulos, K. Ikaros fingers on lymphocyte differentiation. *Int. J. Hematol.* **100,** 220–9 (2014).

275. Quirion, M. R., Gregory, G. D., Umetsu, S. E., Winandy, S. & Brown, M. a. Cutting edge: Ikaros is a regulator of Th2 cell differentiation. *J. Immunol.* **182,** 741–745 (2009).

276. Thomas, R. M. *et al.* Ikaros enforces the costimulatory requirement for IL2 gene expression and is required for anergy induction in CD4+ T lymphocytes. *J. Immunol.* **179,** 7305–7315 (2007).

277. Kimura, M. IRF2-binding protein-1 is a JDP2 ubiquitin ligase and an inhibitor of ATF2-dependent transcription. *FEBS Lett.* **582,** 2833–7 (2008).

278. Cai, S., Lee, C. C. & Kohwi-Shigematsu, T. SATB1 packages densely looped, transcriptionally active chromatin for coordinated expression of cytokine genes. *Nat. Genet.* **38,** 1278–88 (2006).

279. Cohn, M. A., Kee, Y., Haas, W., Gygi, S. P. & D'Andrea, A. D. UAF1 is a subunit of multiple deubiquitinating enzyme complexes. *J. Biol. Chem.* **284,** 5343–51 (2009).

280. Kreßner, C., Nollau, P., Grosse, R. & Brandt, D. T. Functional interaction of SCAI with the SWI/SNF complex for transcription and tumor cell invasion. *PLoS One* **8,** e69947 (2013).

281. Chapman, N. M. & Chi, H. mTOR signaling, Tregs and immune modulation. *Immunotherapy* **6,** 1295–311 (2014).

282. Cobbold, S. P. The mTOR pathway and integrating immune regulation. *Immunology* **140,** 391–8 (2013).

283. Yang, T. T. C. *et al.* Integration of protein kinases mTOR and extracellular signal-regulated kinase 5 in regulating nucleocytoplasmic localization of NFATc4. *Mol. Cell. Biol.* **28,** 3489–501 (2008).

284. Rocha, S., Garrett, M. D., Campbell, K. J., Schumm, K. & Perkins, N. D. Regulation of NF-kappaB and p53 through activation of ATR and Chk1 by the ARF tumour suppressor. *EMBO J.* **24,** 1157–1169 (2005).

285. Patil, M., Pabla, N. & Dong, Z. Checkpoint kinase 1 in DNA damage response and cell cycle regulation. *Cell. Mol. Life Sci.* **70,** 4009–21 (2013).

286. Wang, L., Guo, Q., Fisher, L. A., Liu, D. & Peng, A. Regulation of polo-like kinase 1 by DNA damage and PP2A/B55α. *Cell Cycle* **14,** 157–66 (2015).

287. Benada, J., Burdová, K., Lidak, T., von Morgen, P. & Macurek, L. Polo-like kinase 1 inhibits DNA damage response during mitosis. *Cell Cycle* **14,** 219–31 (2015).

288. de Souza, E. E. *et al.* Characterization of the human NEK7 interactome suggests catalytic and regulatory properties distinct from those of NEK6. *J. Proteome Res.* **13,** 4074–90 (2014).

289. Shou, J. *et al.* Nuclear factor of activated T cells in cancer development and treatment. *Cancer Lett.* **361,** 174–184 (2015).

290. Sun, L. *et al.* Cabin 1, a negative regulator for calcineurin signaling in T lymphocytes. *Immunity* **8,** 703–11 (1998).

291. Zou, Y., Lim, S., Lee, K., Deng, X. & Friedman, E. Serine/threonine kinase Mirk/Dyrk1B is an inhibitor of epithelial

cell migration and is negatively regulated by the Met adaptor Ran-binding protein M. *J. Biol. Chem.* **278,** 49573–81 (2003).

292. Gertz, J. *et al.* Distinct properties of cell-type-specific and shared transcription factor binding sites. *Mol. Cell* **52,** 25–36 (2013).
293. Rauscher, F. J., Voulalas, P. J., Franza, B. R. & Curran, T. Fos and Jun bind cooperatively to the AP-1 site: reconstitution in vitro. *Genes Dev.* **2,** 1687–99 (1988).
294. Jolma, A. *et al.* DNA-dependent formation of transcription factor pairs alters their binding specificity. *Nature* **527,** 384–8 (2015).
295. Geimer Le Lay, A.-S. *et al.* The tumor suppressor Ikaros shapes the repertoire of notch target genes in T cells. *Sci. Signal.* **7,** ra28 (2014).
296. Vahedi, G. *et al.* STATs shape the active enhancer landscape of T cell populations. *Cell* **151,** 981–93 (2012).
297. Choi, J.-M., Sohn, J.-H., Park, T.-Y., Park, J.-W. & Lee, S.-K. Cell permeable NFAT inhibitory peptide Sim-2-VIVIT inhibits T-cell activation and alleviates allergic airway inflammation and hyper-responsiveness. *Immunol. Lett.* **143,** 170–6 (2012).
298. Lozano, T. *et al.* Inhibition of FOXP3/NFAT interaction enhances T cell function after TCR stimulation. *J. Immunol.* **195,** 3180–9 (2015).
299. Elloumi, H. Z. *et al.* A cell permeable peptide inhibitor of NFAT inhibits macrophage cytokine expression and ameliorates experimental colitis. *PLoS One* **7,** e34172 (2012).

List of Abbreviations

ABC	ammonium bicarbonate
ACN	acetonitrile
AP	activator protein
APS	ammonium peroxodisulfate
ATCC	American tissue culture collection
ATF	activating transcription factor
ATP	adenosine monophosphate
AVI	biotinylation signal sequence for the BirA biotin ligase
AVITEV	combination of AVI site and TEV protease cleavage site
BCA	bicinchoninic acid
BCL	B-cell lymphoma
BiFC	bimolecular fluorescence complementation
BIRC	baculoviral IAP repeat-containing protein
BRET	bioluminescence resonance energy transfer
BSA	bovine serum albumin
CABIN	calcineurin binding protein
CaM	calmodulin
CaMK	Ca2+/CaM-dependent protein kinase
cAMP	cyclic adenosine monophosphate
CaN	calcineurin
CARD	caspase recruitment domain
CARMA	CARD containing MAGUK protein
CBH	hybrid chicken beta-actin promoter
CBL	Cbl proto-oncogene
CBM-complex	CARMA1-MALT1-BCL10-complex
CD	cluster of differentiation
cDNA	copy DNA
CHEK	checkpoint kinase
ChIP	chromatin immunoprecipitation
cIAP	cellular inhibitor of apoptosis
CK	casein kinase
CoIP	co-immunopurification
CREB	cyclic AMP response element binding protein
CREBBP	CREB binding protein
CRISPR	clustered regularly interspaced short palindromic repeats
CsA	Cyclosporine A
CTLA	cytotoxic T lymphocyte-associated protein
DAG	diacylglycerol
DAPI	4’,6-Diamidin-2-phenylindol
DD	death domain
DMEM	Dulbecco’s modified Eagle medium
DMSO	dimethylsulfoxid
DNA	deoxyribonucleic acid
DTT	dithiothreitol
DYRK	dual-specificity tyrosine-phosphorylation regulated kinase
E. coli	Escherichia coli
EB	elution buffer
EDTA	ethylene diamintetraacetic acid
EF	elongation factor
EGR	early growth response
ELK	Ets-like transcription factor

ER	endoplasmatic reticulum
ERK	extracellular signal related kinase
ESI	electro-spray ionization
FACS	fluorescence activated cell sorting
FCS	fetal calf serum
FOX	forkhead-box protein
FRET	Förster resonance energy transfer
FYN	feline yes-related protein
GATA	GATA binding protein
GEO	Gene Expression Omnibus
GFP	green fluorescent protein
GITR	glucocorticoid-induced TNF receptor-related protein
GM-CSF	granulocyte/macrophage-colony stimulating factor
GRAIL	gene related to anergy in lymphocytes
gRNA	guide RNA
GSK	glycogen synthase kinase
GST	glutathione-S-transferase
HBS	HEPES buffered saline
HEK	human embryonal kidney cells
HEPES	2-[4-(2-hydroxyethyl)piperazin-1-yl]ethanesulfonic acid
HIOP	heme-oxidized IRP2 ubiquitin ligase
HOIL	HOIL1 interacting protein
HPK	hematopoietic progenitor kinase-
IFN	interferon
IκB	inhibitor of NFκB
IKK	inhibitor of NFκB-kinase
IL	Interleukin
IP_3	inositol 1,4,5-trisphosphate
IRES	internal ribosome entry site
IRF	interferon regulatory factor
IRF2BP	IRF2 binding protein
ITAM	immune receptor tyrosine-based activation motif
ITCH	E3 ubiquitin-protein ligase itchy homolog
ITK	interleukin-2 inducible T cell kinase
JNK	Jun N-terminal kinase
kDa	kilo Dalton
KO	knock-out
LAT	linker of activation in T cells
LB	lysis buffer
LC	liquid chromatography
LCK	lymphocyte specific protein tyrosine kinase
LTQ	linear trap quadrupole
LUBAC	linear ubiquitin assembly complex
MACS	magnet activated cell sorting
MAGUK	membrane-associated guanylate kinase
MALDI	matrix-assisted laser desorption/ionization
MALT	mucosa-associated lymphoid tissue lymphoma (translocation protein)
MAPK	mitogen associated protein kinase
MAPKK	MAP-kinase-kinase
MAPKKK	MAP-kinase-kinase-kinase
MEF	myocyte enhancer factor
MEK	MAPK/ERK-kinase
MIB	mind bomb homolog
MIG	MSCV-IRES-GFP
MS	mass spectrometry

MSCV	murine stem cell virus
mTOR	mammalian target of rapamycin
NEK	never in mitosis related kinase
NEMO	NFκB essential modifier
NFAT	nuclear factor of activated T cells
NFκB	nuclear factor of κ light chain enhancer of activated B cells
NHR	NFAT homology domain
NOTCH	notch homolog
NRON	non-coding repressor of NFAT
PAGE	polyacrylamide gel electrophoresis
PARP	poly-ADP polymerase
PBMC	peripheral blood mononuclear cell
PBS	phosphate buffered saline
PCR	polymerase chain reaction
PI3K	phosphoinositide 3-kinase
PIM	pim proto-oncogene
PIP_2	phosphatidylinositol-4,5-bisphosphate
PKA	protein kinase A
PLA	proximity ligation assay
PLCγ	phospholipase C-γ
PLK	polo-like kinase
PMA	phorbol-12-myristat-13-acetate
PRKDC	Protein kinase DNA activated, catalytic polypeptide
qPCR	quantitative PCR
RAC	ras-related C3 botulinum toxin substrate
RAS-GRP	rat sarcoma guanyl releasing protein
RBCK	RanBP-type and C3HC4-type zinc finger-containing protein
RHR	REL homology domain
RIP	receptor-interacting protein
RNA	ribonucleic acid
RNF	ring finger protein
RP-HPLC	reverse phase-high performance liquid chromatography
RPMI	Roswell Memorial Park Institute
RPTOR	regulatory associated protein of mTOR
RUNX	runt-related transcription factor
SATB	special AT-rich sequence binding homeobox
SCAI	suppressor of cancer cell invasion
SCID	severe combined immune defect
SDS	sodium dodecyl sulfate
SHARPIN	SHANK-associated RH domain interacting protein
SILAC	stable isotope labeling by amino acids in cell culture
siRNA	small interfering RNA
SLP	SH2 domain-containing leukocyte protein
SO	StrepOne tag
SOCE	store operated calcium entry
STIM	stromal interaction molecule
SUMO	small ubiquitin-like modifiers
SWI/SNF	switch/sucrose non-fermentable
TAB	TAK1-binding protein
TACI	transmembrane activator, calcium modulator, and cyclophilin ligand interactor
TAK	TGFβ-activated kinase
TCR	T cell receptor
TEMED	N,N,N′,N′-Tetramethylethane-1,2-diamine
TEV	tobacco etch virus (protease)
TFA	trifluoroacetic acid

TGF	transforming growth factor
T_H cells	T helper cells
TLR	toll-like receptor
TNF	tumor necrosis factor
TNFAIP	TNFα induced protein
TRAF	TNF receptor-associated factor
T_{reg}	regulatory T cells
VRK	vaccinia-related kinase
VSVG	vesicular stomatitis virus glycoprotein G
WB	western blot
WBU	washing buffer
WDR	WD repeat domain
wt	wild-type
XRCC	X-ray repair cross-complementing protein
YFP	yellow fluorescent protein
ZAP	ζ-chain associated protein

Der Lebenslauf ist in der Online-Version aus Gründen des Datenschutzes nicht enthalten.

Acknowledgment

Zuerst möchte ich mich bei Ria Baumgrass für die Möglichkeit bedanken, in ihrer Gruppe an dieser Dissertation arbeiten zu können. Vielen Dank für all die Unterstützung und Finanzierung in den letzten Jahren. Vielen Dank an Prof. Rupert Mutzel für die Bereitschaft, als Gutachter dieser Arbeit und als Vorsitzender der Promotionskommision zu fungieren.

Des Weiteren gilt mein Dank allen jetzigen und früheren Mitarbeitern der AG Baumgrass für die Hilfe bei größeren und kleineren Problemen. Danke an: Claudia B., Claudia S., Manja J., Melanie V., Stefan F., Stefan K., Maria J., Lina B., Enrico F., Katja B., Janine A., Katharina H., Martin K., Tobias S., Timo L., Stefanie G., Yen H., Flori H. und Mathias S. Danke auch an Melanie W., Jakob Z., Farzin M., Patrick M., Daniel S., Claudia H., Jenny, Toralf, Heike H., Yuri S., Mathias P., Anna N., Christian N., Andrey K., Heidi S., Heidi H., Regina, Stefanie S., Stefanie R., Imme S., für Diskussion, Reagenzien, know-how und Alltägliches.

Besonderer Dank gilt Heike Stephanowitz und Eberhard Krause für die Messung und Auswertung der MS-Versuche, Ivo Bachmann und Fridolin Gross für die bioinformatischen Analysen, Flori für die Erstellung der KO-Zelllinien, Mela fürs Korrekturlesen sowie Kristin Wendland für die Einführung in die Welt des PLA.

Einen großen Dank an Lars Baumann, Richard Clarkson und Annette Beck-Sickinger, sowie alle anderen, die mich während meiner wissenschaftlichen Entwicklung gefördert, geprägt und inspiriert haben.

Ein ganz besonderer Dank gilt auch meiner Familie, die mich immer in Allem unterstützt hat. Schön, dass es euch gibt.

Und last but not least: Janina. Danke für so unendlich Vieles!

Appendix

TABLE A 1. MS data of all proteins that were enriched in CoIPs with NFATc1S as a bait. The list shows all proteins that were identified by at least two unique peptides and enriched by a factor of >3 in both runs.

Gene ID	Average unique peptides	Unique sequence coverage [%]	Average ratio count	Enrichment factor Run 1	Enrichment factor Run 2	Gene ID	Average unique peptides	Unique sequence coverage [%]	Average ratio count	Enrichment factor Run 1	Enrichment factor Run2
SCAI;C9orf126	9.0	19.6	7.5	15.2	13.9	CREB1; CREM;ATF1	2.0	10.0	2.0	5.9	3.9
CSNK1D; CSNK1E	2.5	22.2	7.0	12.0	12.5	IKZF1	2.0	9.4	6.0	5.1	3.9
GSK3B	3.0	14.3	2.0	8.8	12.1	CAD	8.0	5.8	9.5	3.3	3.5
WDR48	3.0	4.7	3.0	7.4	6.5	RFC5	2.0	6.6	2.0	3.1	3.8
CSNK1A1; CSNK1A1L	9.5	33.5	9.5	7.1	7.8						

TABLE A 2. MS data of all proteins that were enriched in CoIPs with NFATc1L as a bait. The list shows all proteins that were identified by at least two unique peptides and enriched by a factor of >3 in at least two of three runs.

Gene ID	Average unique peptides	Unique sequence coverage [%]	Average ratio count	Enrichment factor Run 1	Enrichment factor Run 2	Enrichment factor Run 3	Gene ID	Average unique peptides	Unique sequence coverage [%]	Average ratio count	Enrichment factor Run 1	Enrichment factor Run 2	Enrichment factor Run 3
NFATC1	40.7	50.5	138.0	33.7	9.6	15.2	SMARCE1	10.3	46.4	14.0	5.2	6.0	4.2
RPTOR	20.0	23.4	10.0	31.0	1.8	19.5	IFI16	7.7	24.2	8.3	5.0	3.8	3.4
CREB1	4.0	25.7	4.3	28.5	30.4	3.5	CHAMP1	5.0	8.0	3.5	4.9	n.d.	3.9
CSNK1D	2.0	5.1	12.0	27.2	43.6	n.d.	MDH2	3.5	19.9	3.5	4.8	n.d.	3.6
TRMT61B	4.5	13.8	4.5	23.0	n.d.	15.1	XRCC6	22.3	51.6	51.7	4.8	5.0	1.3
SCAI;C9orf126	16.3	40.3	18.0	21.1	25.2	19.9	HLTF	2.5	5.2	2.0	4.7	n.d.	5.1
GSK3B	6.0	33.8	4.0	15.9	44.4	27.9	DNAJC7	4.5	12.1	4.5	4.7	n.d.	4.9
MOSPD2	7.0	21.8	5.0	12.2	n.d.	20.3	MTHFD1L	5.0	10.2	7.5	4.7	2.6	3.3
WDR48	7.3	18.3	5.0	11.7	8.0	14.0	CBFB	2.0	13.4	2.0	4.6	3.5	n.d.
CSNK1E;CSNK1D	2.5	8.9	3.5	10.7	70.5	n.d.	XRCC5	25.0	43.2	65.0	4.4	4.7	4.3
IKZF2	5.0	14.7	7.0	9.8	13.8	n.d.	SMARCA4	23.3	21.9	30.7	4.4	4.7	3.9
NEK7;NEK6	3.0	13.9	3.0	9.5	6.2	7.7	ACTL6A	10.7	35.4	11.3	4.4	4.5	3.2
FOXK2	4.0	15.1	3.5	8.2	n.d.	6.0	RPA1	4.7	20.5	6.0	4.4	2.2	3.7
PHGDH	8.0	18.2	11.3	7.9	0.6	6.2	CTBP1	3.5	8.6	3.0	4.3	3.5	n.d.
CHEK1	5.5	22.5	3.5	7.6	n.d.	11.9	SMARCC1	13.3	24.6	40.0	4.2	4.8	3.3
JUNB	3.0	22.5	3.0	7.5	14.6	n.d.	SATB1	13.7	21.0	18.3	4.0	3.5	3.2
CREBBP	9.5	10.8	3.5	7.3	32.5	24.5	HSPA5	31.0	49.8	82.3	3.9	3.3	3.5
MTHFD2	3.0	14.4	3.7	7.0	5.4	3.8	RUNX1	6.7	24.3	7.3	3.9	4.7	3.0
IKZF1	6.7	32.2	12.3	7.0	9.6	7.0	RFC4	4.7	23.8	4.3	3.9	4.5	2.6
LRRC47	2.7	9.1	2.7	7.0	3.5	3.0	FOXK1	4.0	15.0	3.7	3.9	7.3	6.1
NFATC2	12.3	39.9	79.3	6.5	13.0	0.7	HSPA9	41.7	53.3	123.7	3.7	3.7	2.4
FXR1	4.7	15.4	7.3	6.4	5.3	3.5	SMARCD1	8.3	29.5	7.3	3.6	4.2	3.2
ACAD9	14.0	26.4	13.0	6.3	5.1	2.9	ARID1A	14.0	11.4	23.7	3.5	5.2	4.6
ZBTB40	2.5	3.1	2.0	6.3	n.d.	8.3	LIG3	4.3	5.4	4.0	3.4	3.7	3.8
RANBP9	4.5	11.5	3.0	6.2	n.d.	6.5	TUFM	15.0	39.4	25.3	3.3	3.0	2.4
DPF2	4.7	22.5	4.3	6.0	7.1	2.3	NUP210	13.7	16.1	16.0	3.3	2.2	3.0
SMARCC2	13.0	24.0	14.7	6.0	8.0	4.7	SARS2	6.7	26.8	6.3	3.2	2.1	4.4
SMARCD2	8.7	31.1	10.0	6.0	7.5	5.0	BCL11B	6.7	23.9	8.0	3.2	3.7	2.3
LEF1	3.0	15.1	3.7	5.7	6.1	3.8	CREBBP	9.5	10.8	3.5	n.d.	32.5	24.5
RFC2	2.3	12.2	2.7	5.4	4.9	4.7	EP300	12.0	11.8	15.5	n.d.	19.3	15.2
VAPA	8.3	45.0	15.0	5.4	4.0	5.6	TRRAP	22.0	7.8	17.0	n.d.	14.8	7.8
ATF7	3.0	30.0	3.5	5.4	12.5	n.d.							

TABLE A 3. MS data of all proteins that were enriched in CoIPs with NFATc2 as a bait. The list shows all proteins that were identified by at least two unique peptides and enriched by a factor of >3 in both runs.

Gene ID	Average unique peptides	Unique sequence coverage [%]	Average ratio count	Enrichment factor Run 1	Enrichment factor Run2	Gene ID	Average unique peptides	Unique sequence coverage [%]	Average ratio count	Enrichment factor Run 1	Enrichment factor Run 2
ZNF384	3.5	10.9	13.0	30.6	13.4	HIRA	4.0	9.9	4.0	5.5	7.8
JUN	2.0	8.8	3.5	18.8	17.7	ERCC3	7.0	14.7	3.0	5.5	7.6
RPTOR	15.0	18.0	9.0	17.1	20.8	UBE2S	3.0	32.9	3.5	5.4	5.8
IKZF1	3.5	8.3	26.0	16.7	41.0	SUPT6H	6.0	5.2	4.5	5.4	6.0
ATF7	5.5	33.2	7.5	16.6	16.8	ARID1A	20.5	15.3	26.5	5.3	6.3
CREB1	2.5	13.5	4.5	16.0	66.2	HSPA9	45.0	55.5	192.5	5.3	3.2
EP300	17.5	10.2	20.5	14.7	18.2	POGZ	9.5	13.4	6.0	5.2	6.4
ZNF131	4.0	12.7	4.0	14.6	13.9	UHRF1	3.5	7.1	3.0	5.1	7.8
FOS	4.0	21.1	3.5	14.1	16.1	SUCLA2	2.0	6.6	2.0	5.1	5.5
MAFK	4.0	38.5	6.0	13.7	25.6	HSPA5	33.5	52.4	94.0	5.0	9.6
XRCC5	40.5	61.3	90.0	13.5	51.3	DPF2	5.5	18.7	3.5	4.9	6.5
PRKDC	114.5	30.9	104.0	13.5	18.8	YWHAZ	8.5	37.6	16.0	4.9	16.0
CHEK1	10.5	34.6	5.5	13.4	4.7	GATAD2A	16.5	37.3	16.0	4.9	5.6
SCAI;C9orf126	15.0	34.0	10.0	12.7	45.8	LRRC47	2.0	7.0	2.0	4.8	6.8
CSNK1D	2.0	5.1	14.0	12.2	33.7	ZMYM2	7.0	10.2	5.5	4.7	4.2
JUNB	6.0	38.6	6.5	12.2	19.7	DNAJA1	10.5	38.5	17.5	4.7	4.3

TABLE A 3 (continued)

Gene ID	Average unique peptides	Unique sequence coverage [%]	Average ratio count	Run 1	Run 2	Gene ID	Average unique peptides	Unique sequence coverage [%]	Average ratio count	Run 1	Run 2
NFYC	3.5	15.5	6.5	11.1	10.4	IDH3A	5.5	22.1	4.0	4.7	3.9
PLK1	7.5	22.2	5.0	10.7	23.3	SDHA	3.5	8.4	3.0	4.7	4.2
LIG3	15.0	21.1	6.5	10.6	21.4	CBX5	2.0	9.9	2.5	4.6	7.4
NFATc2	58.5	62.7	365.5	10.6	95.2	CABIN1	4.5	3.8	4.0	4.6	5.8
XRCC1	3.0	8.6	2.5	10.4	12.6	VAPA	10.5	42.2	23.5	4.4	5.3
IKZF2;ZNFN1A2	11.5	27.9	21.0	10.4	62.3	CBX3	2.0	7.7	7.0	4.4	5.1
HSPA1A	9.5	13.7	12.5	10.3	29.8	MRE11A	3.0	6.9	2.5	4.4	5.8
HLTF	20.0	29.4	4.0	10.2	24.7	SMARCA5	11.5	17.1	8.5	4.4	4.3
BTAF1	7.5	6.3	7.0	10.1	12.8	EEF2	16.5	24.2	22.0	4.4	5.3
YWHAB	4.5	31.1	6.0	10.1	12.1	RB1	7.0	10.3	5.0	4.3	5.5
GSK3B	5.5	24.8	7.0	9.8	10.6	MCRS1	4.0	11.1	4.0	4.3	3.9
CHAF1B	7.0	19.1	3.0	9.8	17.4	EMD	3.0	17.8	4.0	4.3	3.2
LEF1	6.0	18.5	11.5	9.7	36.6	GTF2H2C; GTF2H2	2.0	13.4	2.5	4.2	7.2
IRF2BP1	7.5	24.0	7.0	8.8	12.3	SUPT5H	5.0	11.3	3.0	4.2	5.6
JUND	2.0	8.4	3.0	8.3	3.6	RCOR1	4.5	19.3	13.5	4.1	5.8
TFAM	3.5	22.4	5.0	8.1	11.1	VAPB	5.0	25.9	10.0	4.1	6.0
MAFG	2.5	22.2	2.0	8.0	30.1	MRPL17	3.0	18.3	3.0	4.1	5.2
SSBP1	11.5	69.6	20.0	8.0	10.3	UQCRC2	3.0	10.7	3.5	4.1	3.4
RANBP9	8.5	19.3	3.0	8.0	15.4	TCF12	7.0	17.4	6.5	4.1	6.3
CHAMP1	6.0	12.3	4.0	7.9	9.7	BEND3	3.0	6.2	2.0	4.1	3.9
RPA1	17.0	42.2	13.0	7.8	14.2	SMARCA4	29.5	21.9	39.5	4.0	5.0
WDR26	2.5	5.7	2.5	7.8	9.8	KDM1A	20.0	32.0	27.0	4.0	5.6
IRF2BP2	6.0	21.5	5.5	7.7	20.4	SMARCD2	10.0	28.9	13.5	3.9	4.8
ZNF148	3.5	8.8	4.0	7.7	7.9	AIFM1	11.0	26.9	10.5	3.9	3.9
FOXK1	3.5	10.9	3.5	7.7	9.7	MCM2	7.0	11.6	6.0	3.8	3.3
ZNF217	5.0	10.9	4.5	7.6	5.7	H2AFY	7.0	32.5	8.0	3.8	6.8
DEK	7.0	22.9	5.0	7.6	9.8	HSPA8	21.0	40.9	207.0	3.8	6.2
RPA3	2.0	32.9	2.0	7.6	8.5	POLDIP2	6.5	22.3	8.0	3.8	3.7
POLG	10.5	17.3	9.5	7.5	11.3	RAD50	15.0	17.8	8.5	3.8	5.0
CACYBP	9.0	64.0	8.0	7.5	9.7	SMARCC1	26.0	30.5	54.5	3.8	4.7
RPA2	4.5	17.8	4.5	7.5	13.2	POLR1C	4.0	19.3	6.5	3.7	4.6
NFYB	2.0	13.0	2.5	7.2	12.0	TIMM50	6.5	26.6	7.5	3.7	3.7
PARP1	30.5	38.1	25.0	7.1	21.1	MTA2	14.5	28.6	21.0	3.7	4.8
ETV6	3.0	6.9	4.0	7.1	8.7	HADHA	22.5	36.3	38.5	3.7	3.1
XRCC6	50.0	65.8	102.0	7.0	48.5	TLK2;TLK1	3.5	6.5	2.5	3.7	7.4
KIF4A	11.0	15.8	6.5	7.0	7.5	RBBP4	4.5	18.0	28.5	3.6	4.9
RUNX1	8.5	26.5	10.5	7.0	14.4	GATAD2B	6.0	19.2	5.0	3.6	5.4
RFC4	14.0	41.6	16.0	6.8	9.7	RANBP2	24.5	11.6	37.0	3.6	4.7
RFC3	9.0	32.6	9.5	6.8	11.4	CEBPE	3.0	22.1	3.0	3.6	15.1
EGR1	5.5	12.7	5.5	6.8	25.5	ADNP	10.0	16.0	7.0	3.6	4.4
CAD	30.0	17.5	24.5	6.7	8.4	SMARCE1	13.0	38.3	17.5	3.6	4.6
RFC5	9.0	44.8	10.5	6.6	11.3	CNP	6.5	18.7	5.0	3.5	3.4
CTBP1	5.0	15.4	4.5	6.3	7.0	CBX1	2.0	11.3	2.0	3.5	5.6
RFC2	6.0	24.6	7.0	6.3	10.9	SMARCC2	11.5	15.9	10.5	3.5	4.7
BCL11B	7.0	18.4	4.0	6.2	8.9	ZNF24	3.5	15.2	5.5	3.5	3.6
YWHAG	7.5	33.6	9.5	6.2	20.1	CHD4	20.0	14.8	36.0	3.4	4.1
KIF2C	4.0	11.9	3.0	6.2	7.4	SMARCD1	9.5	26.2	6.5	3.4	5.4
SATB1	19.5	33.2	25.0	6.2	10.4	MBD3	5.0	23.9	9.0	3.4	4.5
RNGTT	2.5	6.6	2.5	6.1	3.2	NUDC	7.0	24.2	8.0	3.3	3.7
PRDM15; ZNF298	4.0	7.0	2.0	6.1	8.1	ACTL6A	9.0	30.8	14.0	3.3	4.7
YY1;ZFP42;YY2	2.0	14.7	2.0	6.0	4.3	MTA1	4.5	8.9	6.0	3.3	4.2
ALDH18A1	2.5	5.3	3.0	6.0	5.4	IDH3B	5.0	14.6	8.0	3.3	3.3
MTHFD2	2.5	14.4	3.0	6.0	5.6	CSTF1	5.5	21.3	8.0	3.3	3.3
YWHAE	11.5	50.2	23.0	6.0	9.2	RPL23	6.0	30.7	13.5	3.2	3.9
MRPL39	10.0	37.7	11.5	5.9	7.3	PPP1CA	4.0	14.5	8.0	3.2	3.1
TUFM	18.5	50.7	39.5	5.9	5.4	HSPH1	12.0	23.3	11.5	3.2	3.5
IFI16	13.5	27.6	15.0	5.9	6.9	PMPCB	4.0	11.9	3.5	3.1	5.0
TP53BP1	5.0	4.9	3.0	5.9	4.5	GTF3C5	4.0	16.2	4.0	3.0	3.3
WDR48	4.5	10.3	5.0	5.9	12.8	TCP1	16.0	39.7	25.5	3.0	3.6
ERAL1	6.0	21.1	5.5	5.8	6.0	GTF3C4	6.0	9.0	6.0	3.0	3.9
SSRP1	6.0	10.9	4.0	5.6	8.4	DCAF7	4.0	14.6	3.0	3.0	4.0
TRRAP	23.0	8.4	19.5	5.6	7.1	H3F3B;HIST2H3A;HIST3H3;H3F3A;HIST1H3A;H3F3C	2.0	13.6	22.5	3.0	6.9
YWHAQ	5.5	21.6	6.0	5.5	52.0	HDAC1	5.5	16.6	37.5	3.0	4.0